R-04-52

Transverse dispersion in heterogeneous fractures

Bill Dershowitz, Dawn Shuttle, Kate Klise,
Nils Outters, Jan Hermanson
Golder Associates

December 2004

Svensk Kärnbränslehantering AB
Swedish Nuclear Fuel
and Waste Management Co
Box 5864
SE-102 40 Stockholm Sweden
Tel 08-459 84 00
+46 8 459 84 00
Fax 08-661 57 19
+46 8 661 57 19

ISSN 1402-3091
SKB Rapport R-04-52

Transverse dispersion in heterogeneous fractures

Bill Dershowitz, Dawn Shuttle, Kate Klise,
Nils Outters, Jan Hermanson
Golder Associates

December 2004

Keywords: Advection, Dispersion, Diffusion, Modeling, Processes, Retention, Sorption, Tracer tests, Safety Assessment, Discrete Fracture Network.

Foreword

Dispersion within fractures is caused by a combination of classic hydrodynamic dispersion and the effect of roughness and heterogeneity within the planes. Many repository safety assessment approaches consider the possible effect of longitudinal dispersion, in the direction of flow, but neglect the effect of transverse dispersion perpendicular to the primary flow path direction. However, the processes of fracture heterogeneity which cause longitudinal dispersion are equally strong in producing transverse dispersion. This report evaluates the possible influence of transverse dispersion within fracture planes on conservative and sorbing tracer transport. The report considers a wide variety of fracture plane heterogeneity assumptions, at both experimental and performance assessment time scales. Results of fracture network simulations are compared against corresponding single pipe safety assessment simulations.

Abstract

Twenty stochastic realizations were implemented for each of four types of heterogeneous fracture spatial fields at the 20-meter scale. Parameters for each of these stochastic fields were adjusted to be consistent with observations of tracer breakthrough within the STT1b experiments at the Äspö TRUE-1 rock block. Simulations were then carried out to evaluate the effect of alternative transverse dispersion assumptions on tracer breakthrough at experimental and safety assessment time scales. These simulations were carried out using both particle tracking and Laplace Transform Galerkin methods. Results of these simulations were then compared against one-dimensional safety-assessment style simulations carried out using the GoldSim simulator, based on FARF31 transport assumptions.

Simulations carried out with transverse dispersions from 0.01 to 10 m show a clear difference in tracer breakthrough with transverse dispersion. This can also be seen in both breakthrough calculated using the LTG approach, and in particle transport visualizations. However, transverse dispersion's effect on tracer breakthrough and pathways statistics is frequently within the variability between stochastic realizations, and could therefore be considered a second order effect. The primary effect of increased transverse dispersion is in delaying and increasing the tail of breakthrough, such that simulations which ignore transverse dispersion effects produce early breakthrough and higher peaks than those which include this effect. The influence of transverse dispersivity on the range of transport behaviors is much less than the range of transmissivity within fractures would lead one to expect. This is due to power law relationships of transmissivity to aperture, and thus velocity, that dampen the effect of transmissivity on the velocity fields.

Sammanfattning

Tjugo stokastiska realiseringar genomfördes för vardera av fyra typer av heterogena sprickfält på skalan 20 meter. För varje stokastisk realisering anpassades parametrarna utifrån observationer av genombrottskurvor för spårämnen vid STT1b-experimenten inom projektet Äspö TRUE-1 berg-block. Simuleringar utfördes för att uppskatta effekten av alternativa antaganden gällande transversiell dispersion på genombrottskurvor för spårämnen, på tidsskalor som är relevanta dels för experiment och dels för ”Safety Assessment”. Simuleringarna genomfördes med både particle tracking- och Laplace Transform-Galerkin-metoder. Resultaten från simuleringarna jämfördes sedan med endimensionella simuleringar av ”Safety Assessment”-typ. De senare simuleringarna genomfördes med GoldSim, baserat på FARF31-antaganden för transport.

Simuleringar med en transversiell dispersion i intervallet 0,01–10 m visar på en tydlig effekt av den transversella dispersionen. Detta kan också observeras i de genombrottskurvor som beräknats med LTG-metoden och genom visualisering av partikeltransporten. Effekten av transversell dispersion på genombrottskurvorna och på statistiken för transportbanorna är dock ofta av samma storleksordning som skillnaderna mellan de olika stokastiska realiseringarna. Med utgångspunkt från denna observation kan effekten av transversell dispersion anses vara sekundär. Den dominerande effekten av ökad transversell dispersion är dels att en ökad ”fördröjning” av genombrottskurvan, och dels en förlängning av kurvans ”svans” – simuleringarna utan någon transversell dispersion ger ett snabbare genombrott med en högre ”topp” på genombrottskurvan, jämfört med de simuleringar där transversell dispersion beaktas.

Inverkan av transversell dispersion på transporten är mycket mindre än vad som kan förväntas utifrån det breda transmissivitetsintervall som är förknippat med sprickor. Detta beror på det exponentiella förhållandet mellan transmissivitet och spricköppning (och därmed flödeshastigheten), vilket minskar effekten av transmissiviteten på hastighetsfältet.

Executive summary

Objectives

This report evaluates the significance of transverse dispersion processes for solute transport in a single fracture. Transverse dispersion is a potentially significant process because it increases the fracture surface area available for sorptive and diffusive properties, and has the potential to transport solute between what would otherwise be distinctive, streamline pathways. Transverse dispersion processes are generally ignored in one-dimensional repository performance assessment approaches.

This report provides an initial assessment of the magnitude of transverse dispersion effect in a single heterogeneous fracture on repository safety assessment. This study builds on a previous report /Outters et al. 2003/ which considered the network effects on transport dispersion including streamline routing and mixing at fracture intersections.

Simulations

The project uses FracMan software /Dershowitz et al. 2003/. This platform has been extensively used by SKB in other projects. FracMan software is designed to generate and analyze DFN's as well as to compute fluid flow in DFN's with the MAFIC Finite element method (FEM) code /Miller et al. 2002/. Solute transport was modeled using the particle tracking inside MAFIC, the 2-D Laplace Transform Galerkin inside PAWorks/LTG, and the 1-D Laplace Transform approach designed to replicate FARF31 /Norman and Kjellbert, 1990/ inside GoldSim /Miller and Kossik, 2002/.

The study reported here focuses on a single, 20-meter scale discrete fracture, with simplified boundary conditions intended to represent the position of this fracture within a fracture network. The range of assumptions made regarding fracture heterogeneity were as follows (Figures 2-1 through 2-5):

- Base case, Heterogeneous fracture, geostatistical field, correlation length 0.01 m (Figure 2-1).
- Case 1a, Homogeneous fracture, transmissivity = $5\times10^{-7}m^2/s$.
- Case 1b, Heterogeneous fracture, non-channeled geostatistical field correlation length 5 m (Figure 2-2).
- Case 1c, Heterogeneous fracture, channeled, anisotropic geostatistical field (Figure 2-3).
- Case 1d, Heterogeneous fracture, fracture intersection zone (FIZ) permeability enhanced (Figure 2-4).
- Case 5, Simple channelized fracture (Figure 2-5).

The transport properties of these fractures were adjusted to be consistent with the STT1b tracer transport experiment of the Äspö TRUE-1 in situ transport experiment.

For most of the cases simulated, transport aperture, e (m), was correlated to transmissivity, T (m^2/s), according to $e = 15\times T^{0.6}$. This relationship was established based on the results of simulation of STT1b tracer experiments /Marschall and Elert, 2003/ inside the Base case stochastic field fracture. For Case 5, a range of alternative relationships between aperture and transmissivity were considered.

Values for transverse dispersion were simulated between 0.01 m and 10 m. The value of 0.01 m represents a "typical" value of transverse dispersion from the literature, estimated as approximately 1% of the travel distance. The value of 10 is extreme, and is approximately ten times greater than the upper bound realistic value of 1 m (10% of the travel distance).

Simulations were carried out primarily for a basically one-dimensional flow field in the plane of the fracture. This boundary condition was implemented by applying no flow boundaries on the north and south edges of the fracture, and heads of 0.5 m and 0 m to the west and east edges of the fracture respectively.

Results

The breakthrough statistics t_5, t_{50}, and t_{95}, correspond to the time for 5%, 50%, and 95% mass recovery respectively. These results are summarized in Table 0-1 and Table 0-2. In these tables, the designations "L", "F," and "P" refer to Laplace Transform Galerkin (PAWorks) FARF31 Conceptual Model (GoldSim), and Particle Tracking (MAFIC) respectively. These results are based on a correlation between transmissivity and transport aperture et = 15 T0.6 For this correlation, and the range of spatial transmissivity fields considered in Case 1, changes in transverse dispersion did not produce a significant change in the mean conservative tracer breakthrough times, although it did somewhat decrease the standard deviation.

For the simple, channelized fracture considered in Case 5, this same aperture-transmissivity relationship also produced relatively small impacts of even large values of transverse dispersivity. However, when this channelized fracture is given a constant aperture the tracer breakthrough curves are much more strongly affected by transverse dispersivity, with t_{95} delayed by up to almost 50%. This is because when aperture is held constant, velocity varies directly with transmissivity, such that flow outside the high transmissivity channel is slower. However, even for these cases, the effect of transverse dispersivity in these single fracture studies was to increase transport times.

Studies of sorbing tracer transport (Case 3) produced results similar to those found with conservative tracers, in which the magnitude of changes in breakthrough statistics due to transverse dispersion was on the same order as the changes between stochastic realizations of the spatial fields. Similarly, simulations with larger tracer release area (Case 2) also produced variations due to transverse dispersion within the range defined by stochastic realizations.

Table 0-1. Statistical summary of breakthrough times, Base case and Case 1, LTG and GoldSim simulations.

Case	Transverse Dispersion	t_5 (μ,σ)	t_{50} (μ,σ)	t_{95} (μ,σ)
0–L	(A) 0.1 m	1,168.1, 79.3	2,369.4, 139.7	4,512.4, 219.5
	(B) 1 m	1,167.0, 45.7	2,383.5, 80.1	4,536.1, 112.8
	(C) 10 m	1,148.0, 23.3	2.377.0, 38.1	4,542.8, 58.4
0–F	–	990	1,970	3,818
1a–L	(A) 0.1 m	897.7	1,845.1	3,596.4
	(B) 1 m	898.6	1,845.6	3,597.4
	(C) 10 m	899.4	1,846.8	3,598.9

Case	Transverse Dispersion	t_5 (μ,σ)	t_{50} (μ,σ)	t_{95} (μ,σ)
1b–L	(A) 0.1 m	1,134.5, 72.6	2,309.3, 121.5	4,383.4, 178.4
	(B) 1 m	1,129.1, 22.3	2,299.2, 38.3	4,367.5, 59.1
	(C) 10 m	1,118.3, 16.7	2,305.0, 31.7	4,409.2, 55.3
1c–L	(A) 0.1 m	882.3, 358.1	1,757.7, 743.7	3,520.3, 1,495.1
	(B) 1 m	778.6, 170.7	1,609.9, 369.7	3,391.4, 772.6
	(C) 10 m	753.5, 153.0	1,584.1, 331.6	3,240.1, 607.2
1d–L	(A) 0.1 m	8,909.9, 1,231.6	Na	Na
	(B) 1 m	8,221.5, 958.9	Na	Na
	(C) 10 m	8,503.3, 71.7	Na	Na

Table 0-2. Statistical summary of tracer retention statistics, Base case and Case 1, particle tracking and GoldSim simulations.

Case	Transverse dispersion	Q (μ,σ)	1/v (μ,σ)	1/bv (μ,σ)	β (μ,σ)	τ (μ,σ)
0–P	(A) 0.1 m	1.5×10^{-8}, 8.3×10^{-6}	2.4×10^{5}, 3.3×10^{4}	2.4×10^{11}, 2.6×10^{13}	2.6×10^{9}, 5.5×10^{8}	5.2×10^{6}, 8.1×10^{5}
	(B) 1 m	1.8×10^{-8}, 1.5×10^{-5}	2.2×10^{5}, 4.4×10^{4}	5.8×10^{11}, 4.6×10^{13}	3.0×10^{9}, 7.3×10^{8}	5.9×10^{6}, 1.3×10^{5}
	(C) 10 m	2.2×10^{-8}, 1.8×10^{-5}	2.3×10^{5}, 5.7×10^{4}	3.9×10^{11}, 2.1×10^{13}	3.2×10^{9}, 9.2×10^{8}	6.4×10^{6}, 1.7×10^{5}
0–F	–	6.25×10^{-10}	1.99×10^{5}	1.6×10^{8}	3.2×10^{9}	3.98×10^{6}
1a–P	(A) 0.1 m	1.7×10^{-8}, 1.2×10^{-7}	2.0×10^{5}, 6.3×10^{4}	3.0×10^{12}, 1.7×10^{14}	1.7×10^{9}, 5.6×10^{8}	4.2×10^{6}, 1.4×10^{6}
	(B) 1 m	1.9×10^{-8}, 1.6×10^{-7}	1.9×10^{5}, 7.1×10^{4}	2.5×10^{12}, 1.1×10^{14}	2.0×10^{9}, 7.9×10^{8}	5.1×10^{6}, 2.0×10^{6}
	(C) 10 m	2.1×10^{-8}, 2.5×10^{-7}	1.9×10^{5}, 9.2×10^{4}	1.3×10^{12}, 6.1×10^{13}	2.2×10^{9}, 1.1×10^{9}	5.4×10^{6}, 2.6×10^{6}
1b–P	(A) 0.1 m	1.5×10^{-8}, 9.5×10^{-6}	2.3×10^{5}, 3.1×10^{4}	4.3×10^{11}, 2.8×10^{13}	2.7×10^{9}, 5.2×10^{8}	5.2×10^{6}, 7.6×10^{5}
	(B) 1 m	1.8×10^{-8},1.8×10^{-5}	2.1×10^{5}, 4.5×10^{4}	7.7×10^{11}, 4.7×10^{13}	2.9×10^{9}, 7.3×10^{8}	5.6×10^{6}, 1.3×10^{6}
	(C) 10 m	2.4×10^{-8},1.9×10^{-5}	2.2×10^{5}, 5.7×10^{4}	5.6×10^{11}, 3.8×10^{13}	3.2×10^{9}, 9.2×10^{8}	6.0×10^{6}, 1.7×10^{6}
1c–P	(A) 0.1 m	2.5×10^{-8}, 5.0×10^{-6}	2.0×10^{5}, 3.4×10^{4}	2.5×10^{11}, 1.7×10^{13}	1.6×10^{9}, 7.3×10^{8}	4.4×10^{6}, 8.3×10^{5}
	(B) 1 m	3.1×10^{-8}, 8.4×10^{-6}	1.8×10^{5}, 5.2×10^{4}	5.0×10^{11}, 3.2×10^{13}	1.6×10^{9}, 6.6×10^{8}	4.9×10^{6}, 1.5×10^{6}
	(C) 10 m	5.0×10^{-8}, 1.3×10^{-5}	1.9×10^{5}, 7.3×10^{4}	3.6×10^{11}, 2.4×10^{13}	1.9×10^{9}, 8.6×10^{8}	5.4×10^{6}, 2.1×10^{6}
1d–P	(A) 0.1 m	1.4×10^{-8}, 7.6×10^{-6}	3.6×10^{-5}, 7.5×10^{4}	4.1×10^{11}, 3.5×10^{13}	1.3×10^{10}, 5.7×10^{9}	8.6×10^{6}, 1.9×10^{6}
	(B) 1 m	1.5×10^{-8}, 1.3×10^{-5}	3.5×10^{-5}, 9.3×10^{4}	3.2×10^{12}, 2.9×10^{14}	1.4×10^{10}, 5.6×10^{9}	9.9×10^{6}, 2.7×10^{6}
	(C) 10 m	1.5×10^{-8}, 1.5×10^{-5}	3.7×10^{-5}, 1.2×10^{-5}	2.1×10^{12}, 1.8×10^{14}	1.5×10^{10}, 6.5×10^{9}	1.1×10^{7}, 3.5×10^{6}

The influence of transverse dispersion on breakthrough and recovery times is much smaller than the variability of transmissivity would lead one to expect. This is due to the assumed power law relationship of transmissivity to aperture. In this relationships, the ratio of transmissivity to aperture varies less than the transmissivity. Since local velocity varies with this ratio, rather than directly with transmissivity, the effect of transverse dispersion, which moves tracer mass to areas of lower transmissivity, is significantly reduced. Hence different realizations of the same stochastic field do not exhibit larger variability in transport behavior. Larger variability of transverse dispersion behavior could be observed if the range of the transmissivity fields is greater than that used in this exercise or if transmissivity and aperture (and hence velocity) are weakly correlated. This would seem unlikely for simple open fractures, but more complex relationships between transmissivity and apparent aperture could exist for conducting features with complex internal structures.

Contents

1 Introduction

1.1 Background

Streamline approaches for solute transport in fractured rock assume that solute follows distinct, unique pathways with constant properties through the geosphere all the way from the waste form to the biosphere. While this assumption is convenient for most mathematical models used in performance assessment, there are three important mechanisms that interfere with streamline pathways in nature:

- transverse dispersion, according to which a certain percentage of solute mass moves perpendicular to the average flow direction at any location in the network,
- network mixing, according to which a certain percentage of solute mass moves into each branch,
- changes in groundwater chemistry and boundary conditions both in time and in space over the distance from the waste form to the biosphere.

This report addresses the first of theses mechanisms, using discrete feature network (DFN) modeling. The report provides an initial assessment of the magnitude of transverse dispersion effect in a single heterogeneous fracture on repository safety assessment. This study builds on a previous report /Outters et al. 2003/, which considered the network effects on transport dispersion including streamline routing and mixing at fracture intersections.

1.2 Purpose and objective

The purpose of this project is to understand the effect of transverse dispersion and heterogeneity on transport in fractured rock. To achieve this, this study focuses on a single, 20×20 meter discrete fracture from within a fracture network, using a broad range of assumptions about both heterogeneity and transverse dispersion.

Because one-dimensional transport approaches generally neglect transverse dispersion, the objective of this project is to provide a quantitative and graphical comparison of solute transport with and without transverse dispersion. To provide a broad range of applicability, the magnitude of transverse dispersivity is varied from 0 to 20 meters, on the fracture surfaces that have a variety of heterogeneous, homogeneous, and anisotropic properties, along with varying degrees of channelization. Sensitivity studies are carried out for a range of assumptions regarding dispersion processes and results are compared to those which would be obtained by SKB's FARF31 pipe transport code.

Based on the simulations carried out, this report provides a discussion of the implications of neglecting transverse dispersion in the use of stream tube (pipe transport) approaches.

2 Modelling strategy

The project uses FracMan software /Dershowitz et al. 2003/. This platform has been extensively used by SKB in other projects, including studies of solute transport in fractured rock /e.g. Outters and Shuttle, 2000/. FracMan software is designed to generate and analyze DFN's as well as to compute fluid flow in DFN with the MAFIC Finite element method (FEM) code /Miller et al. 2002/.

2.1 Scope

While transport in fractured rock is controlled by fracture networks, the fundamental building block for these networks is the individual fracture. In order to make quantitative conclusions about the role of transverse dispersion in solute transport, it is therefore necessary to first focus on the effect of transverse dispersion in single fractures.

2.1.1 Fractures studied

This study includes a range of heterogeneous fields on discrete fracture surfaces in order to evaluate the range of applicability. Figure 2-1 through Figure 2-5 illustrate the heterogeneous fractures implemented for this study:

- Base case, heterogeneous fracture, geostatistical field, correlation length 0.01 m (Figure 2-1).
- Case 1a, homogeneous fracture, transmissivity = $5\times10^{-7}m^2/s$.
- Case 1b, heterogeneous fracture, non-channeled geostatistical field correlation length 5 m (Figure 2-2).
- Case 1c, heterogeneous fracture, channeled, anisotropic geostatistical field (Figure 2-3).
- Case 1d, heterogeneous fracture, fracture intersection zone (FIZ) permeability enhanced (Figure 2-4).
- Case 5, simple channelized fracture (Figure 2-5).

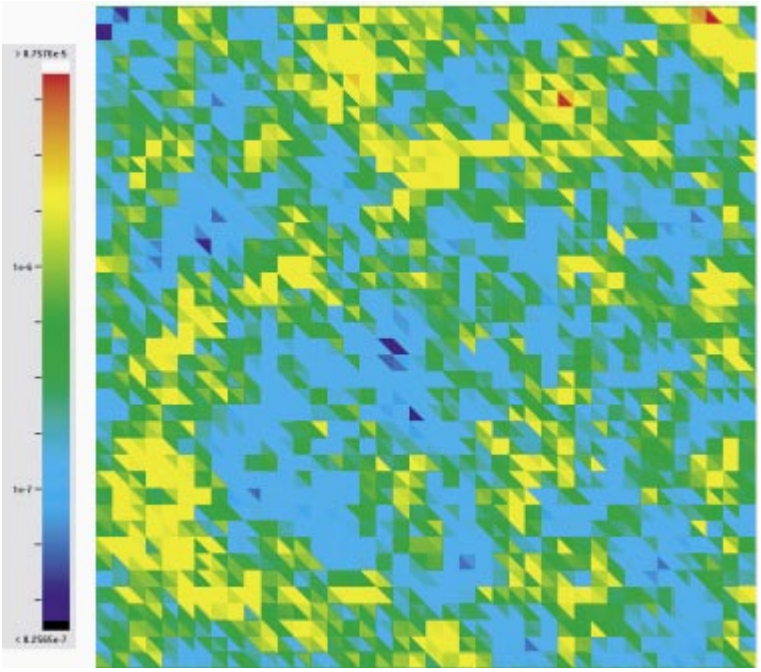

Figure 2-1. *Base case, heterogeneous fracture, geostatistical field, correlation length 0.01 m.*

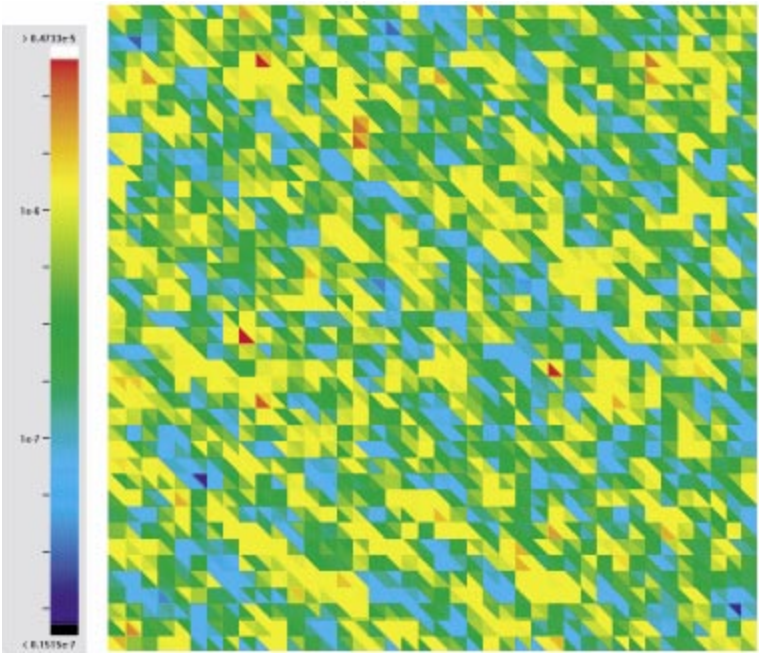

Figure 2-2. *Case 1b, heterogeneous fracture, non-channeled geostatistical field correlation length 5 m.*

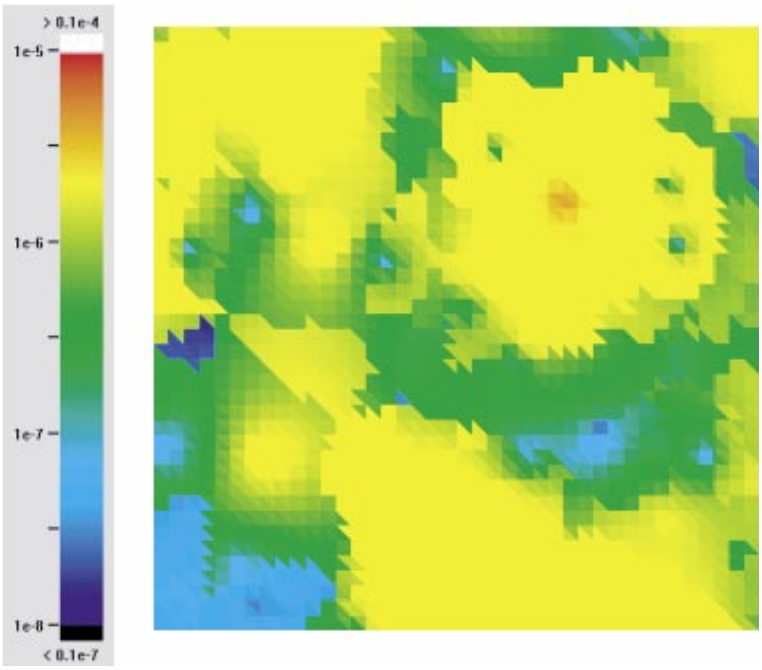

Figure 2-3. *Case 1c, heterogeneous fracture, channeled, anisotropic geostatistical field.*

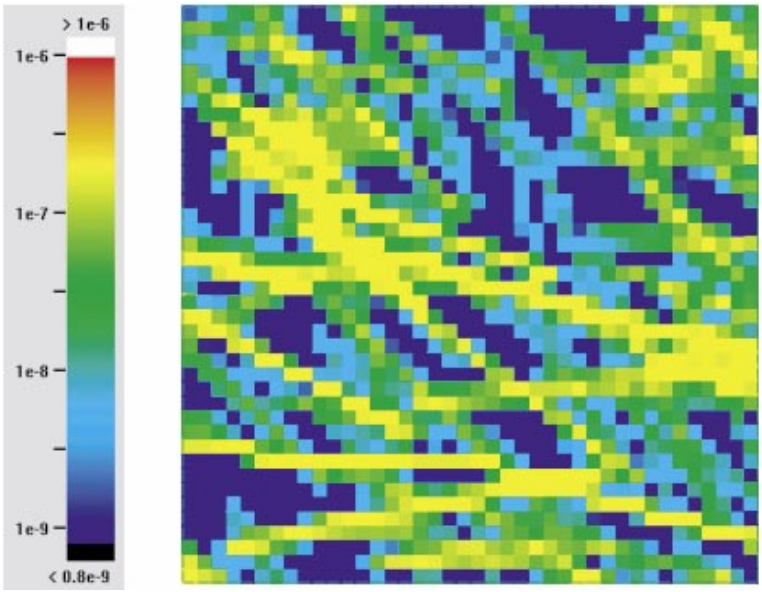

Figure 2-4. *Case 1d, heterogeneous fracture, Fracture Intersection Zone (FIZ) permeability enhanced.*

The fracture intersection zone model was generated by using the TRUE-1 rock block DFN of /Dershowitz et al. 2001/. The parameters for this DFN are provided in Table 2-2. For the stochastic field of Case 1d, the transmissivity of each element was calculated from the fracture intersections in the cell according to the formula,

$$T = \sum T_f \, L_i \; / \sum L_i$$

Where T_f is the transmissivity of fracture i intersecting that cell, and L_i is the trace length in the cell of fracture i.

This equation is based on the approach of /Oda, 1984/, which is referred to as the "Oda Tensor" approach. This approach assumes that the maximum transmissivity will be locations containing the greatest length of fracture intersections. Since the discretization is crude relative to the detailed geometry of the fracture intersections, the actual pathways formed by the fracture intersections are only represented approximately by this approach.

Case 5 was defined after the completion of Cases 1 through 4, in order to better understand the physics behind the results observed. Case 5 (Figure 2-5) combines a simple linear flow channel with zones to the side which can be either stagnant or advective, depending on the assigned properties and boundary conditions.

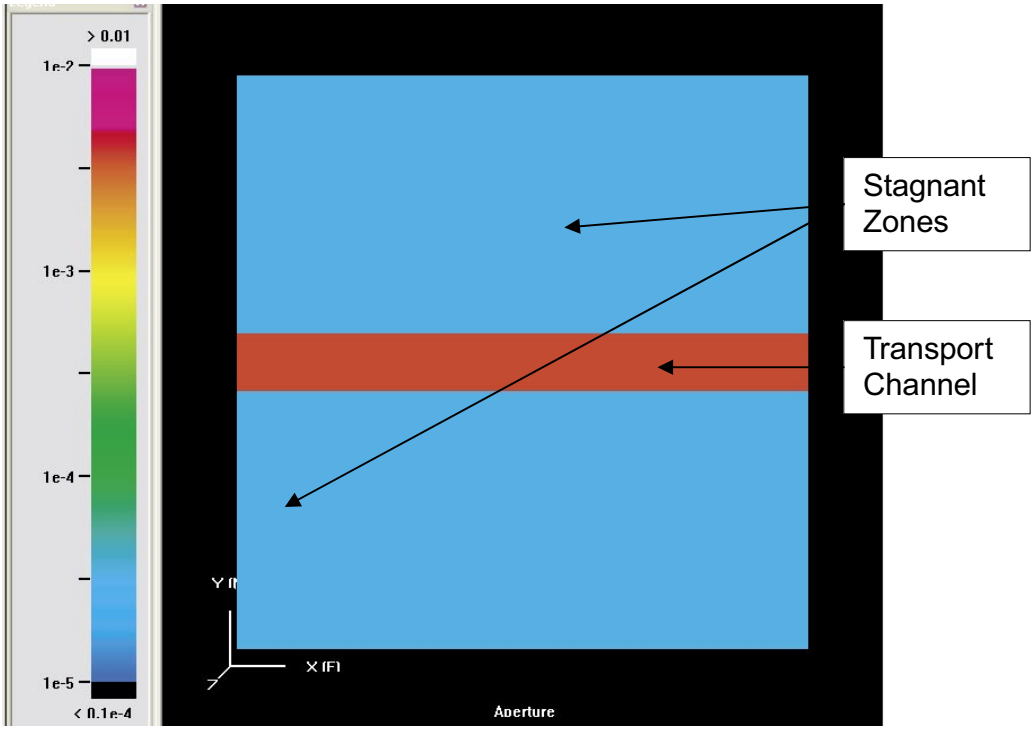

Figure 2-5. *Case 5, simple channelized fracture.*

2.1.2 Simulation approaches

The basic simulation approach used in this study is particle tracking. In particle tracking, the flow field in the fracture is solved using finite elements based on the applied boundary condition. Particles are then released from a number of elements on the edge of the fracture, and tracked through the flow field to the down-gradient side of the fracture. In the MAFIC implementation of particle tracking, particles are instantaneously translated with in each time step laterally and transverse based on a normal distribution defined from the dispersion term in the advection dispersion equation /Miller et al. 2002/.

Two alternative approaches for solute transport are used in this project, the Laplace Transform Galerkin (LTG) method /Sudicky and McLaren, 1992/, and the FARF31 /Norman and Kjellbert, 1990/ pipe transport approach. The Laplace Transform Galerkin method solves the solute transport equation for the triangular finite elements in Laplace space. The transport equation solved is given in /Dershowitz et al. 2002/. The transport solution includes the effects of advection, longitudinal and transverse dispersion, sorption, decay, diffusion to immobile zones, and sorption in immobile zones. LTG is solving essentially the same case treated by particle tracking, since concentrations are calculated at each element within the finite element grid, based on the flow field calculated using the finite element method. In LTG, both transverse and longitudinal dispersion are solved as part of the underlying partial differential equation.

The FARF31 approach utilizes a single, homogeneous pipe from the radionuclide source to the environmental release. Consequently, it cannot consider heterogeneity along the transport pathway, or the effects of 2D or 3D flow. The breakthrough curves from the FARF31 approach can be compared directly to those obtained by the LTG and particle tracking approaches. However, the FARF31 result does not provide any information about the transport process between the source and the release. For this study, FARF31 transport is approximated in GoldSim /Miller and Kossik, 2002/.

2.1.3 Boundary conditions

This study uses a gradient of 2.5% for the Base case, from the upgradient (0.5 m head) to downgradient (0 m head) sides of the fracture. For long-term (1 million year) simulations, the study uses a gradient of 0.00025% over the fracture, from the upgradient (0.00005 m head) to downgradient (0 m head) sides of the fracture.

For the Base case, the solute is injected to the model over a length of 0.05 m at the center of the upgradient edge of the fracture. This is designed to provide a source which represents solute entering the modeled fracture from an intersecting fracture near to a leaking waste canister. In Case 3, this source considers alternative injection lengths of 0.1 m and 10 m to check the influence of source size on results. It is anticipated that the effect of transverse dispersion would be greatest for the smaller source, and smallest for the larger source.

2.1.4 Output formats

Solute transport results are compared in terms of

- breakthrough curves,
- statistics of tracer breakthrough (t_5, t_{50}, t_{95} times for 5%, 50%, and 95% of tracer breakthrough),
- spatial patterns of breakthrough to the downstream face,
- distribution of solute residence time $f(\tau)$,

- distribution of flux Q_i, Eulerian velocity v_i, inverse Lagrangian velocity $1/v_i$, and weighted inverse Lagrangian velocity $1/(b_i v_i)$, where Q_i is flux (m^3/s), b_i is aperture (m), and v_i is velocity (m/s),
- distribution of normalized transport retention factor f(β).

The Eulerian velocity v is the groundwater velocity as measured in the global coordinate system along the pathway. The inverse of the Lagrangian velocity $1/v_i$ in the local coordinate system is calculated along the particle pathway as the residence time divided by the path length. The weighted inverse Lagrangian velocity $1/(b_i v_i)$ are weighted by the aperture of each element traversed by the particles.

The distribution f(β) is used in the /Cvetkovic et al. 1999/ analytical solution for solute transport, and controls the rate of diffusion and surface sorption. In this study, β is calculated as

$$\beta_j = \sum_{i=1}^{n} \frac{l_i}{v_i \cdot b_i}$$

where l_i is the distance traveled by the particle j in the element, v_i is the Lagrangian velocity of the particle j in the element i where a particle is located at a given time, and b_i is the half aperture of the element i.

3 Simulations

Fourteen cases were simulated to understand the effect of transverse dispersion on solute transport in a single fracture. For the first eleven cases, variant simulations were carried out using particle tracking, LTG (2D), and GoldSim (1D). Three values of transverse dispersion were considered for each of these cases, 0.01 m, 1 m, and 10 m. As a percentage of the 20-m travel length, these are 0.05%, 5%, and 50%, respectively. For reference, EPM methods typically assume on the order of 1% transverse dispersion. The final three cases were simulated using a deterministic, channelized fracture, with a more limited range of assumptions, focusing on understanding the physical processes controlling the significance of transverse dispersion.

The simulations carried out are numbered as listed in Table 3-1. Each of the simulations described in Table 3-1 was carried out as 20 Monte Carlo realizations, with the exception of homogeneous/uncorrelated case, FARF31/GoldSim simulations, and the simple channel case, for which only a single realization was considered.

Table 3-1. Simulations carried out.

Case		Variants	Transverse dispersion
0	Base case heterogeneous, correlated, channeled	0–P particle tracking 0–L LTG 0–F FARF31 (GoldSim)	(A) 0.1 m (B) 1 m (C) 10 m
1a	Homogeneous, uncorrelated	1a–P particle tracking 1a–L LTG	(A) 0.1 m (B) 1 m (C) 10 m
1b	Heterogeneous, correlated, non-channeled	1b–P particle tracking 1b–L LTG	(A) 0.1 m (B) 1 m (C) 10 m
1c	Heterogeneous, correlated, channeled, anisotropic	1c–P particle tracking 1c–L LTG	(A) 0.1 m (B) 1 m (C) 10 m
1d	Fracture Intersection Zone	1d–P particle tracking 1d–L LTG	(A) 0.1 m (B) 1 m (C) 10 m
2a	Source 1 m	2a–P particle tracking 2a–L LTG	(A) 0.1 m (B) 1 m (C) 10 m
2b	Source 5 m	2b–P particle tracking 2b–L LTG	(A) 0.1 m (B) 1 m (C) 10 m
2c	Source 10 m	2c–P particle tracking 2c–L LTG	(A) 0.1 m (B) 1 m (C) 10 m
3a	Immobile zone no immobile zones	3a–L LTG 3a–F FARF31 (GoldSim)	(A) 0.1 m (B) 1 m (C) 10 m
3b	Immobile zone Maximized immobile zones	3b L LTG 3b–F FARF31 (GoldSim)	(A) 0.1 m (B) 1 m (C) 10 m
4a	Million years reduced gradient	4–L LTG 4–F FARF31 (LTG)	(A) 0.1 m (B) 1 m (C) 10 m

Case		Variants	Transverse dispersion
5a	Simple deterministic channel – aperture correlated to transmissivity	5a–P particle tracking 5a–L LTG	(A) 0.01 m (B) 1 m
5b	Simple deterministic channel – aperture constant on entire fracture	5b–P particle tracking 5b–L LTG	(A) 0.01 m (B) 1 m
5c	Simple deterministic channel – aperture constant on entire fracture, no-flow boundary on “stagnant zones”	5c–P particle tracking 5c–L LTG	(A) 0.01 m (B) 1 m

3.1 STT1b calibration

The first stage of this study was designed to ensure that the different stochastic fields could be compared directly. To achieve this, the correlation between transport aperture and transmissivity for each of the stochastic fields was adjusted to obtain a reasonable match to the STT1b tracer test /Marschall and Elert, 2002/. The calibration was done once for each case, and subsequent realizations of that field were assumed to follow the same parameters. These simulations are carried out using LTG.

For consistency with FARF31, a solute transport assumed a single immobile zone for the fracture. This is a significant assumption, and obviates study of the important effects of multiple immobile zones /see e.g. Dershowitz et al. 2001/. The single immobile zone is assumed to surround the fracture on both sides.

Solute transport parameter assumptions are summarized in Table 3-2. Table 3-2 provides the values obtain from calibrating the Base case. These values were also applied to Case 1a through 1d.

Table 3-2. Solute transport parameters.

Parameters	Parameter value
Transport aperture (m)	$e = 15\ T^{0.6}$
Longitudinal dispersion	2 m
Immobile zone porosity	2%
Immobile zone diffusion thickness	50 mm
Tortuosity	0.5
Fraction of perimeter available for diffusion	100%
Density	2,700 kg/m^3
Sorption Kd	HTO = 0 m^3/kg Cs = 8.0e–4 m^3/kg Na = 1.4e–6 m^3/kg
Diffusion coefficient (Free water)	HTO = 2.4e–9 m^2/s Cs = 2.02e–9 m^2/s Na = 1.33e–9 m^2/s

Figure 3-1 and Figure 3-2 show the matches against STT1b for the first realizations of the fracture heterogeneity Base case model. Figure 3-3 and Figure 3-4 contain results from fracture heterogeneity of case 1a, 1b, 1c, and 1d. These matches were obtained for the conservative tracers HTO and I–131.

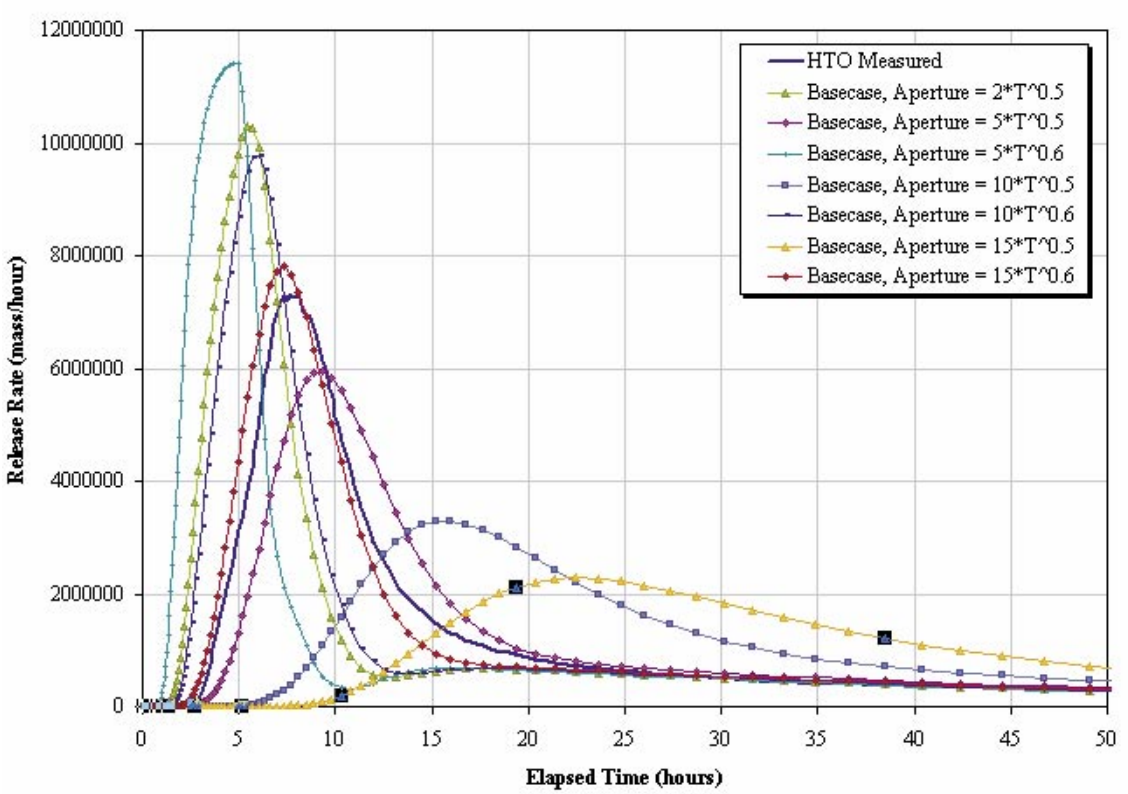

Figure 3-1. *Calibration to STT1b, Base case, HTO, LTG.*

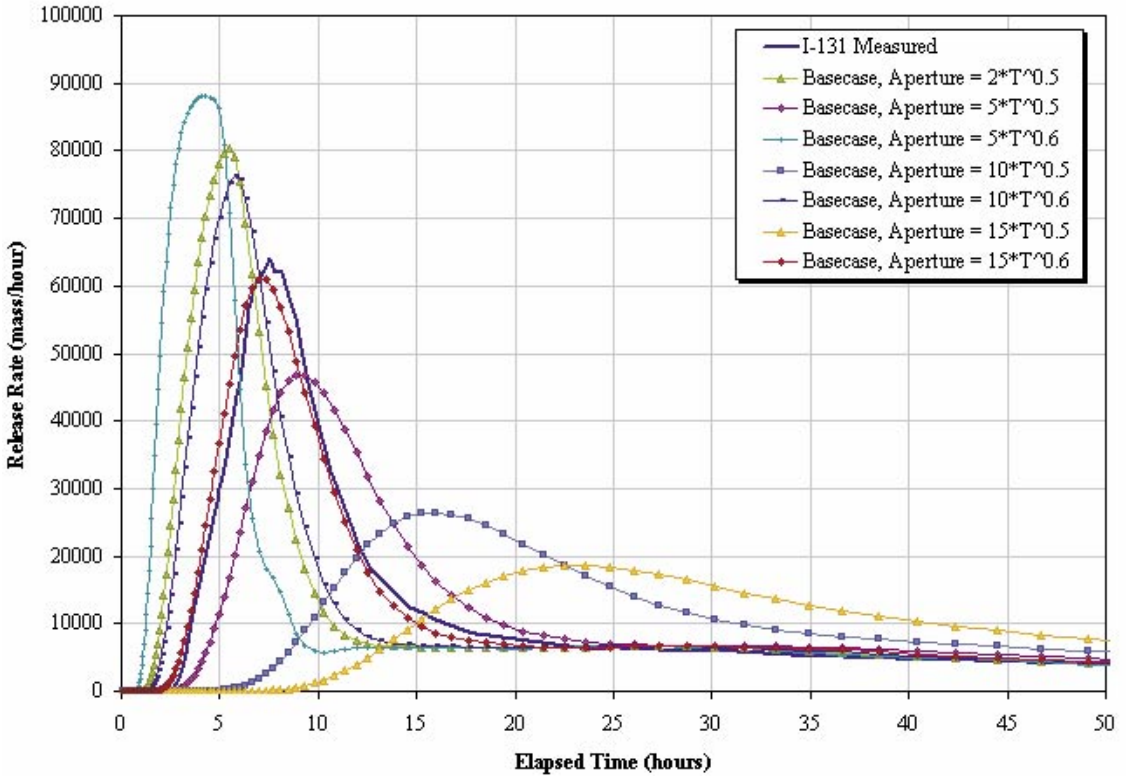

Figure 3-2. *Calibration to STT1b, Base case, I–131, LTG.*

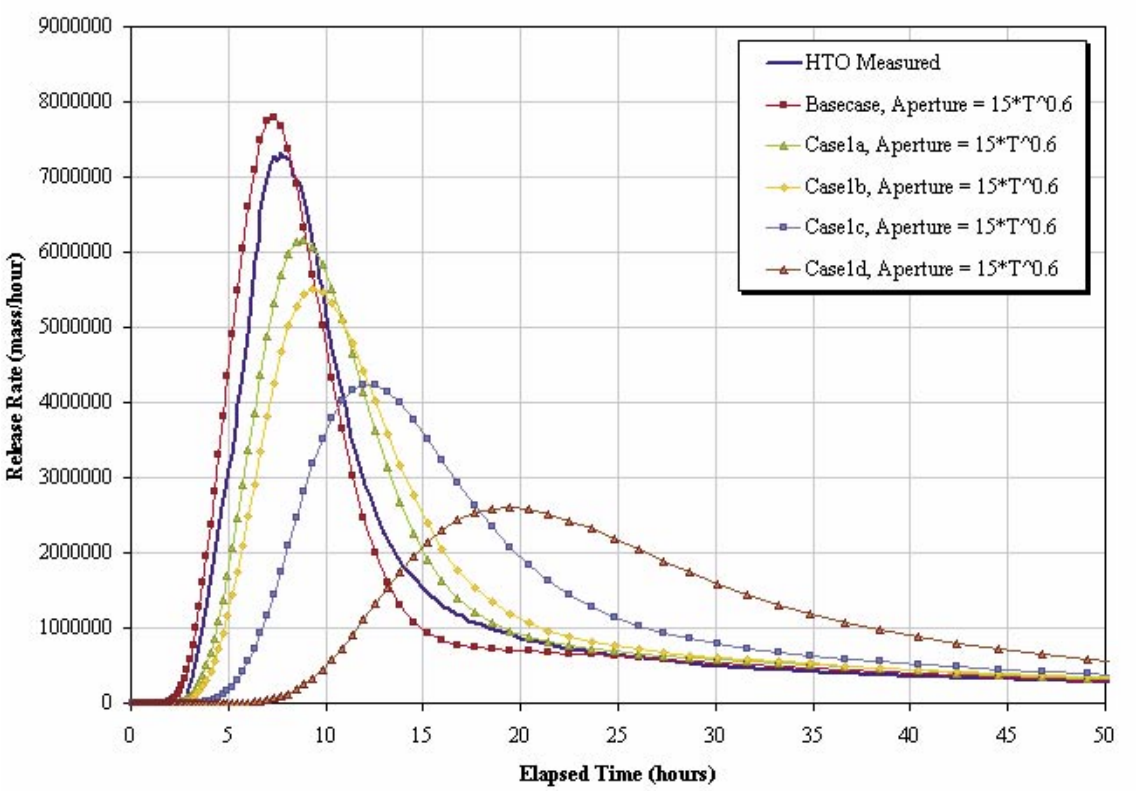

Figure 3-3. *STT1b Base case aperture calibration. Simulations with Case 1a, Case 1b, Case 1c, and Case 1d transmissivity fields, HTO, LTG.*

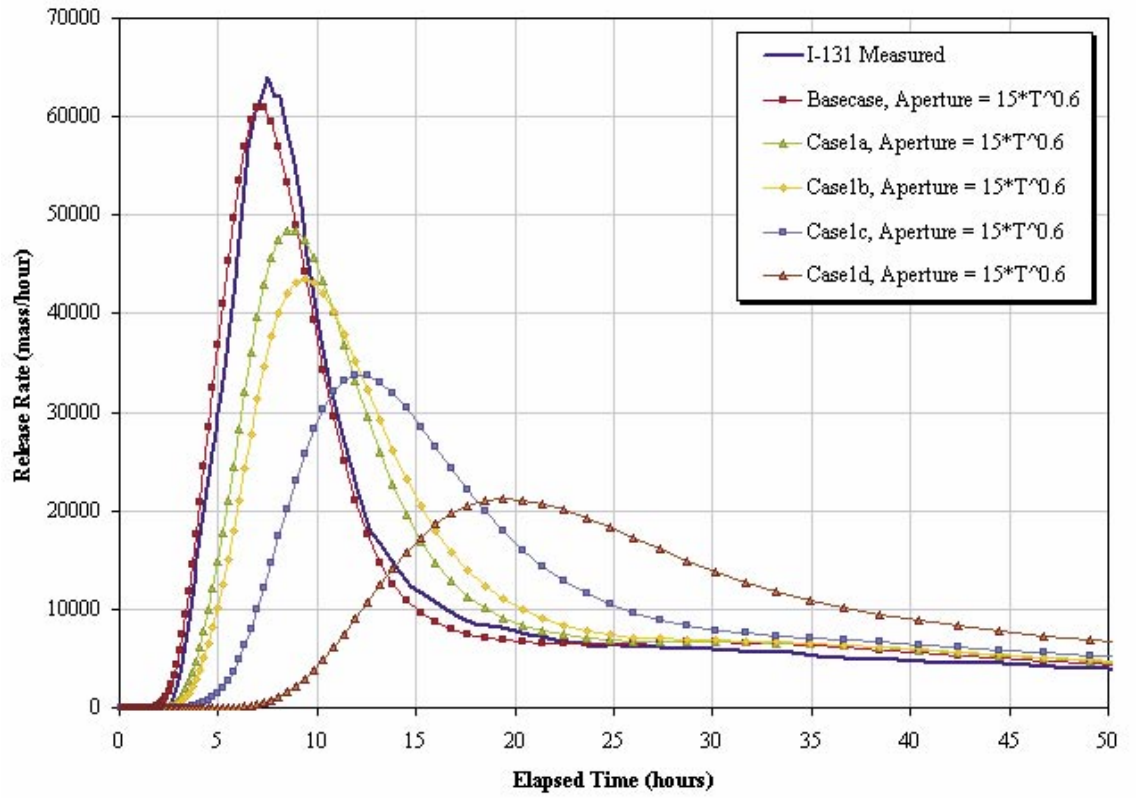

Figure 3-4. *STT1b Base case aperture calibration. Simulations with Case 1a, Case 1b, Case 1c, and Case 1d transmissivity fields, I–131, LTG.*

3.2 Base case and alternative transmissivity fields

The major question addressed by this study is how strong an effect transverse dispersion has on transport in fractures. Statistical results for the simulations of the Base case and Case 1a, b, c, and d are summarized in Table 3-3 and Table 3-4.

The effect of increased transverse dispersion can be seen in the reduced variability between realizations, as indicated by the standard deviation in Table 3-3. The standard deviation for t_5, t_{50}, and t_{95} decreases consistently and systematically with increase α_T. The change in the mean t_5, t_{50}, and t_{95} with α_T is however, insignificant. Changes in the distribution of β, $1/\nu$ $1/b\nu$, and τ shown in Table 3-4 are more sensitive.

Natural variation in transport between fractures is illustrated by comparing Monte Carlo realizations. Figure 3-5 presents a comparison of the difference between multiple realizations as compared to differences due to values of transverse dispersion between 0.1 m and 10 m. The effect of multiple realizations is comparable to the difference due to transverse dispersion.

Figure 3-6 illustrates the distribution of residence times while varying transverse dispersion. Although there are clear differences, there is not a clear systematic trend. Further, the difference between Base case and the Case 1b Stochastic Field is comparable to the difference due to difference in α_T.

For the Base case $\alpha_T = 0.01$ m results in an increase in shorter travel times. For case 1b, $\alpha_T = 1.0$ m corresponds to the greatest percentage of shorter travel times.

A similar effect can be seen in the distribution of β shown in Figure 3-7. Transverse dispersion α_T clearly changes the distribution of β. However, the differences are comparable to those due to the change in stochastic field.

The mean effect expected from changes to transverse dispersion α_T is in the spatial distribution of breakthrough to the downstream edge of the fracture. This is illustrated in Figure 3-8 through Figure 3-11. Clearly increased transverse dispersion increases the spatial scatter in solute transport. While this would be expected to influence breakthrough curves, the results shown in Figure 3-5 do not show a strong influence.

Table 3-3. Statistical summary Base case and Case 1, LTG simulations.

Case	Transverse dispersion	t_5 (μ,σ)	t_{50} (μ,σ)	t_{95} (μ,σ)
0–L	(A) 0.1 m	1,168.1, 79.3	2,369.4, 139.7	4,512.4, 219.5
	(B) 1 m	1,167.0, 45.7	2,383.5, 80.1	4,536.1, 112.8
	(C) 10 m	1,148.0, 23.3	2,377.0, 38.1	4,542.8, 58.4
0–F	–	990	1,970	3,818
1a–L	(A) 0.1 m	897.7	1,845.1	3,596.4
	(B) 1 m	898.6	1,845.6	3,597.4
	(C) 10 m	899.4	1,846.8	3,598.9
1b–L	(A) 0.1 m	1,134.5, 72.6	2,309.3, 121.5	4,383.4, 178.4
	(B) 1 m	1,129.1, 22.3	2,299.2, 38.3	4,367.5, 59.1
	(C) 10 m	1,118.3, 16.7	2,305.0, 31.7	4,409.2, 55.3
1c–L	(A) 0.1 m	882.3, 358.1	1,757.7, 743.7	3,520.3, 1,495.1
	(B) 1 m	778.6, 170.7	1,609.9, 369.7	3,391.4, 772.6
	(C) 10 m	753.5, 153.0	1,584.1, 331.6	3,240.1, 607.2

Case	Transverse dispersion	t_5 (μ,σ)	t_{50} (μ,σ)	t_{95} (μ,σ)
1d–L	(A) 0.1 m	8,909.9, 1,231.6	Na	Na
	(B) 1 m	8,221.5, 958.9	Na	Na
	(C) 10 m	8,503.3, 71.7	Na	Na

Table 3-4. Statistical summary, Base case and Case 1, particle tracking simulations.

Case	Transverse dispersion	Q (μ,σ)	1/v (μ,σ)	1/bv (μ,σ)	β (μ,σ)	τ (μ,σ)
0–P	(A) 0.1 m	1.5×10^{-8}, 8.3×10^{-6}	2.4×10^{5}, 3.3×10^{4}	2.4×10^{11}, 2.6×10^{13}	2.6×10^{9}, 5.5×10^{8}	5.2×10^{6}, 8.1×10^{5}
	(B) 1 m	1.8×10^{-8}, 1.5×10^{-5}	2.2×10^{5}, 4.4×10^{4}	5.8×10^{11}, 4.6×10^{13}	3.0×10^{9}, 7.3×10^{8}	5.9×10^{6}, 1.3×10^{5}
	(C) 10 m	2.2×10^{-8}, 1.8×10^{-5}	2.3×10^{5}, 5.7×10^{4}	3.9×10^{11}, 2.1×10^{13}	3.2×10^{9}, 9.2×10^{8}	6.4×10^{6}, 1.7×10^{5}
0–F	–	6.25×10^{-10}	1.99×10^{5}	1.6×10^{8}	3.2×10^{9}	3.98×10^{6}
1a–P	(A) 0.1 m	1.7×10^{-8}, 1.2×10^{-7}	2.0×10^{5}, 6.3×10^{4}	3.0×10^{12}, 1.7×10^{14}	1.7×10^{9}, 5.6×10^{8}	4.2×10^{6}, 1.4×10^{6}
	(B) 1 m	1.9×10^{-8}, 1.6×10^{-7}	1.9×10^{5}, 7.1×10^{4}	2.5×10^{12}, 1.1×10^{14}	2.0×10^{9}, 7.9×10^{8}	5.1×10^{6}, 2.0×10^{6}
	(C) 10 m	2.1×10^{-8}, 2.5×10^{-7}	1.9×10^{5}, 9.2×10^{4}	1.3×10^{12}, 6.1×10^{13}	2.2×10^{9}, 1.1×10^{9}	5.4×10^{6}, 2.6×10^{6}
1b–P	(A) 0.1 m	1.5×10^{-8}, 9.5×10^{-6}	2.3×10^{5}, 3.1×10^{4}	4.3×10^{11}, 2.8×10^{13}	2.7×10^{9}, 5.2×10^{8}	5.2×10^{6}, 7.6×10^{5}
	(B) 1 m	1.8×10^{-8},1.8×10^{-5}	2.1×10^{5}, 4.5×10^{4}	7.7×10^{11}, 4.7×10^{13}	2.9×10^{9}, 7.3×10^{8}	5.6×10^{6}, 1.3×10^{6}
	(C) 10 m	2.4×10^{-8},1.9×10^{-5}	2.2×10^{5}, 5.7×10^{4}	5.6×10^{11}, 3.8×10^{13}	3.2×10^{9}, 9.2×10^{8}	6.0×10^{6}, 1.7×10^{6}
1c–P	(A) 0.1 m	2.5×10^{-8}, 5.0×10^{-6}	2.0×10^{5}, 3.4×10^{4}	2.5×10^{11}, 1.7×10^{13}	1.6×10^{9}, 7.3×10^{8}	4.4×10^{6}, 8.3×10^{5}
	(B) 1 m	3.1×10^{-8}, 8.4×10^{-6}	1.8×10^{5}, 5.2×10^{4}	5.0×10^{11}, 3.2×10^{13}	1.6×10^{9}, 6.6×10^{8}	4.9×10^{6}, 1.5×10^{6}
	(C) 10 m	5.0×10^{-8}, 1.3×10^{-5}	1.9×10^{5}, 7.3×10^{4}	3.6×10^{11}, 2.4×10^{13}	1.9×10^{9}, 8.6×10^{8}	5.4×10^{6}, 2.1×10^{6}
1d–P	(A) 0.1 m	1.4×10^{-8}, 7.6×10^{-6}	3.6×10^{-5}, 7.5×10^{4}	4.1×10^{11}, 3.5×10^{13}	1.3×10^{10}, 5.7×10^{9}	8.6×10^{6}, 1.9×10^{6}
	(B) 1 m	1.5×10^{-8}, 1.3×10^{-5}	3.5×10^{-5}, 9.3×10^{4}	3.2×10^{12}, 2.9×10^{14}	1.4×10^{10}, 5.6×10^{9}	9.9×10^{6}, 2.7×10^{6}
	(C) 10 m	1.5×10^{-8}, 1.5×10^{-5}	3.7×10^{-5}, 1.2×10^{-5}	2.1×10^{12}, 1.8×10^{14}	1.5×10^{10}, 6.5×10^{9}	1.1×10^{7}, 3.5×10^{6}

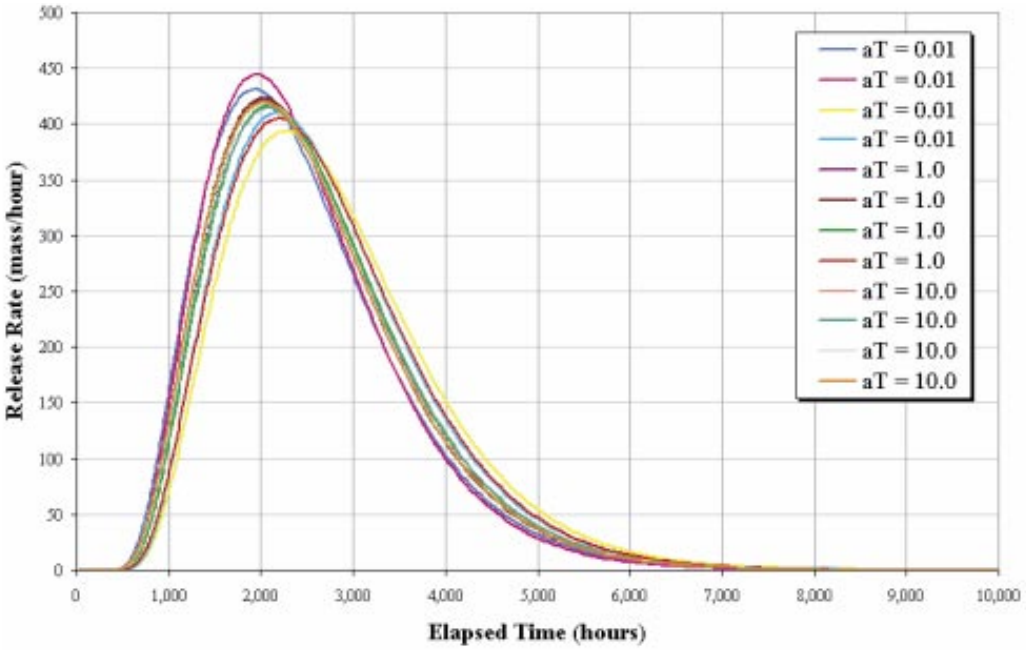

Figure 3-5. *Breakthrough curves for realizations of the Base case (α_T = 0.01, 1, and 10 m), particle tracking.*

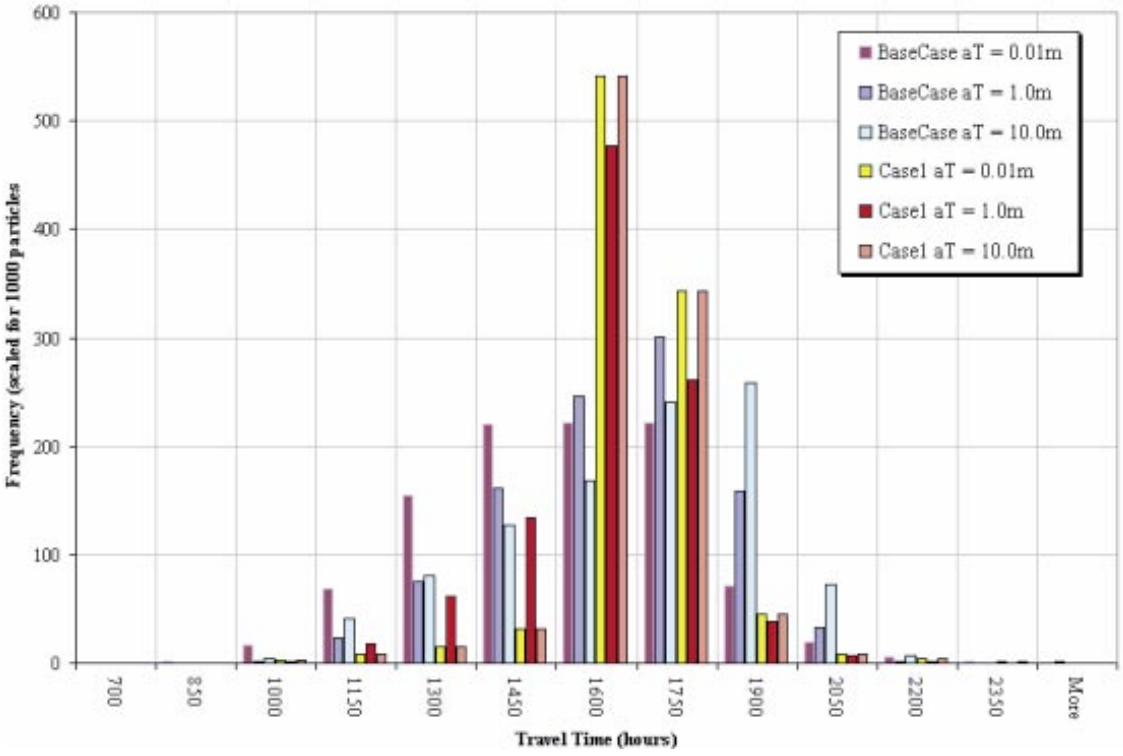

Figure 3-6. *Histogram PDF of residence time τ for one realization each for the Base case and Case 1b (α_T = 0.01, 1 10 m) , particle tracking.*

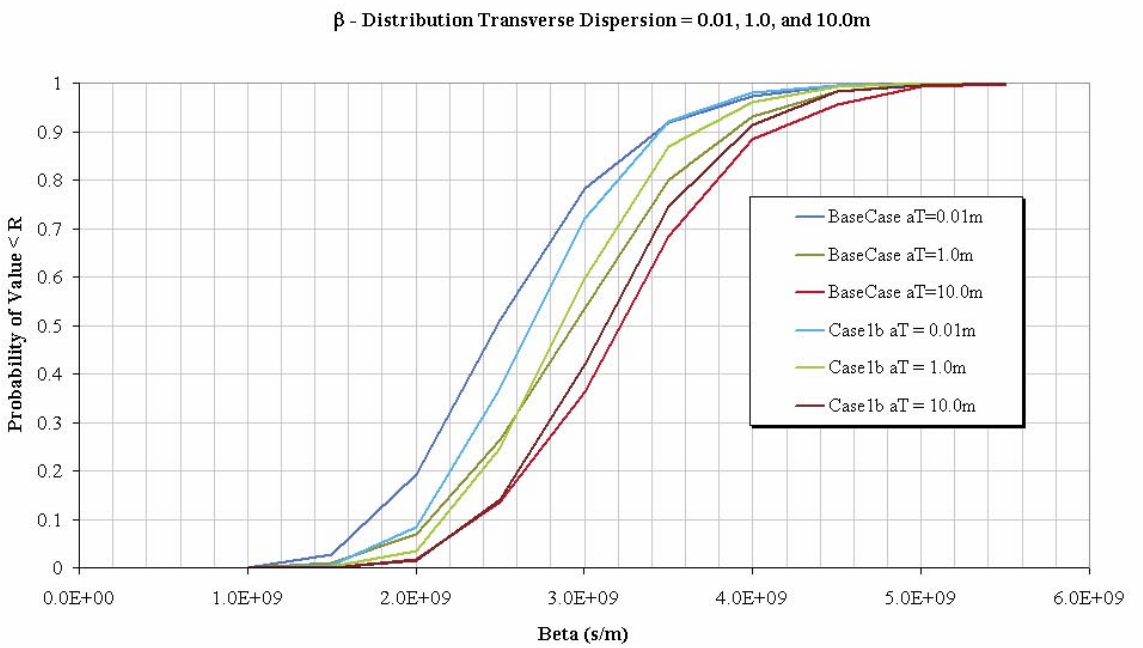

Figure 3-7. *CCDF of average retention factor β for one realization for the Base case, Case 1b (αT = 0.01, 1 10 m), particle tracking.*

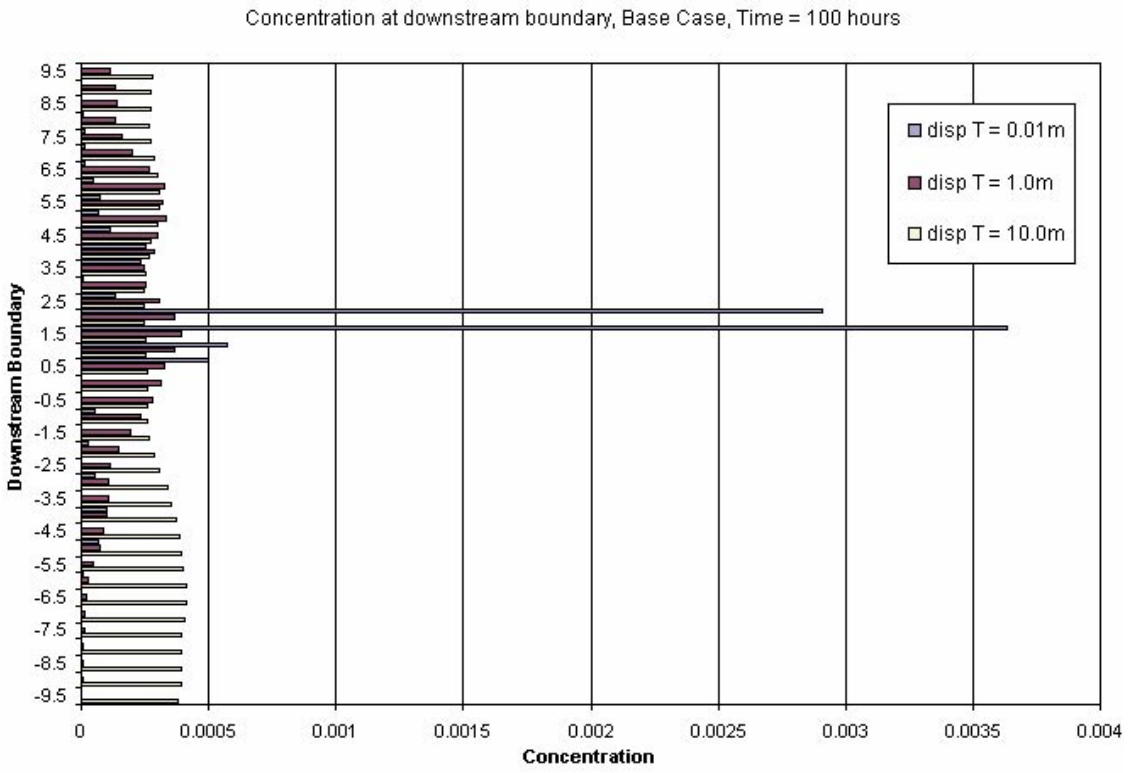

Figure 3-8. *Concentration profile along the downstream edge of the fracture at time 100 hours for one realization of the Base case (α_T = 0.01, 1, 10), LTG.*

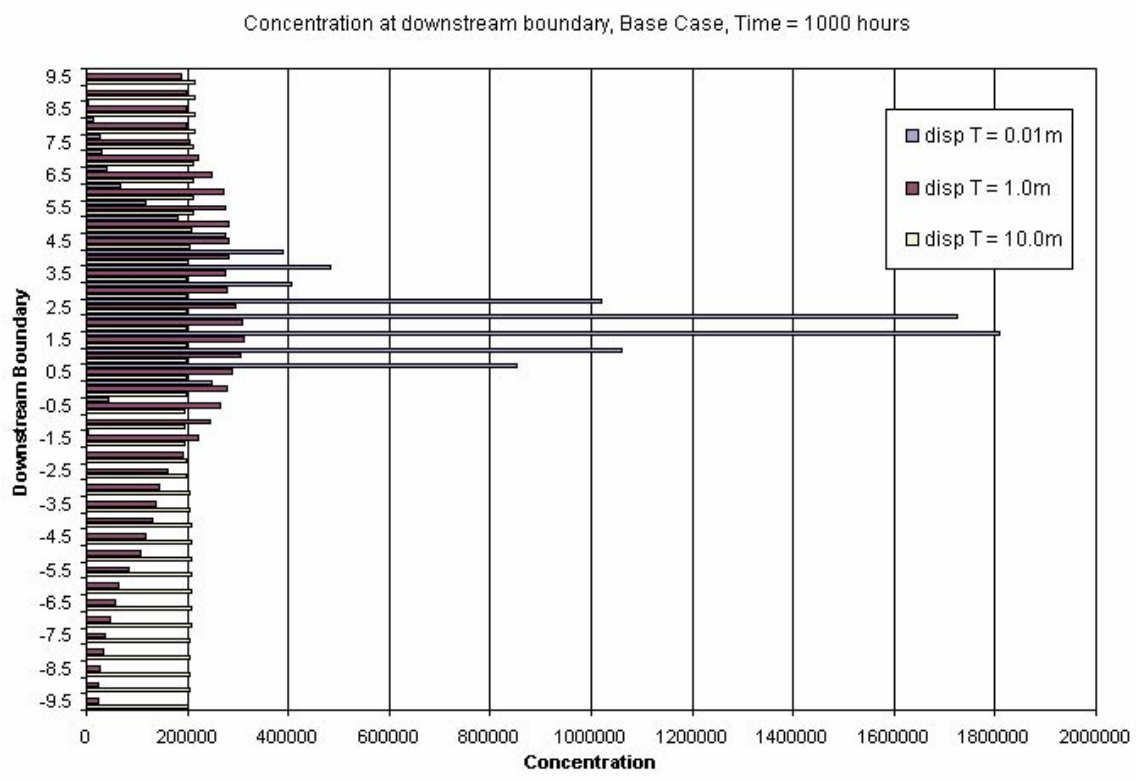

Figure 3-9. *Concentration profile along the downstream edge of the fracture at time 1,000 hours for one realization of the Base case (α_T = 0.01, 1, 10), LTG.*

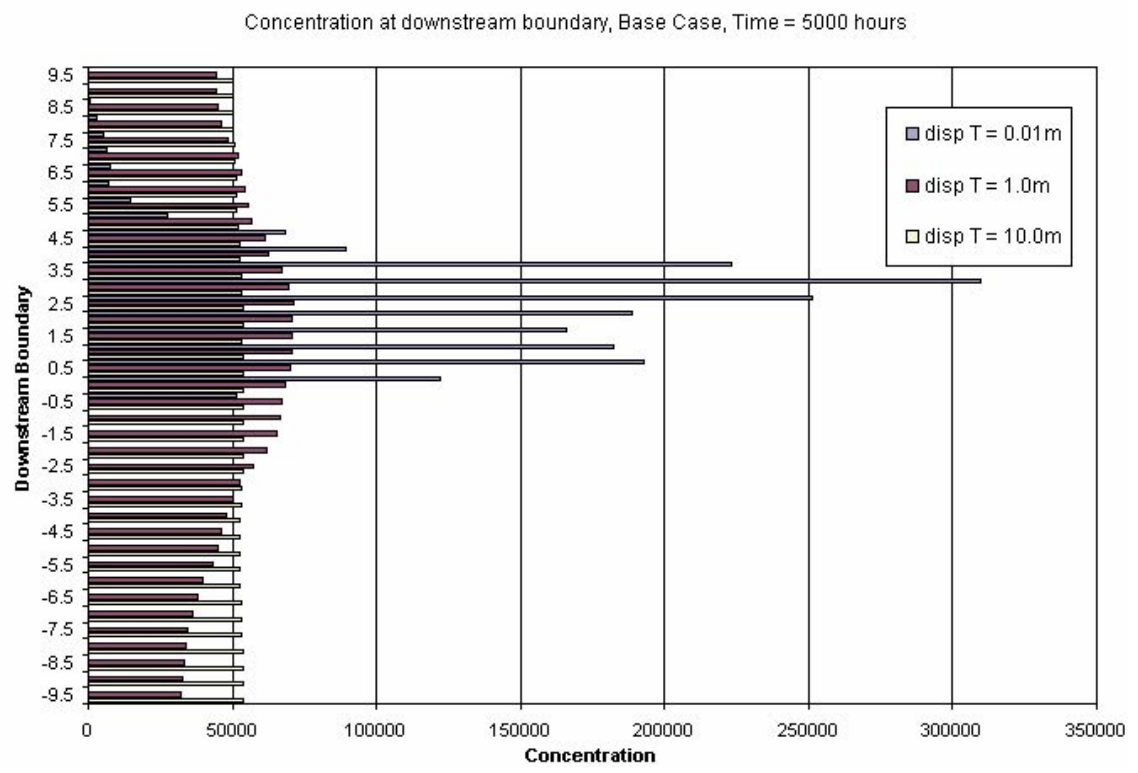

Figure 3-10. *Concentration profile along the downstream edge of the fracture at time 5,000 hours for one realization of the Base case (α_T = 0.01, 1, 10), LTG.*

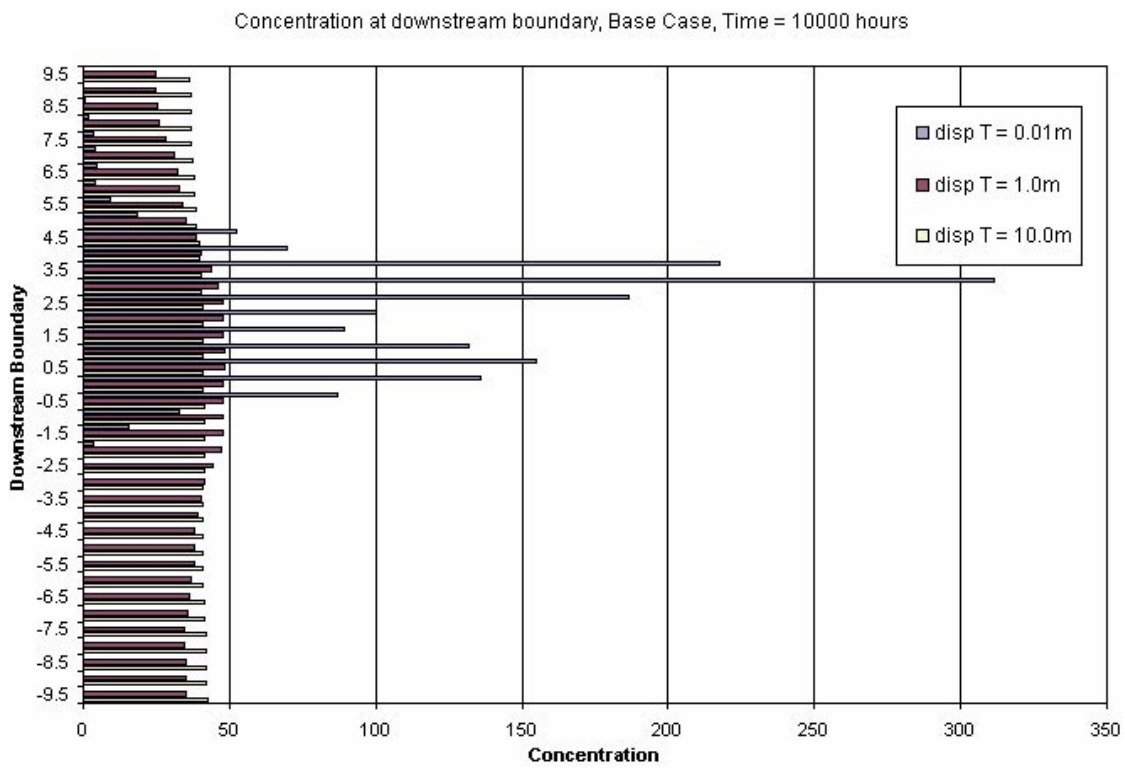

Figure 3-11. *Concentration profile along the downstream edge of the fracture at time 10,000 hours for one realization of the Base case (α_T = 0.01, 1, 10), LTG.*

3.2.1 Base case: heterogeneous field

Figure 3-12, Figure 3-13, and Figure 3-14 show particle tracks for realization 1 of the Base case. In these and subsequent particle track plots, particles are colored by time step, such that particles for each time step plotted share the same color. The plot for low (0.01 m) dispersion clearly shows the formation of a single distinctive transport pathway at low dispersion. This pathway is controlled by local heterogeneity. As the dispersion increases, there is a distinctive spread in the tracer pathways, with more particles entering lower transmissivity fractures. Comparing the location of particles at $t = 2.52\times10^6$ seconds, the particles have traveled further on the 0.01 m dispersion pathways than on the pathways with 1 m and 10 m transverse dispersion pathways. At 0.01 m dispersion, the center of mass at $t = 2.52\times10^6$ seconds is at approximately 17 m, while at 10 m, the center of mass is at approximately 14 m. This implies an influence of transverse dispersion both on the shape of the breakthrough curve and on the pathway statistics.

Figure 3-15 illustrates 20 of the 40 Base case heterogeneous fields. Figure 3-16 through Figure 3-19 present HTO breakthrough curves for all 40 Base case realizations. Within the 40 realizations, the time to peak breakthrough varies from approximately 1,700 to 2,500 hours. This variation is much larger than the variation due to differences in the dispersion as seen in Figure 3-12 through Figure 3-14. Thus, while transverse dispersion has an effect on breakthrough, based on these simulations it does not appear to be significant when compared to the variation between realizations of the Base case heterogeneous field.

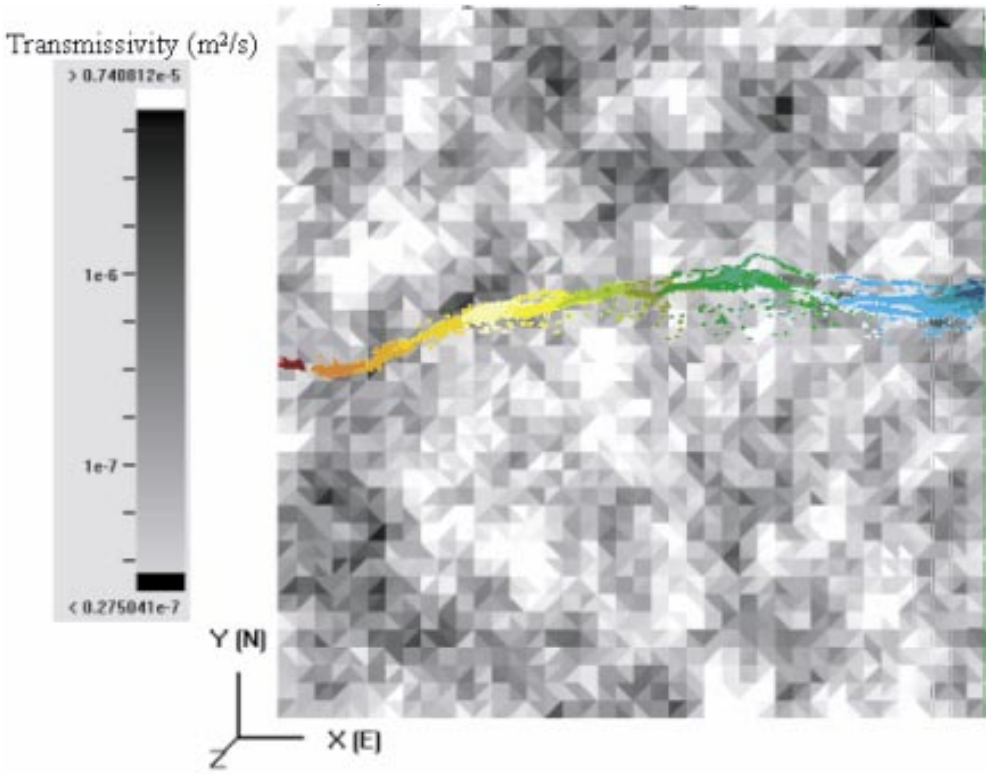

Figure 3-12. *Base case, α_T = 0.01 m., particle tracking.*

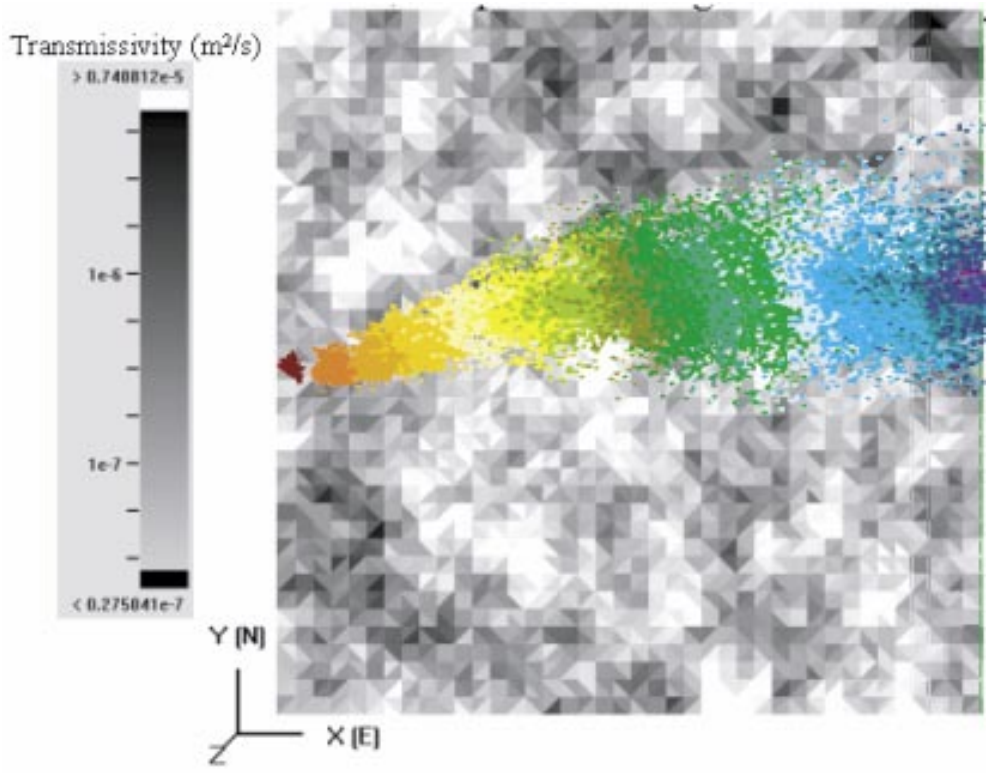

Figure 3-13. *Base case, α_T = 1.0 m, particle tracking.*

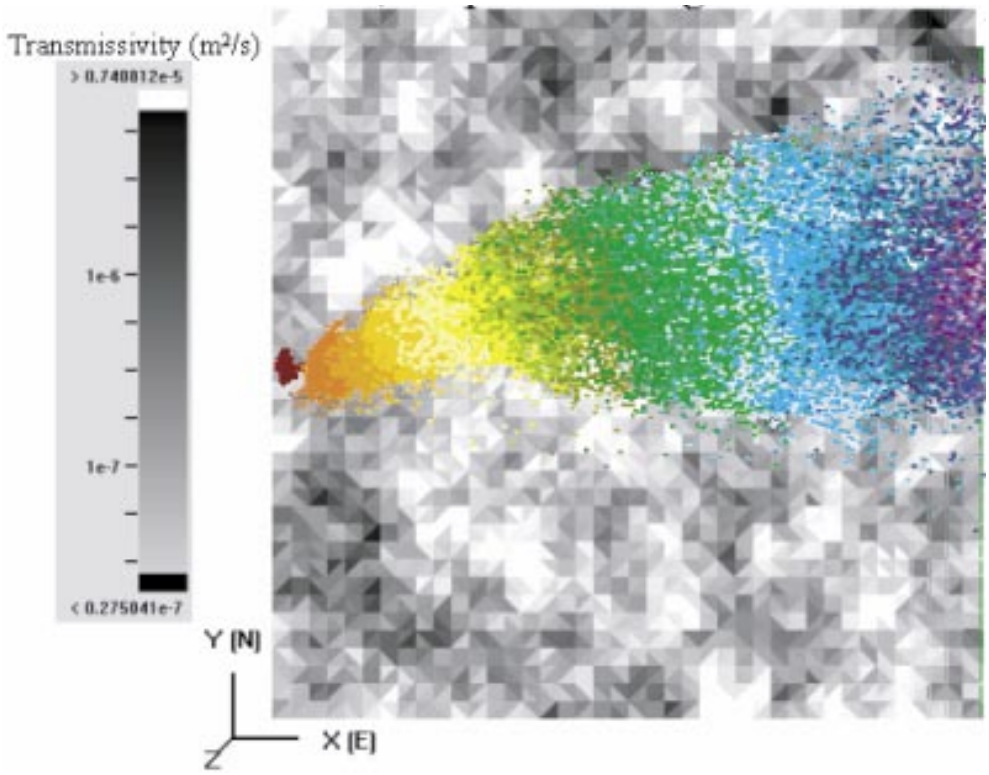

Figure 3-14. *Base case, α_T = 10.0 m, particle tracking.*

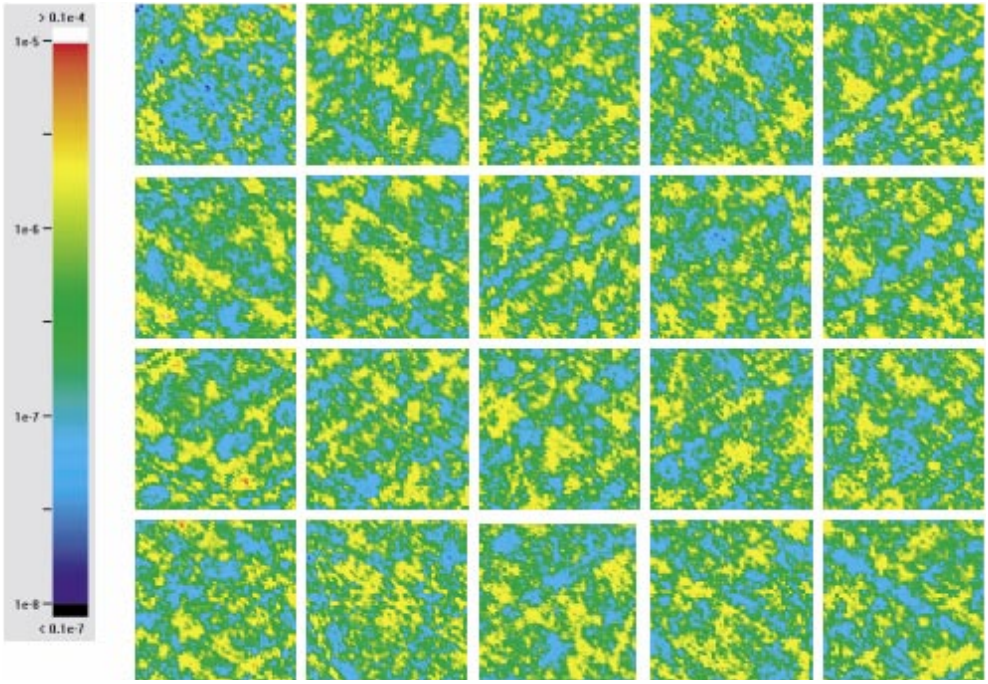

Figure 3-15. *Base case, heterogeneous fields (20 realizations).*

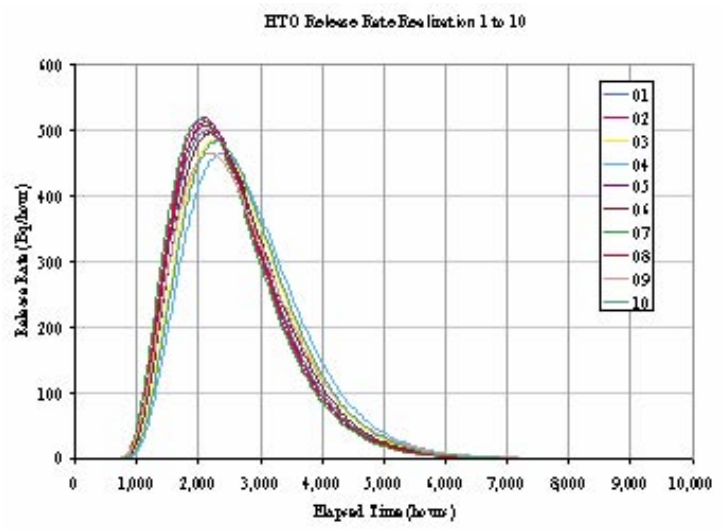

Figure 3-16. *Base case, HTO breakthrough, realizations 1–10, LTG.*

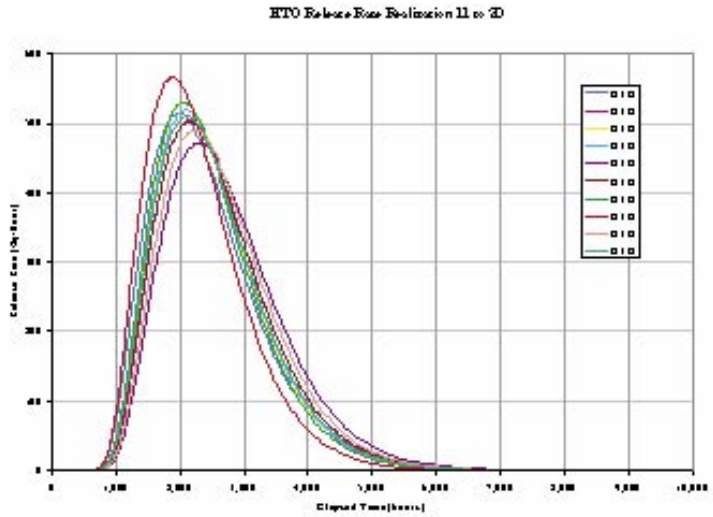

Figure 3-17. *Base case, HTO breakthrough, realizations 11–20, LTG.*

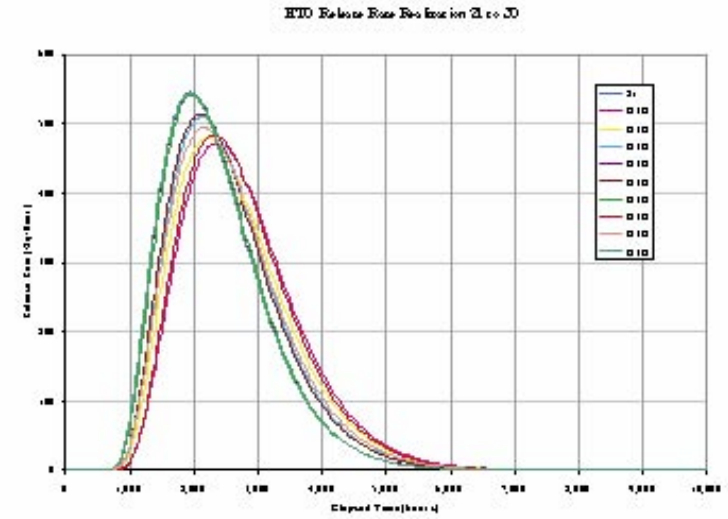

Figure 3-18. *Base case, HTO breakthrough, realizations 21–30, LTG.*

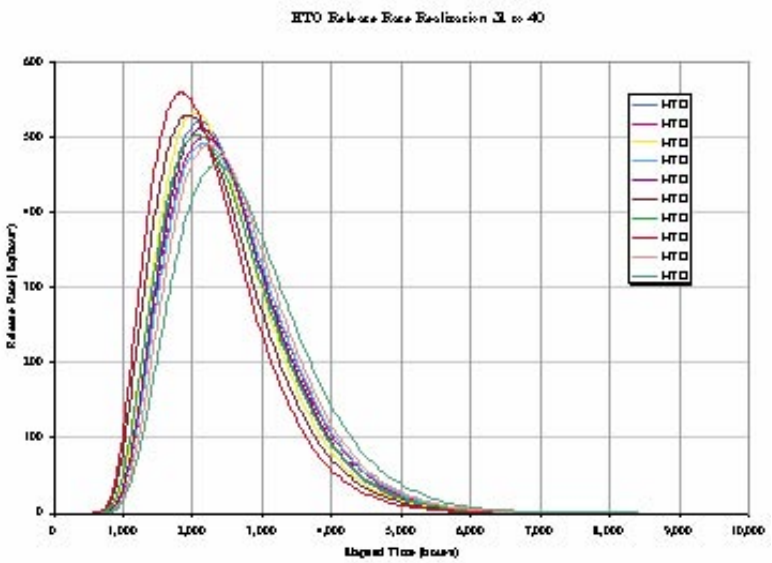

Figure 3-19. *Base case, HTO breakthrough, realizations 31–40, LTG.*

The issue then becomes a comparison of the scatter due to variability between stochastic fields as compared to the change due to different values of transverse dispersion. Figure 3-5 presents a plot of HTO breakthrough curves for four realizations, with three different values of transverse dispersion. The difference due to transverse dispersion is consistent with the dispersion between realizations.

Figure 3-20 shows the variation in t_5, t_{50}, and t_{95} with transverse dispersion for the Base case. For the forty simulations carried out, the mean does not change. The standard deviation of t_5, t_{50}, and t_{95} does however change significantly, as shown in Figure 3-21. Increases in transverse dispersion significantly reduce the importance of variability between stochastic realizations.

Effective dispersion in breakthrough curves can be indicated by the statistic $(t_{95}–t_5)/t_{50}$. This is shown in Figure 3-22. The mean dispersion in the breakthrough curve increases with increased transverse dispersion, as would be expected. The standard deviation between realizations decreases, indicating again a decrease in the importance of dispersion between realizations.

Figure 3-23 through Figure 3-25 show comparable results for the distribution of beta, the normalized travel-time distribution. While there is some shift in the curves with increased transverse dispersion, the shift appears to be within the scatter between realizations.

Figure 3-26 provides a log plot of the statistics for pathway measures Q, 1/bv, beta, and tau. For most of these measures, there is a trend with increased transverse dispersion. However, this trend is generally a factor of 2 to 4, which is not large compared to the variability between realizations.

Perhaps the greatest difference with changing transverse dispersion is in the pattern of flow wetted area, and the spatial pattern of breakthrough to the downstream face as shown in Figure 3-12 through Figure 3-14. Increased transverse dispersion dramatically increases the exposure of fracture surface to solute, which makes much more surface available for sorption. Sorbing tracer transport will be dealt with in the next chapter. The change in the pattern of downstream breakthrough implies significant effect on transport pathways involving fracture networks.

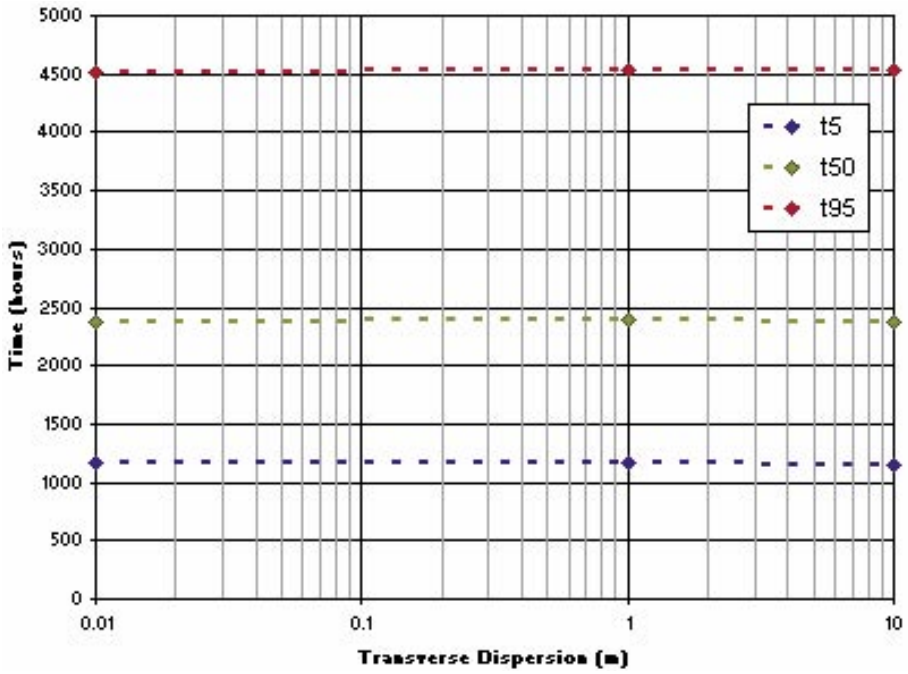

Figure 3-20. *Base case, HTO distribution of mean t_5, t_{50}, t_{95}, LTG.*

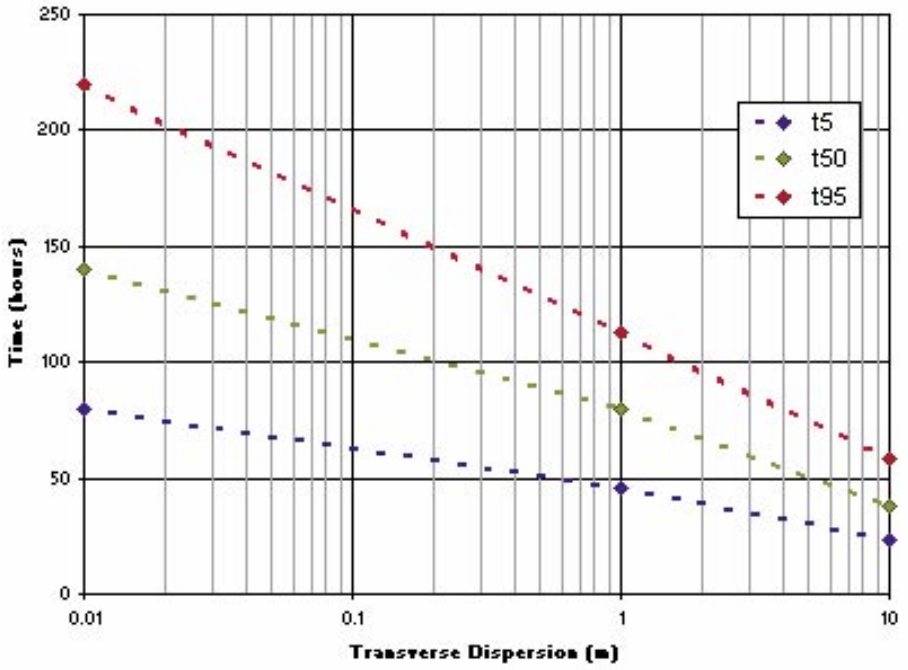

Figure 3-21. *Base case, HTO distribution of standard deviation t_5, t_{50}, t_{95}, LTG.*

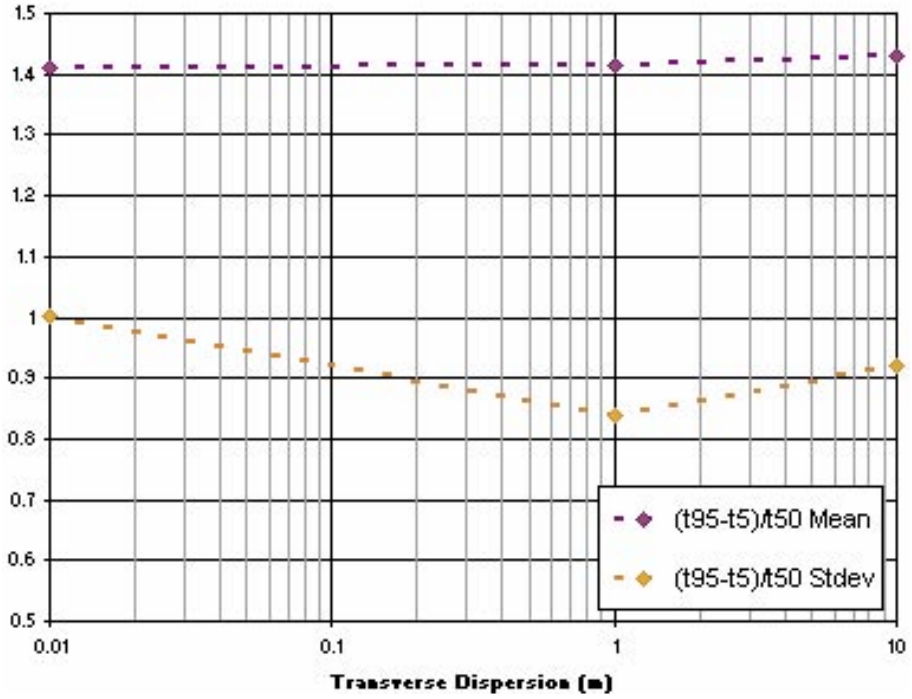

Figure 3-22. *Base case, HTO effective dispersion, LTG.*

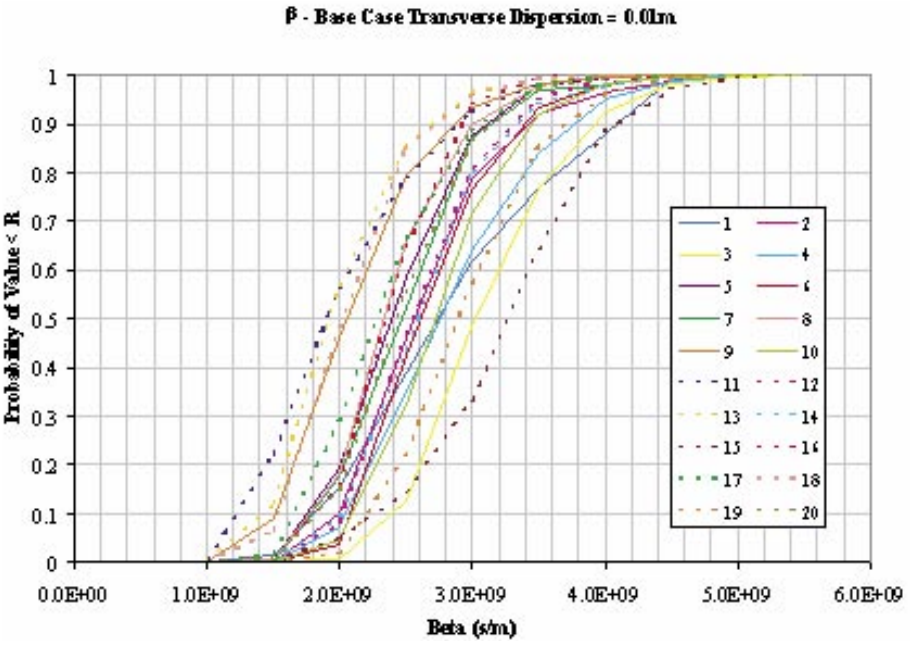

Figure 3-23. *β-Base case αT = 0.01 m, particle tracking.*

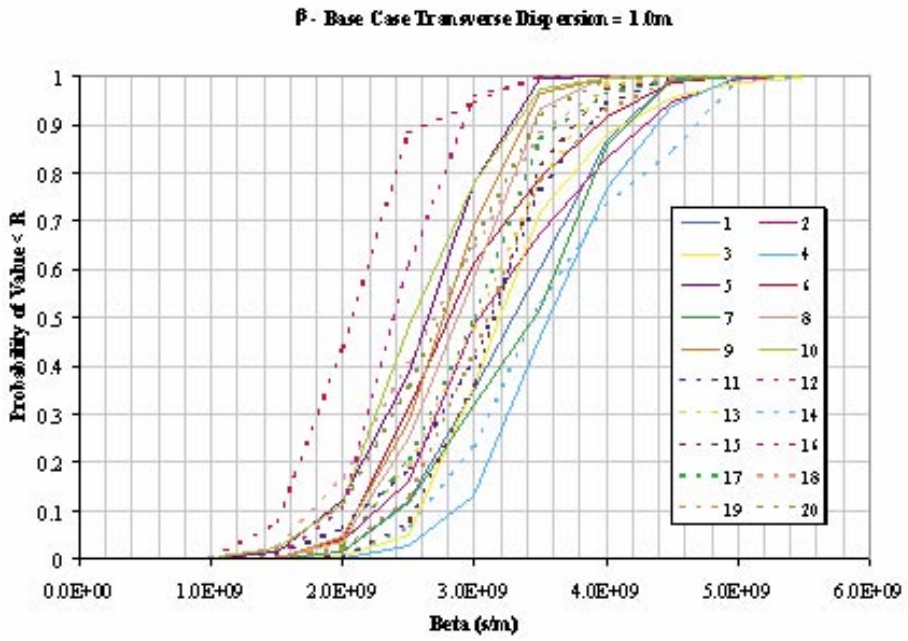

Figure 3-24. *β-Base case αT = 1.0 m, particle tracking.*

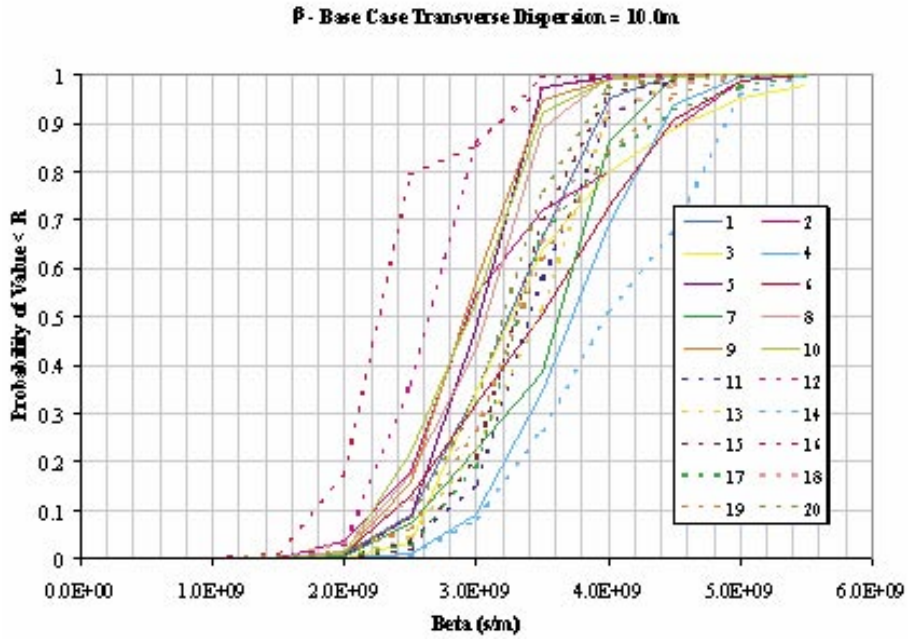

Figure 3-25. *β-Base case αT = 10 m, particle tracking.*

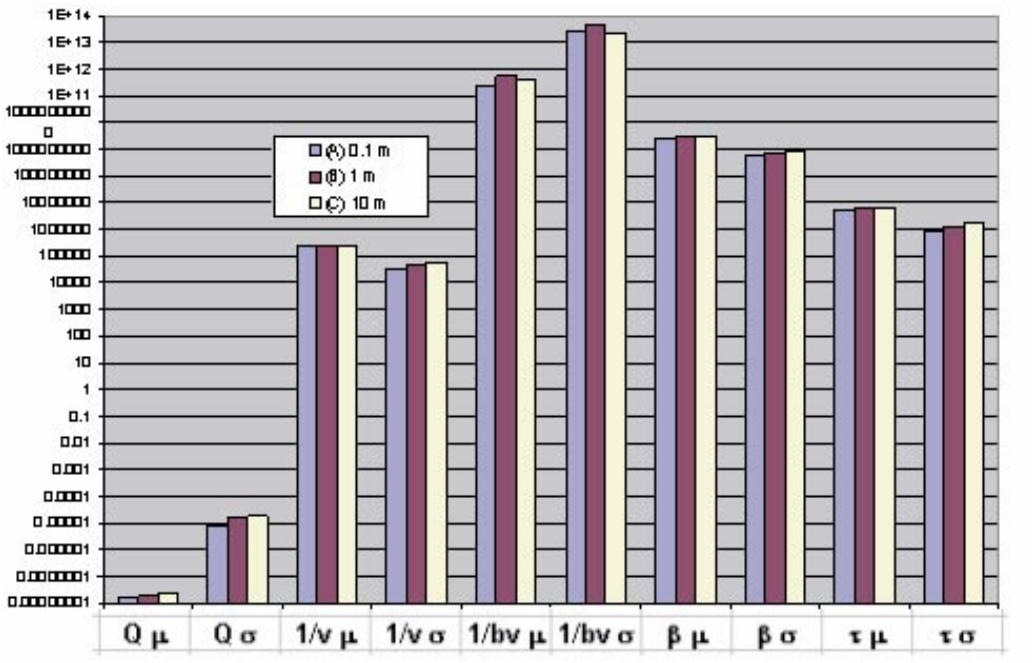

Figure 3-26. *Base case, summary statistic for all transport measures.*

3.2.2 Case 1: alternative heterogeneous and homogeneous fields

The purpose of Case 1 is to evaluate whether the conclusions for the Base case are perhaps prejudiced by the spatial field used. Case 1 considers four different fields, with very different patterns, as described in Chapter 2 above. Forty realizations were run for each of these fields, except for the homogeneous case, which required only a single realization.

- Case 1a: homogeneous, uncorrelated (constant transmissivity).
- Case 1b: heterogeneous, correlated, non-channeled (Figure 2-2).
- Case 1c: heterogeneous, anisotropic, correlated, channeled (Figure 2-3).
- Case 1d: Fracture Intersection Zone (Figure 2-4).

As with the Base case, each of these cases was first run against the STT1b tracer test to derive an appropriate correlation between transmissivity and transport aperture to match the STT1b breakthrough. Each of the matches was obtained using an equation of the form,

$e_t = a_t T^{bt}$

The fitted STT1b breakthrough for each of the cases are provided in Figure 3-3 through Figure 3-4.

The trends for the mean and standard deviation of t_5, t_{50}, and t_{95} for Case 1a through d are shown in Figure 3-27 through Figure 3-33.

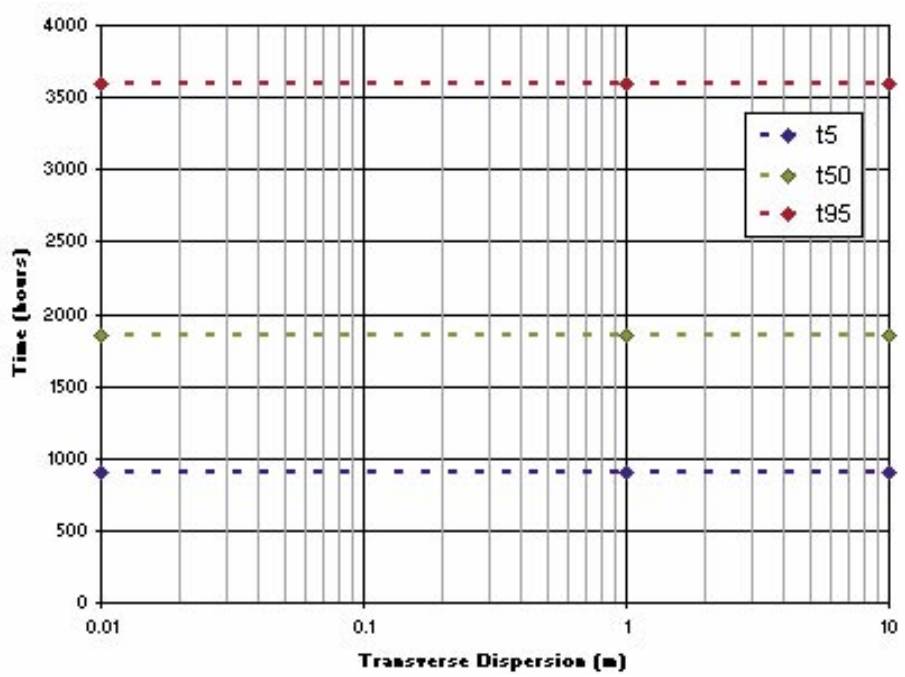

Figure 3-27. *Case 1a, HTO distribution of mean t_5, t_{50}, t_{95}, LTG.*

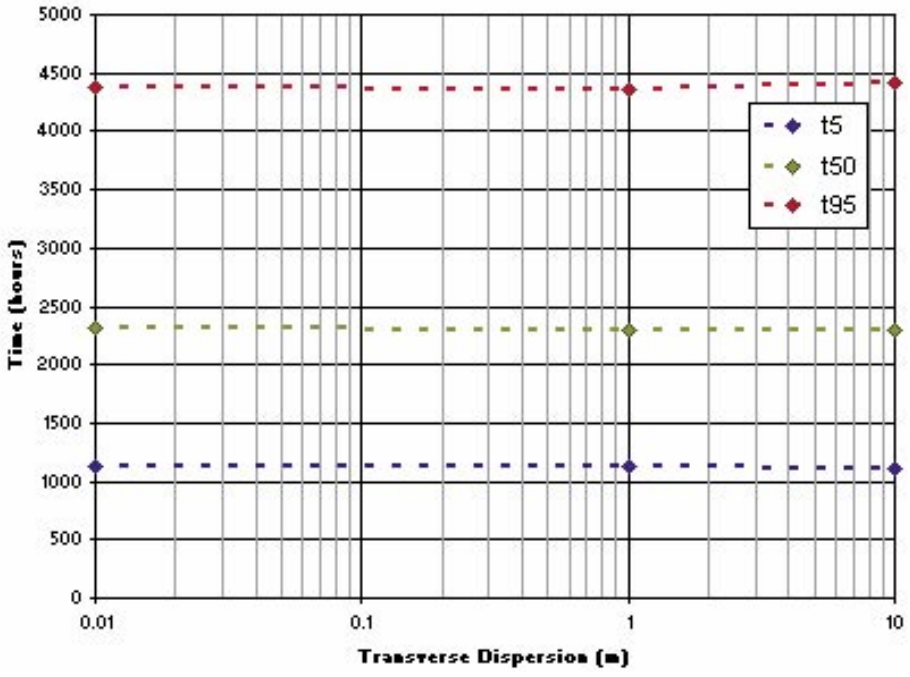

Figure 3-28. *Case 1b, HTO, distribution of mean t_5, t_{50}, t_{95}, LTG.*

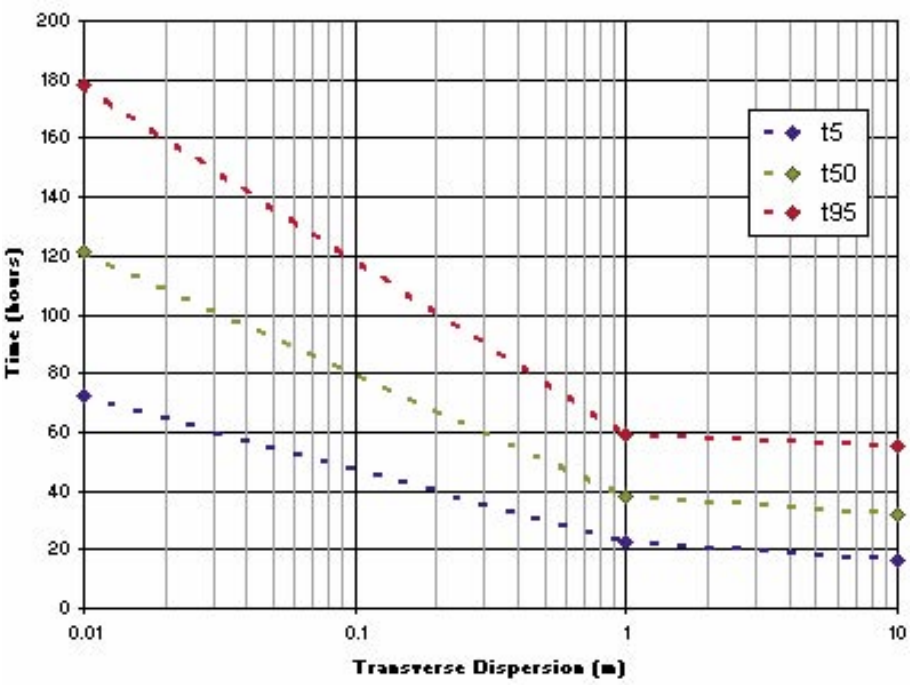

Figure 3-29. *Case 1b, HTO, distribution of st dev t_5, t_{50}, t_{95}, LTG.*

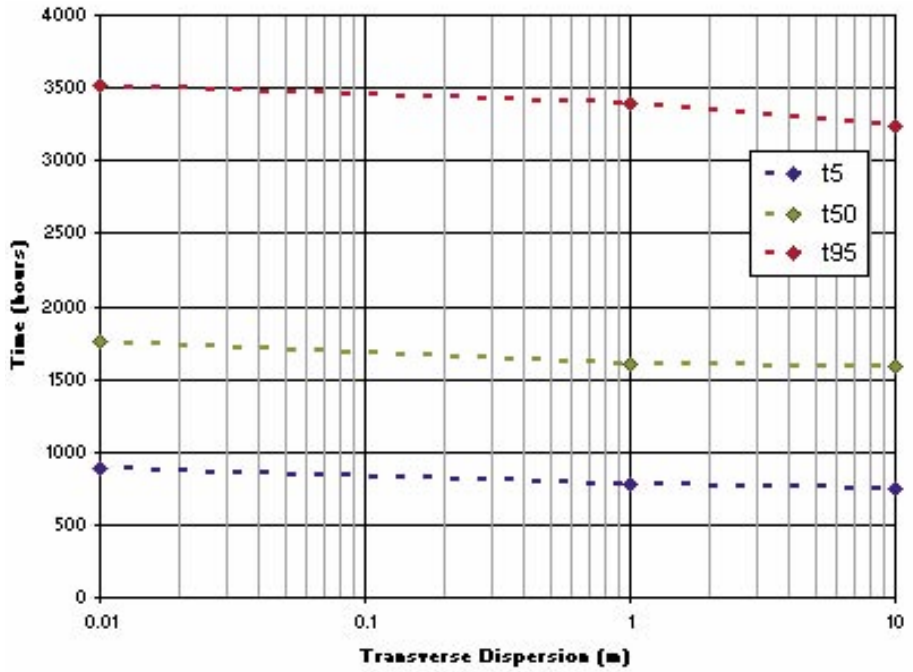

Figure 3-30. *Case 1c, HTO distribution of mean t_5, t_{50}, t_{95}, LTG.*

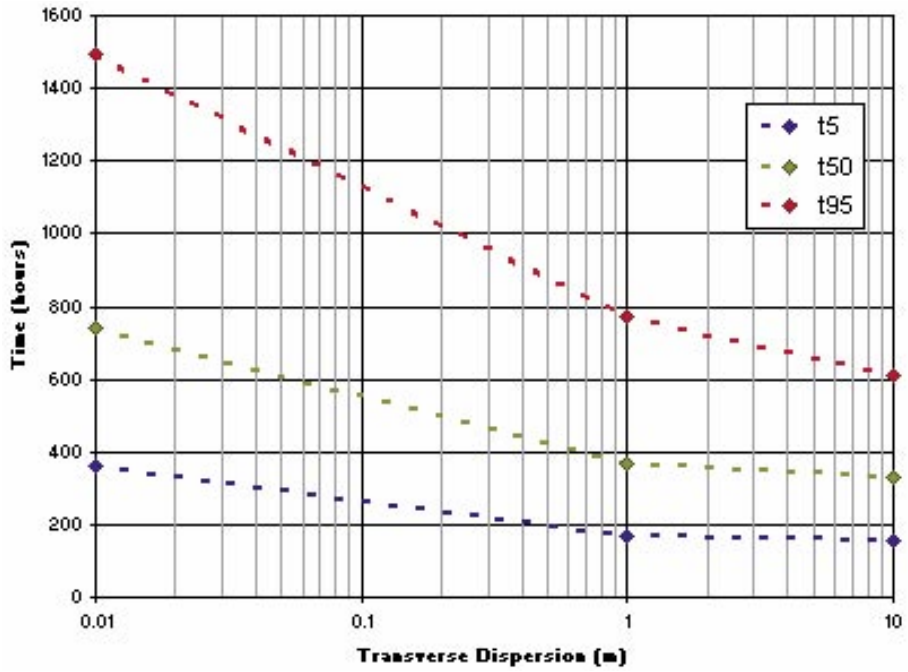

Figure 3-31. *Case 1c, HTO, distribution of st dev t_5, t_{50}, $5_{95,}$ LTG.*

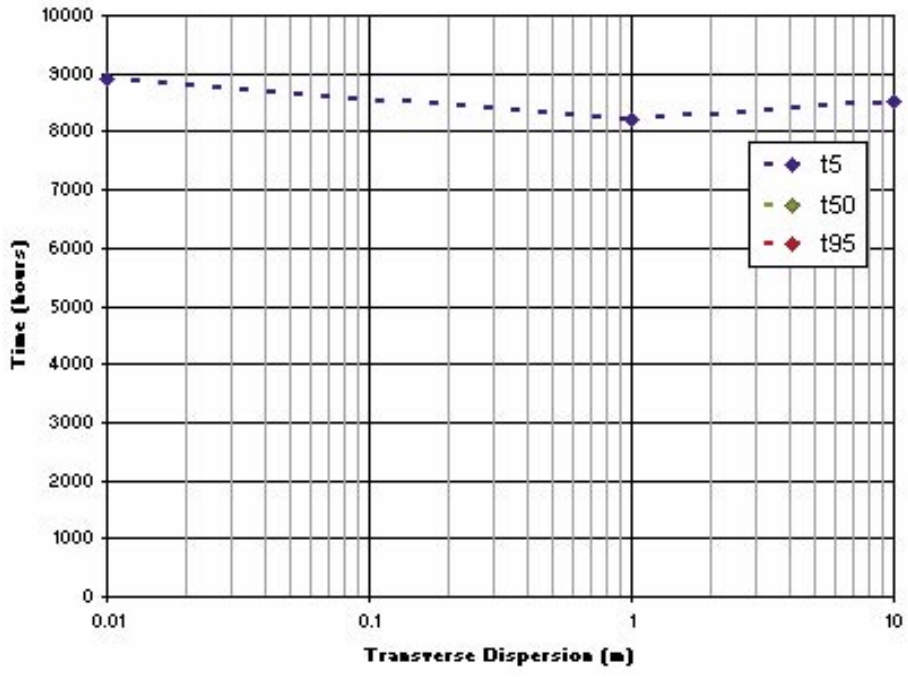

Figure 3-32. *Case 1d, HTO, distribution of mean t_5, t_{50}, t_{95} (total recovery is less than 50%), LTG.*

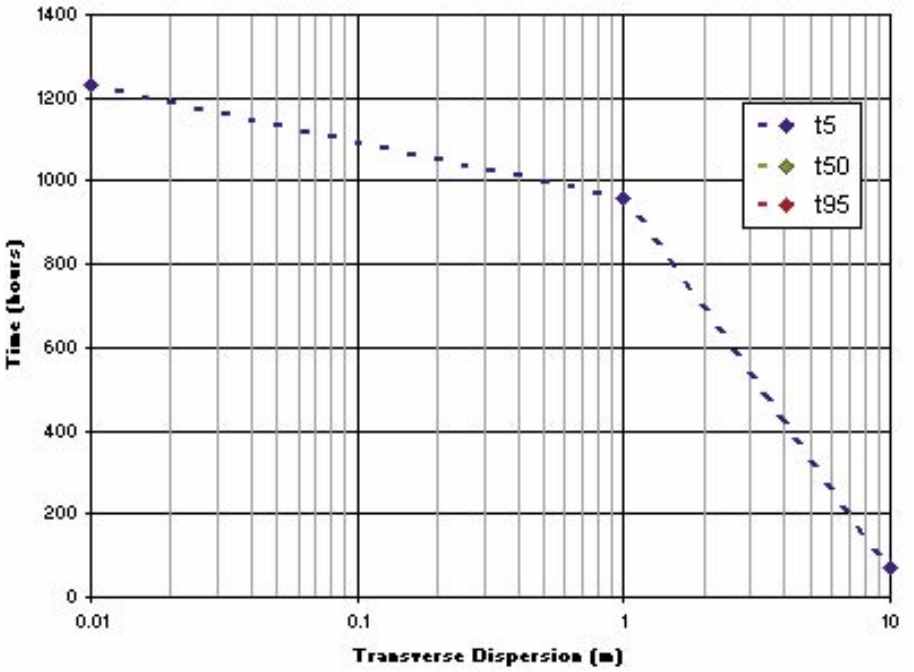

Figure 3-33. *Case 1d, HTO, distribution of st dev t_5, t_{50}, t_{95} (total recovery is less than 50%), LTG.*

3.2.2.1 Case 1a: homogeneous fracture

Transmissivity for Case 1a is constant, so there is only a single realization. The particle pathways for Case 1a are shown in Figure 3-34 through

Figure 3-36 for transverse dispersion values of 0.01 m, 1 m, and 10 m. Despite the absence of spatial heterogeneity, there is considerable transverse dispersion, even for the case of 1 cm transverse dispersion. This results in a change in the spatial patterns of breakthrough to the downstream side. The pattern of breakthrough to the downstream edge from LTG simulations is shown in Figure 3-37. This figure shows the concentration along the edge at approximately time t_{50}.

Within the homogeneous fracture case, the velocity in the direction of the gradient is constant at all locations. Transverse dispersion only moves tracer mass to a parallel location in the flow field. The velocity and distance to the downstream boundary are the same from this location as from the location before transverse dispersion. Therefore the travel time to the downstream boundary should not be sensitive to transverse dispersion in the homogeneous fracture case. This can be seen in Figure 3-38, which presents the breakthrough curves for Case 1a with transverse dispersion values of 0.01 m, 1 m, and 10 m. There are no significant changes to t_5, t_{50}, and t_{95} or to the breakthrough curves with change in transverse dispersion up to 10 m.

Since transverse dispersion in a single homogeneous fracture has no effect on travel times, it is not surprising that it also has no effect on 1/v, 1/bv, tau, and beta, as can be seen from Table 3-4.

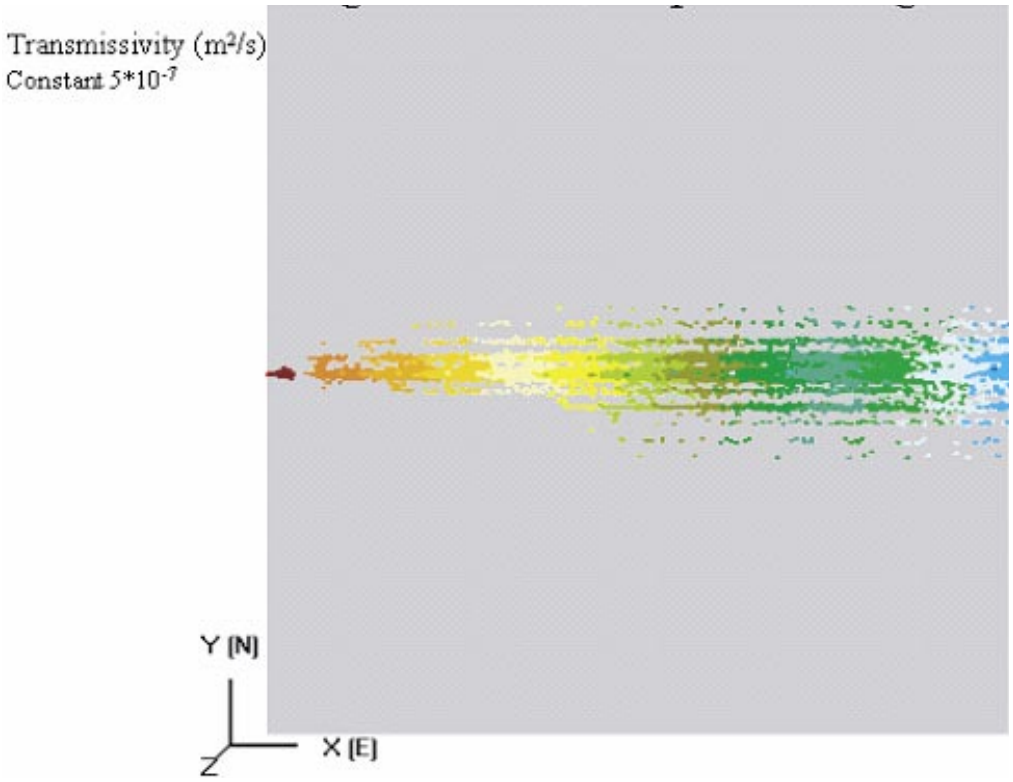

Figure 3-34. *Case 1a, homogenous field, α_T = 0.01 m, particle tracking.*

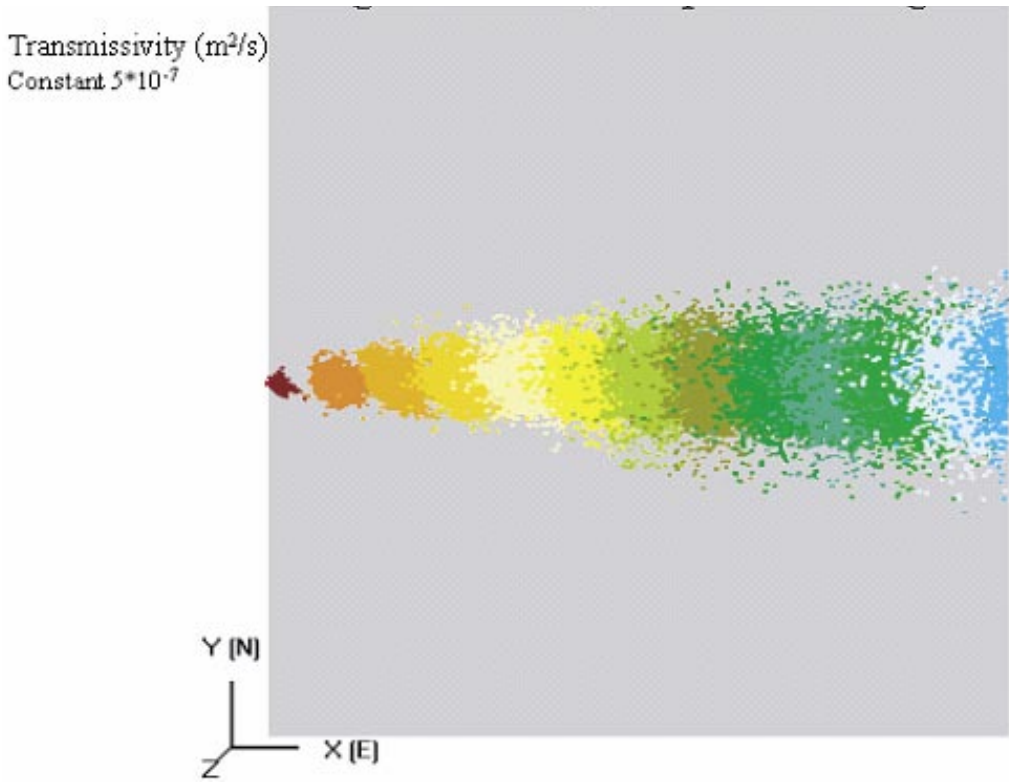

Figure 3-35. *Case 1a, homogenous field, α_T = 1.0 m, particle tracking.*

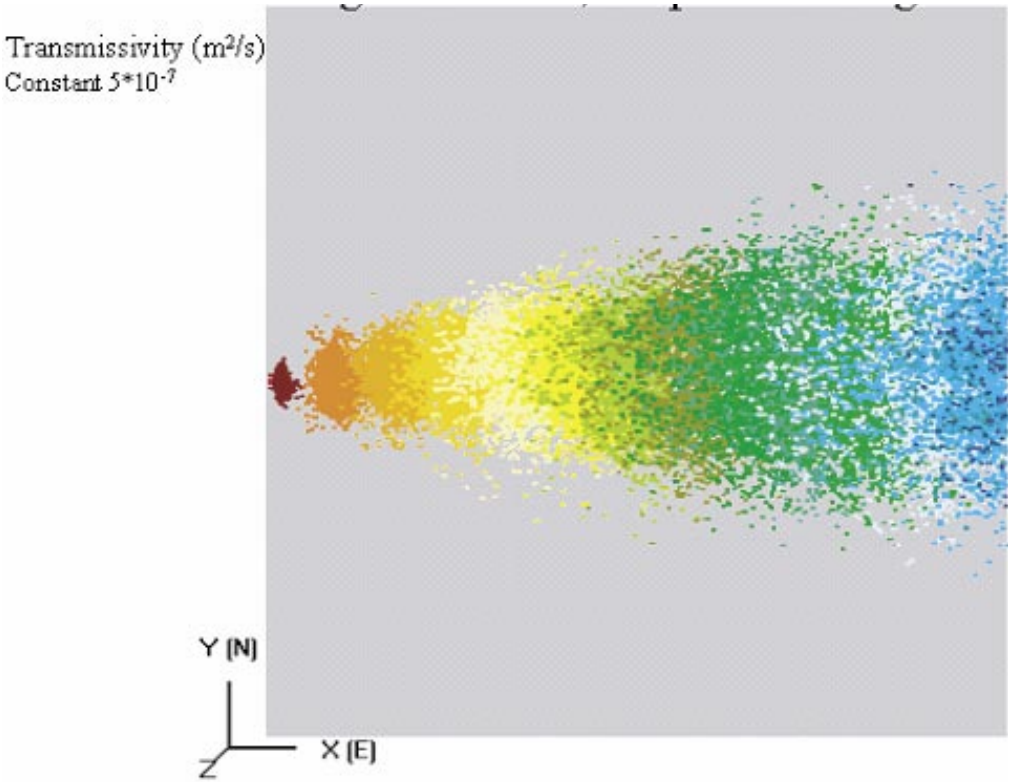

Figure 3-36. *Case 1a homogenous field, α_T = 10.0 m, particle tracking.*

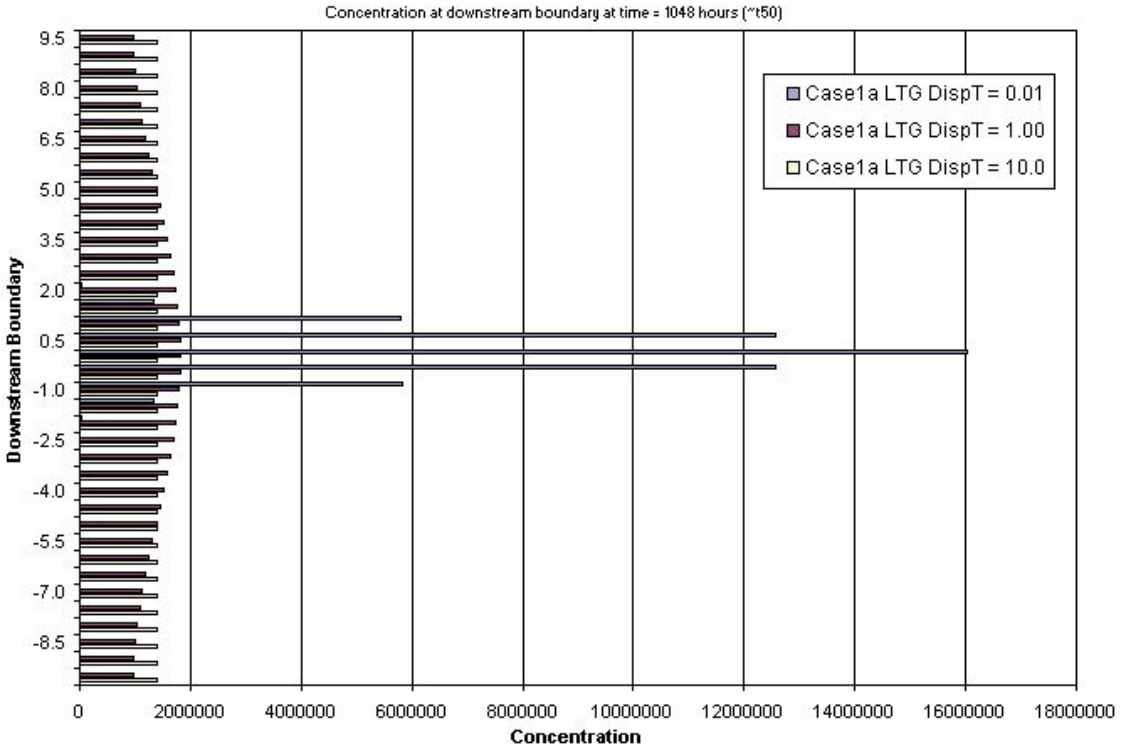

Figure 3-37. *Concentration at downstream boundary at time equal to $t_{50,}$ LTG.*

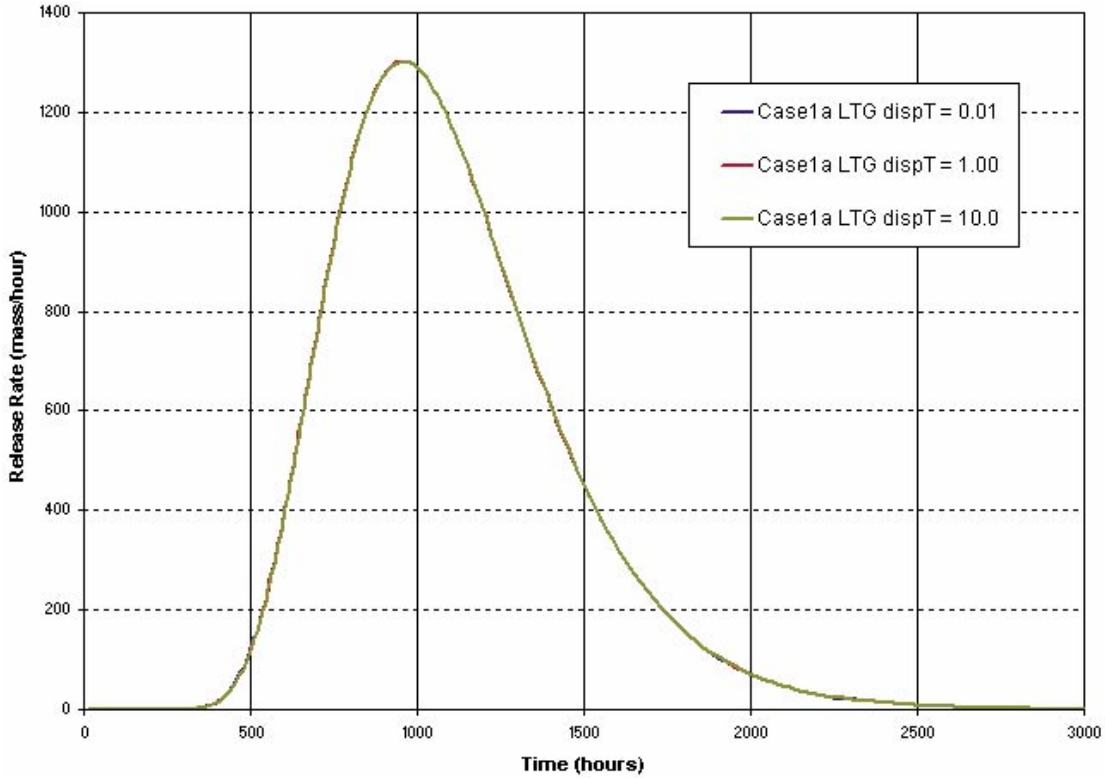

Figure 3-38. *Case 1a breakthrough, αT = 0.01, 1, 10 m, LTG.*

3.2.2.2 Case 1b: heterogeneous, correlated, non-channeled

As shown in Figure 3-39 through Figure 3-41, the fine pattern of the heterogeneous non-channeled fracture of Case 1b, increases the spread of transverse dispersion when compared to the homogeneous Case 1a. However, the spread is fairly comparable to that of the Base case 0. The lack of channeling leads to more symmetrical particle pathways, as compared to the generally non-symmetrical particle pathways of the Base case.

Figure 3-42 shows HTO breakthrough for the first ten realizations of Case 1b. When compared to Figure 3-16 through Figure 3-19, it can be seen that this field is significantly less variable between realizations. This is consistent with the unchanneled, low correlation length pattern, which makes Case 1b almost equivalent to a homogeneous field with effective properties. This can also be seen in the lack of variability in t_5, t_{50}, and t_{95} statistics as shown in Figure 3-28 and Figure 3-29.

The statistical summary of Case 1b results for all transport measures is provided in Table 3-4. Results are similar to those for the Base case.

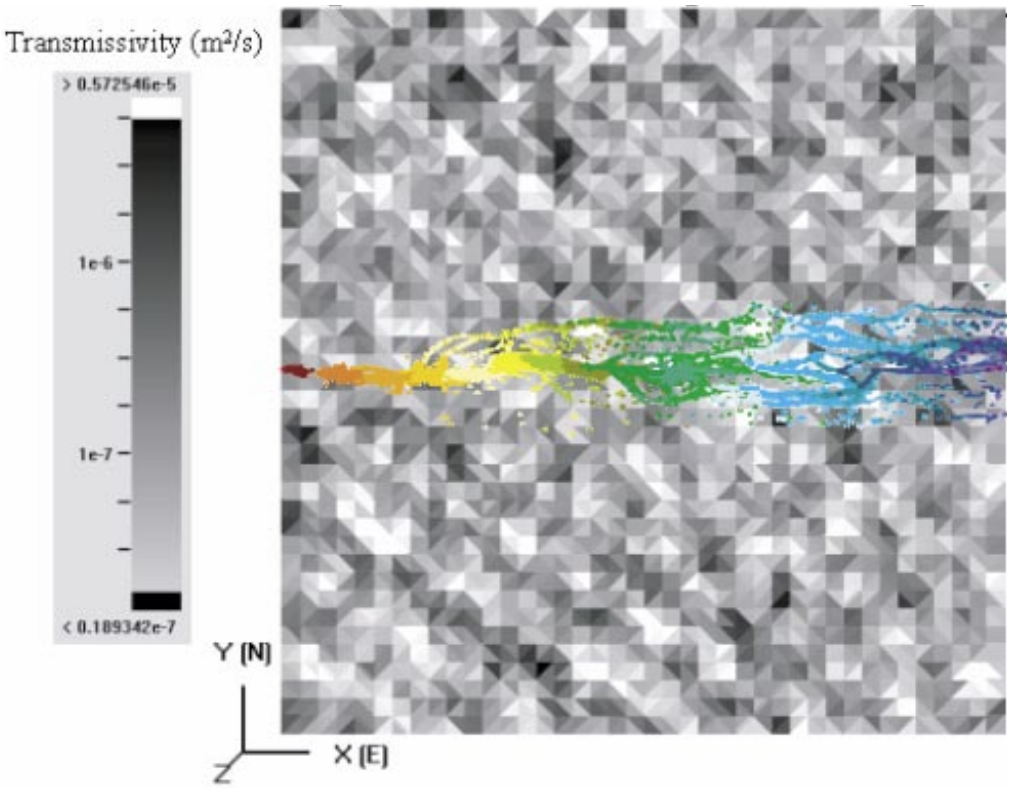

Figure 3-39. *Case 1b, heterogeneous field, α_T = 0.01 m, particle tracking.*

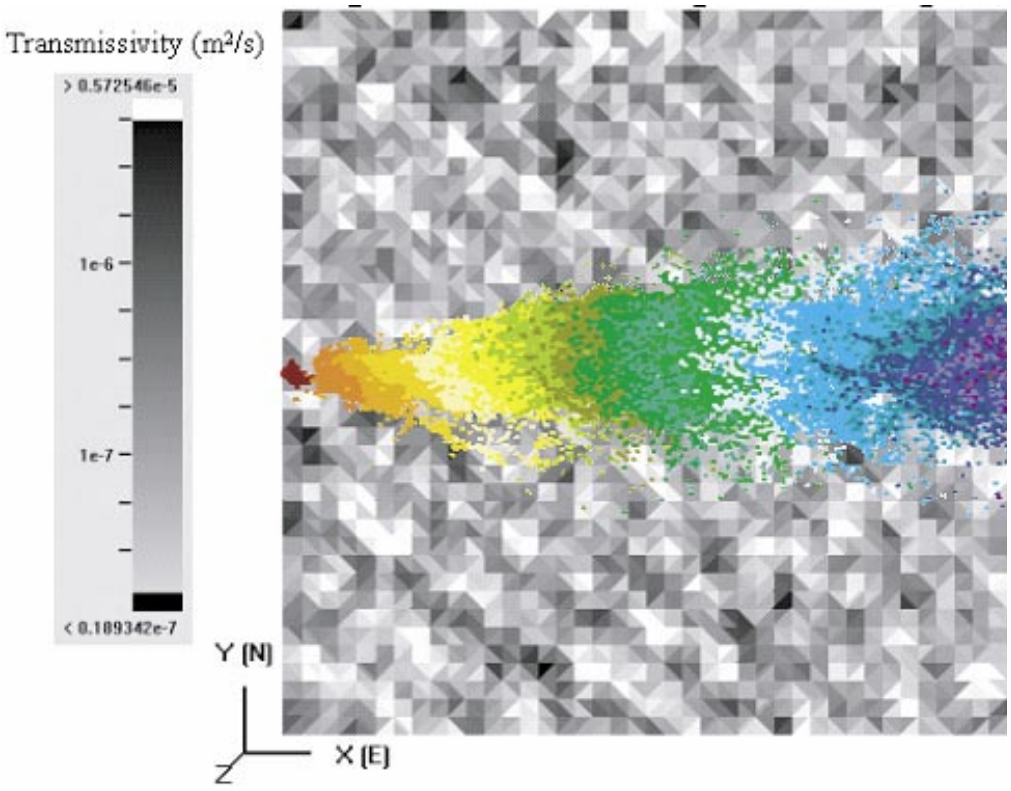

Figure 3-40. *Case 1b, heterogeneous field, α_T = 1.0 m, particle tracking.*

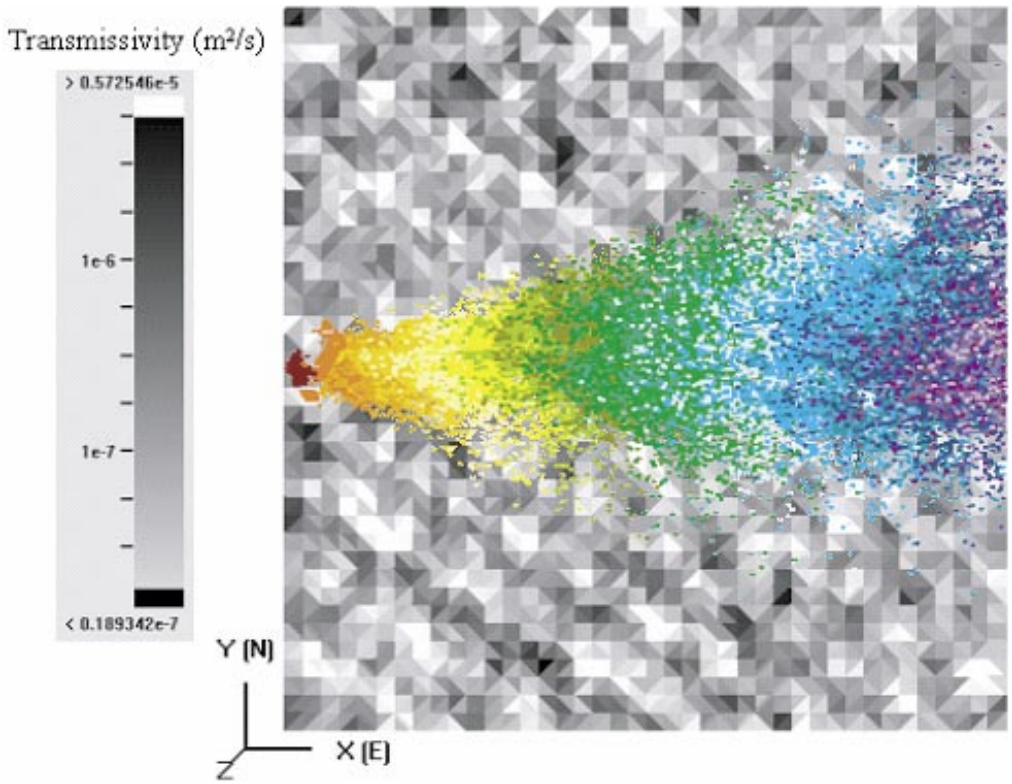

Figure 3-41. *Case 1b, heterogeneous field, α_T = 10.0 m, particle tracking.*

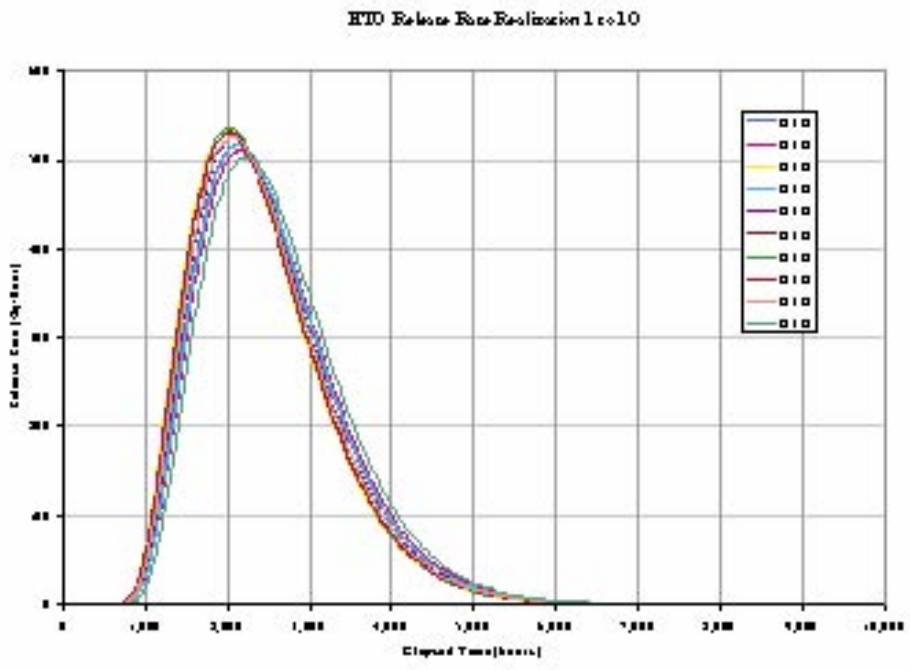

Figure 3-42. *Case 1b, HTO breakthrough for the first ten realizations, LTG.*

3.2.2.3 Case 1c: non-stationary transmissivity

While the spatial field of Case 1b was fairly similar to that of the Base case, the spatial field of Case 1c is clearly quite different (Figure 2-3). Case 1c uses the "peak and valley" approach, with 0.05 peaks and 0.05 troughs per m^2. In between peaks and troughs, the transmissivity field follows a moving average with a local perturbation of 4×10^{-10} m^2/s. These parameters produce clear, broad channels.

Particle tracks for Case 1c are shown in Figure 3-43 through Figure 3-45. The particle pathways clearly show the formation of bifurcating pathways within the fracture plane due to the spatial field. This pattern is clear for the 0.01 m transverse dispersion case, but is also significant when transverse dispersion is larger. Ultimately, this leads to the largest coverage of the fracture surface found in any of the cases studied.

As shown in Figure 3-46, increasing transverse dispersion has little effect on the tracer breakthrough curve t_5, t_{50}, and t_{95}. Increasing transverse dispersion does decrease the variability between realizations. Figure 3-47 shows statistical results from the Case 1c simulations for transport measures Q, 1/v, 1/bv, beta, and tau. Despite the significant difference between Case 1c and the Base case, the trend is very similar. Transverse dispersion does not significantly influence the transport measures for Case 1c.

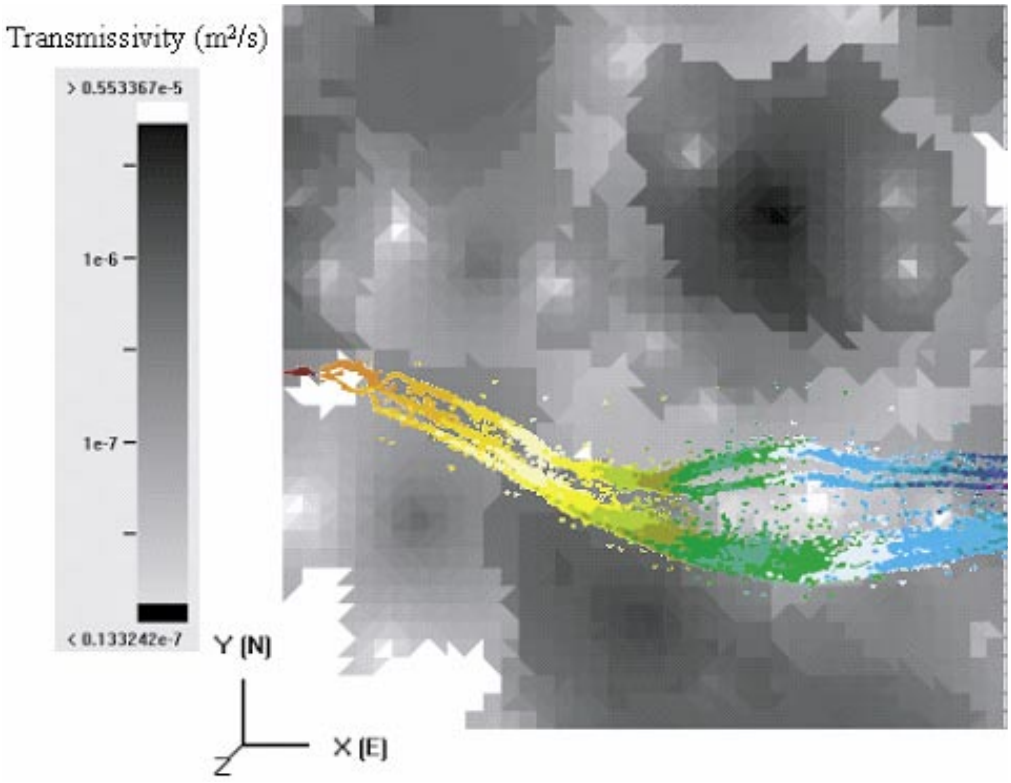

Figure 3-43. *Case 1c, geostatistical field, α_T = 0.01 m, particle tracking.*

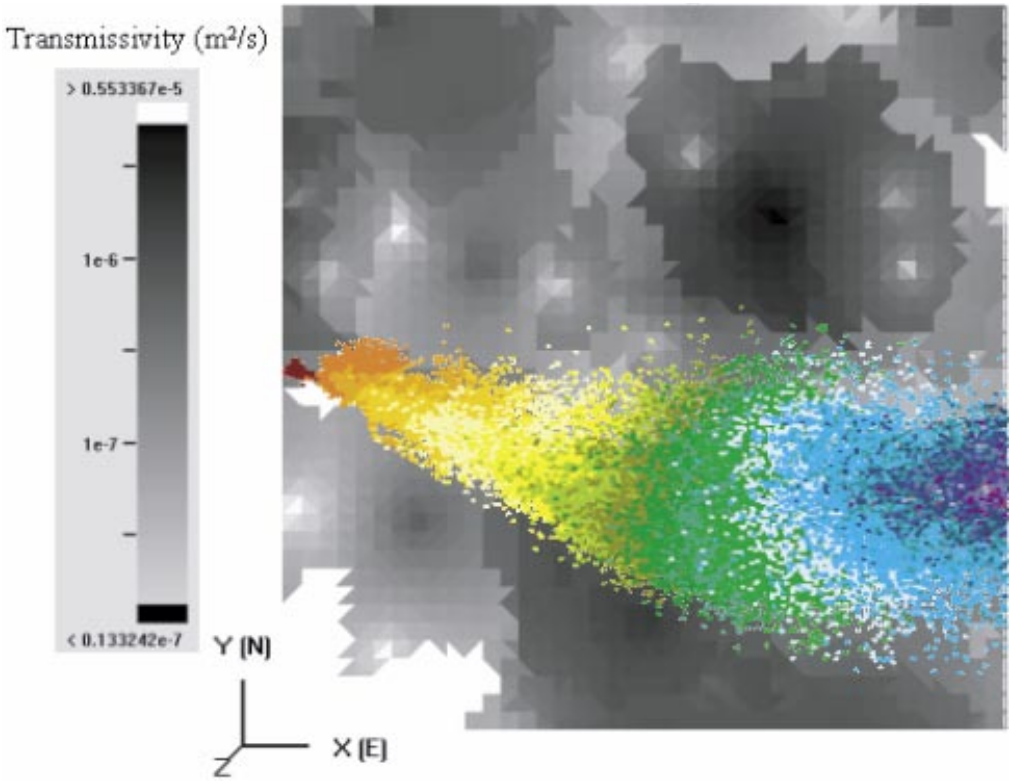

Figure 3-44. *Case 1c, geostatistical field, α_T = 1.0 m, particle tracking.*

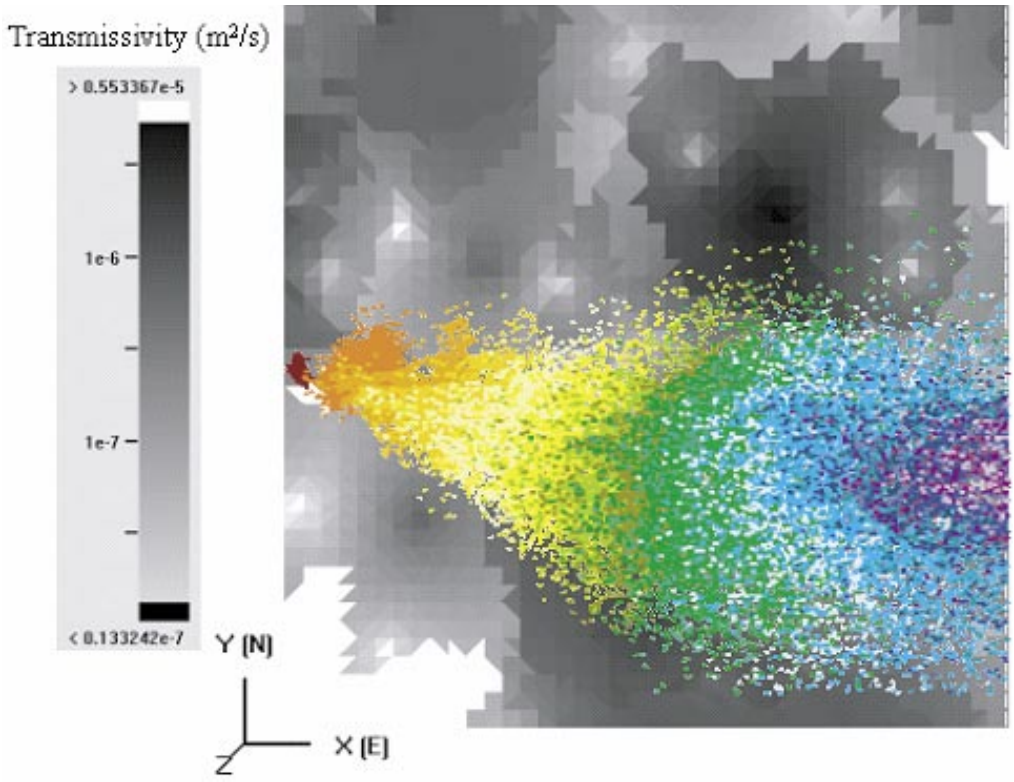

Figure 3-45. *Case 1c, geostatistical field, α_T = 10.0 m, particle tracking.*

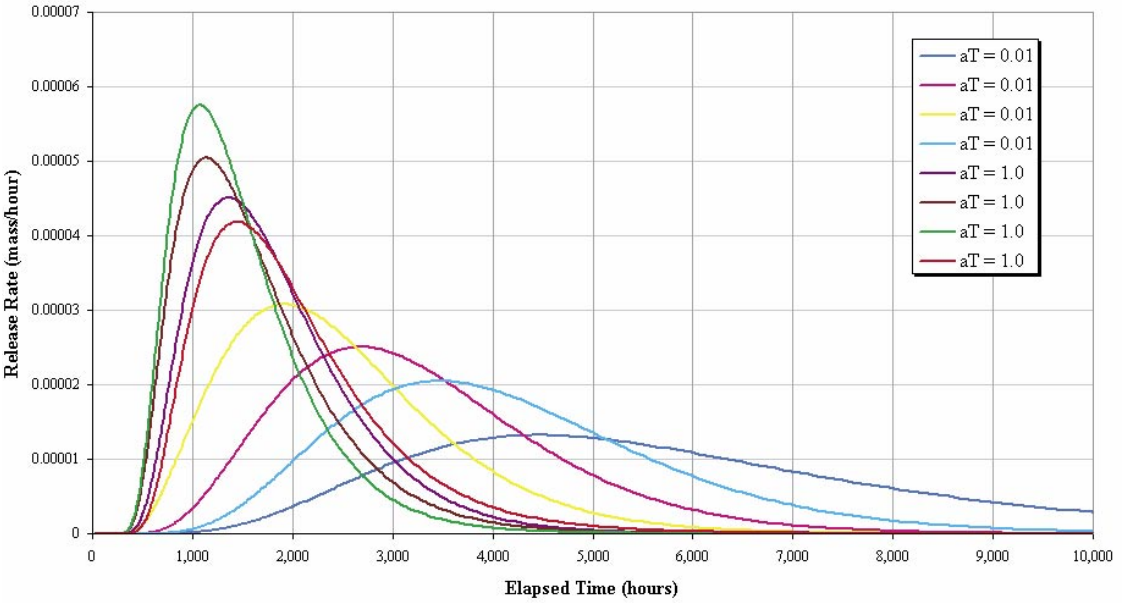

Figure 3-46. *Breakthrough curves for HTO for 4 realizations of Case 1c (α_T = 0.01, 1 m), LTG.*

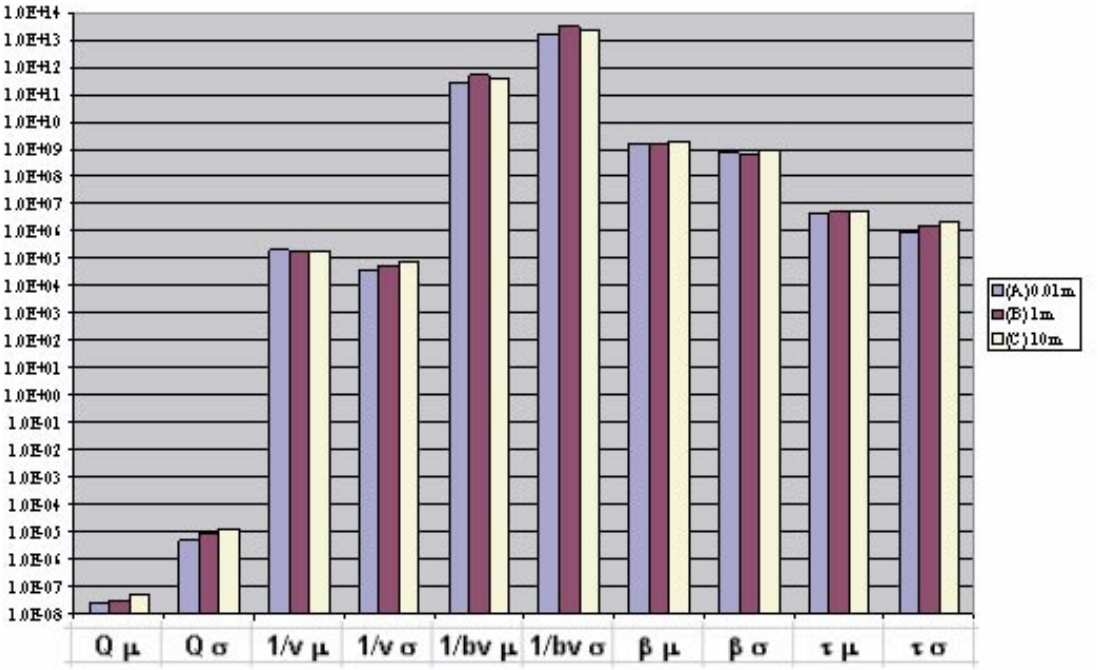

Figure 3-47. *Case 1c, statistics for all transport measures.*

3.2.2.4 Case 1d: Fracture Intersection Zone permeability enhanced

Stochastic continuum models used in the Base case, Case 1b, and Case 1c assume a smooth variation of transmissivity on the fracture surface based primarily on an aperture variation concept. Case 1d used a very different concept, in which transmissivity is enhanced at fracture intersections. For this case, the Oda tensor /Oda, 1984/ is used to assign transmissivity in each cell. Cells with intersecting fractures therefore have enhanced permeability, based on the transmissivity of both the primary and intersecting fractures. This results in the formation of a network of linear channels, surrounded by significantly less transmissive regions.

The pattern of linear channels imbedded in Case 1d means that transport can be relatively rapid, as long as there is a linear connection. However, transverse dispersion can move tracer off the primary pathway, and into slower regions of the fracture. Particle tracks for Case 1d are shown in Figure 3-48 through Figure 3-50. For small transverse dispersion, pathways are dominated by channels defined by fracture intersections. With moderate dispersion (1 m), tracer is spread to multiple channels. With the largest dispersion (10 m), tracer is spread throughout the fracture plane, including regions which would be expected to have much longer pathway travel-times.

Figure 3-32 and Figure 3-33 show the variation in breakthrough statistics with transverse dispersion for Case 1d. This case shows an interesting phenomenon. The increase in transverse dispersivity from 0.01 to 1 m causes an increase in variability, rather than a decrease in variability, and also significantly changes the breakthrough statistics. This may be due to the accessing of more FIZ channels. As transverse dispersivity is increased again to 10 m, the variability decreases, since all realizations share a common mix of pathways including FIZ channels and non-channel fracture area.

Transport measure statistics for Case 1d are provided in Figure 3-51.

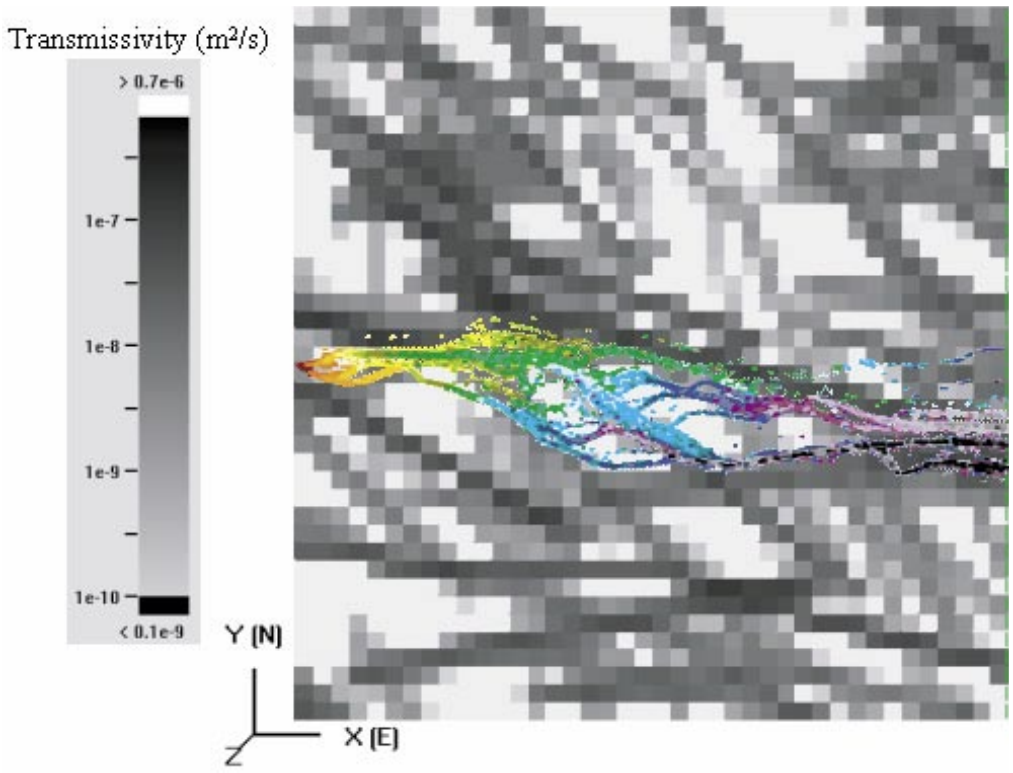

Figure 3-48. *Case 1d, Fracture Intersection Zones, α_T = 0.01 m, particle tracking.*

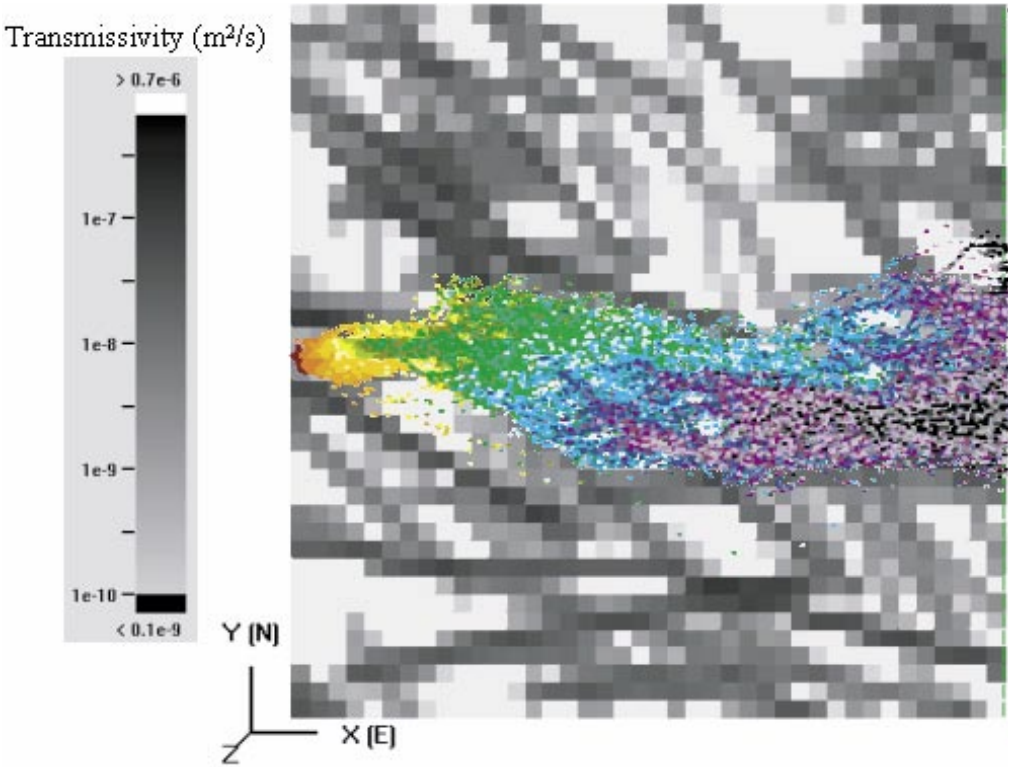

Figure 3-49. *Case 1d, Fracture Intersection Zones, α_T = 1.0 m, particle tracking.*

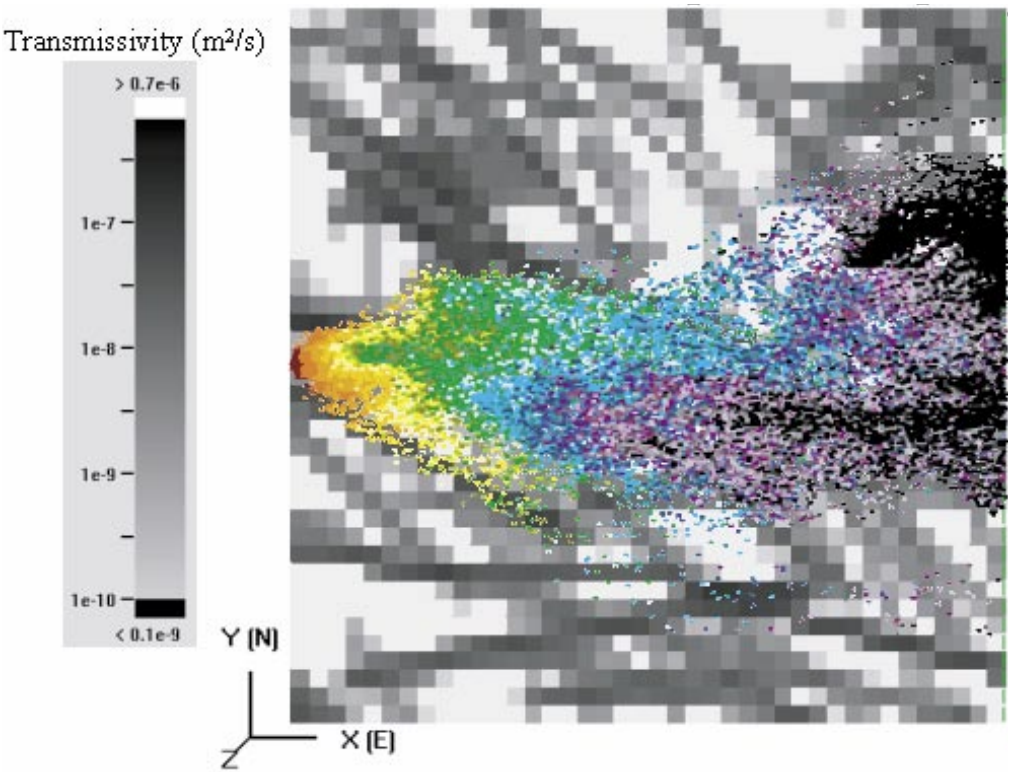

Figure 3-50. *Case 1d, Fracture Intersection Zones, α_T = 10.0 m, particle tracking.*

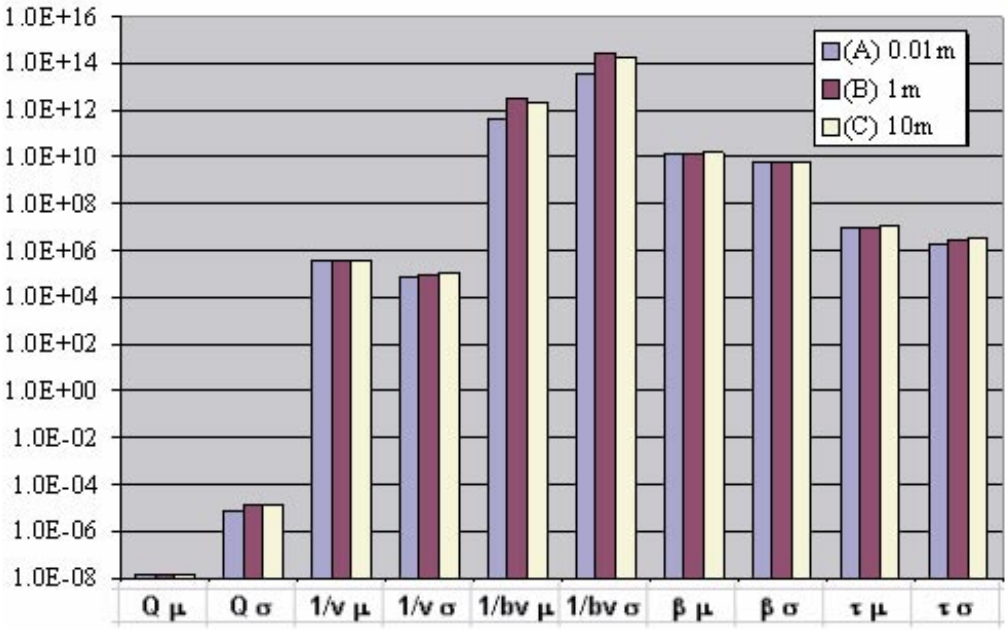

Figure 3-51. *Case 1d, statistics for all transport measures.*

3.3 Case 3: sorbing tracer transport

Simulations presented above assume conservative (HTO) tracer transport. For conservative tracers, the surface area accessed is of only secondary significance at the one year time scales studied. For sorbing tracer transport, retention is directly proportional to available surface area, and transverse dispersion, which accesses more surface area, therefore has a greater potential to influence solute transport.

Sorbing tracer transport was run for the Base case spatial field, using Cesium and Sodium as tracers, using the LTG approach. The following two cases were run:

- no immobile zones (Case 3a),
- maximized immobile zones (Case 3b).

In addition, sorbing tracers were run for the Base case 0. Immobile zone parameters are summarized in Table 3-5. Results using sorbing tracers are summarized in Table 3-6.

Table 3-5. Immobile zone parameters.

	Base case 0, Case 1a,b,c,d Case 2	**Case 3a no immobile zone**	**Case 3b maximum immobile zone**
Distribution coefficient Kd (m^3/kg)	HTO = 0 Cs = 8.0×10^{-4}	HTO = 0 Cs = 8.0×10^{-4}	HTO = 0 Cs = 8.0×10^{-4}
	Na = 1.4×10^{-6}	Na = 1.4×10^{-6}	Na = 1.4×10^{-6}
Porosity		0%	10%
Perimeter fraction	2	2	2
Diffusion thickness		0	0.1 m
Tortuosity		0.5	0.5
Rock density	2,700	2,700	2,700

Table 3-6. Statistical summary Case 3 immobile zone, LTG simulations.

Case	Transverse dispersion	t_5 (μ,σ)	t_{50} (μ,σ)	t_{95} (μ,σ)
0–L HTO	(A) 0.1 m	1,168.1, 79.3	2,369.4, 139.7	4,512.4, 219.5
	(B) 1 m	1,167.0, 45.7	2,383.5, 80.1	4,536.1, 112.8
	(C) 10 m	1,148.0, 23.3	2,377.0, 38.1	4,542.8, 58.4
0–L Cs	(A) 0.1 m	Na	Na	Na
	(B) 1 m	Na	Na	Na
	(C) 10 m	Na	Na	Na
0–L Na	(A) 0.1 m	1,098.4, 72.8	2,471.6, 158.4	5,445.2, 262.6
	(B) 1 m	1,096.1, 42.0	2,488.8, 90.2	5,473.8, 137.8
	(C) 10 m	1,077.4, 22.0	2,482.8, 41.9	5,472.6, 65.3
0–F HTO		818.2	1,909.1	4,363.6
0–F Cs		7,272.7	Na	Na
0–F Na		909.1	2,000	4,909.1
3a–L HTO	(A) 0.1 m	791.6, 33.7	1,298.4, 48.4	2,137.4, 74.7
	(B) 1 m	782.6, 19.4	1,296.1, 28.7	2,151.0, 41.6
	(C) 10 m	763.8, 13.7	1,293.4, 20.5	2,176.7, 33.2
3a–L Cs	(A) 0.1 m	791.6, 33.7	1,298.4, 48.5	2,137.3, 74.8
	(B) 1 m	782.7, 19.4	1,296.1, 28.7	2,150.9, 41.7
	(C) 10 m	763.9, 13.7	1,293.4, 20.5	2,186.6, 33.2
3a–L Na	(A) 0.1 m	791.6, 33.7	1,298.4, 48.5	2,139.3, 74.8
	(B) 1 m	782.7, 19.4	1,296.1, 28.7	2,150.9, 41.7
	(C) 10 m	763.9, 13.7	1,293.4, 20.5	2,176.6, 33.2
3a–F HTO		727.3	1,090.9	1,818.2
3b–L HTO	(A) 0.1 m	9,753.4, 123.5	Na	Na
	(B) 1 m	Na	Na	Na
	(C) 10 m	Na	Na	Na
3b–L Cs	(A) 0.1 m	Na	Na	Na
	(B) 1 m	Na	Na	Na
	(C) 10 m	Na	Na	Na
3b–L Na	(A) 0.1 m	9,033.2, 401.8	Na	Na
	(B) 1 m	9,659.1, 224.7	Na	Na
	(C) 10 m	9,871.2, 131.2	Na	Na
3b–F HTO		4,909.09	Na	Na
3b–F Cs		Na	Na	Na
3b–F Na		3,545.45	Na	Na

The first issue to be addressed is whether the difference in sorbing tracer transport due to transverse dispersion is significant relative to the difference between realizations. Figure 3-52 and Figure 3-53 present breakthrough curves of four realizations of the Base case using each of the dispersion values. Transverse dispersion does have a very clear and significant influence on the solute breakthrough. In general, transverse dispersion increases the length of the tails by increasing area available for diffusion. Also, as for the conservative tracers, transverse dispersion reduces the variability between realizations.

The Base case, Case 3a, and Case 3b are compared in Figure 3-54 through Figure 3-56. Looking at Figure 3-54, it can be seen that even for a non-sorbing tracer, the "maximum immobile zone" provides a strong retention effect. Figure 3-56 can be used to gauge the relative effect of transverse dispersion when compared against the immobile zone properties for a sorbing tracer (Na). The effect of transverse dispersion does not appear significant. So, for a given transmissivity pattern, the transverse dispersion has a significant influence on breakthrough. However, for an ensemble of transmissivity patterns, the influence of transverse dispersion is minor.

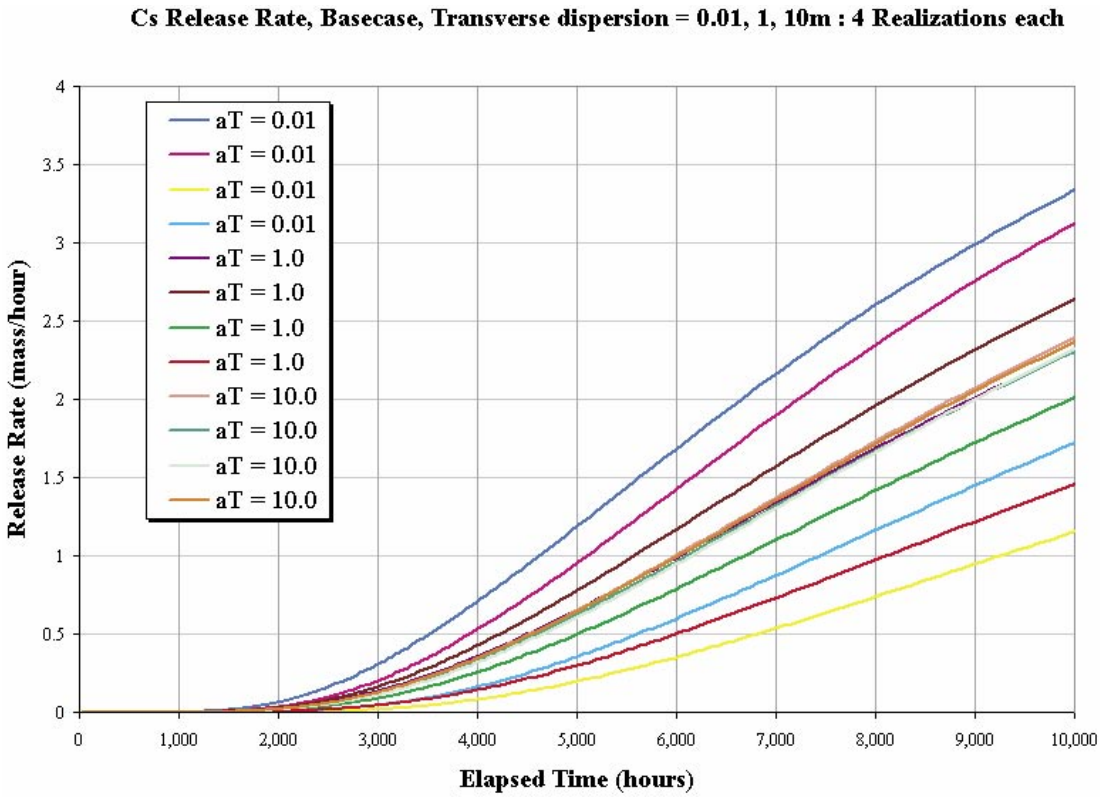

Figure 3-52. *Breakthrough curves for Cs for 4 realizations of the Base case(α_T = 0.01, 1 and 10 m), LTG.*

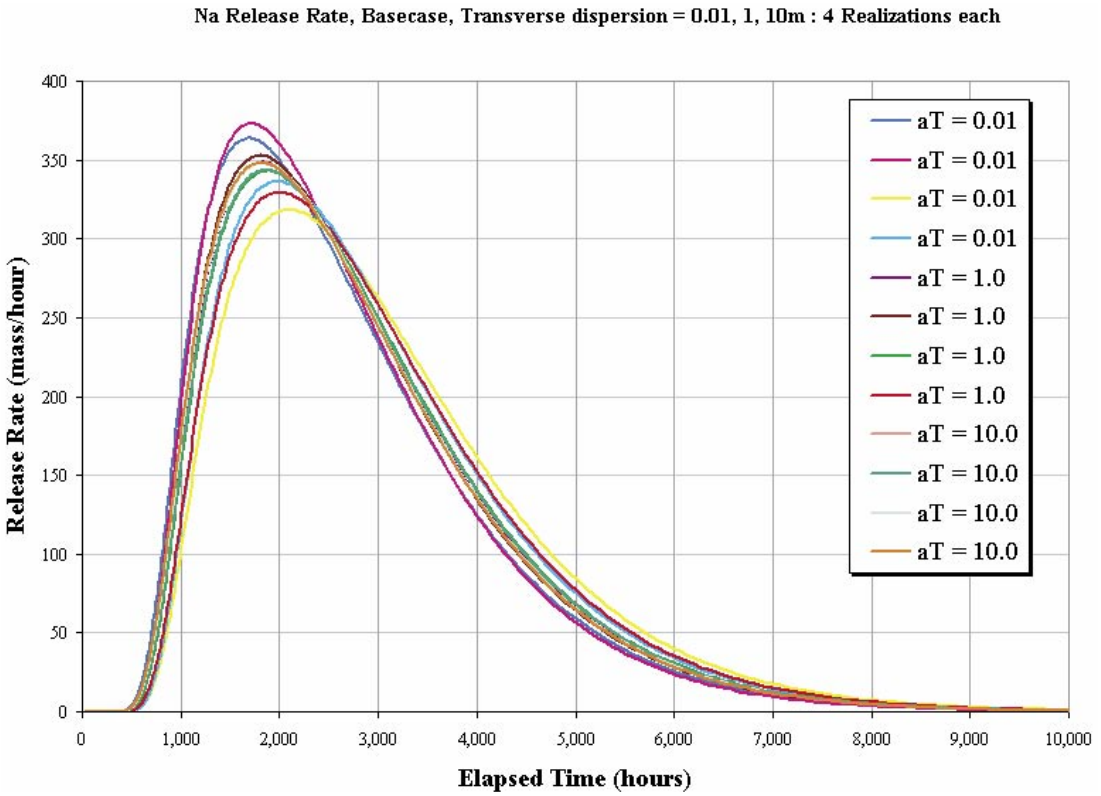

Figure 3-53. *Breakthrough curves for Na for 4 realizations of the Base case(α_T = 0.01, 1 and 10 m), LTG.*

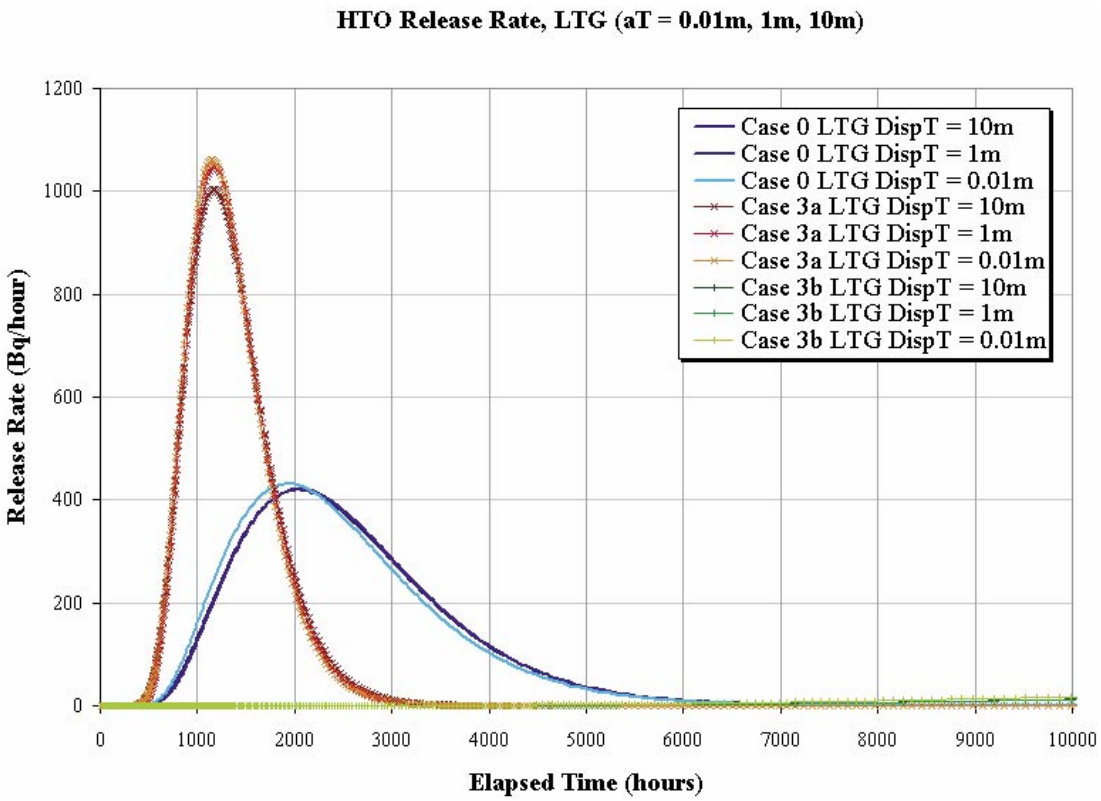

Figure 3-54. *Breakthrough curves for HTO for a single realization of the Base case, Case 3a, and 3b(α_T = 0.01, 1 and 10 m), LTG.*

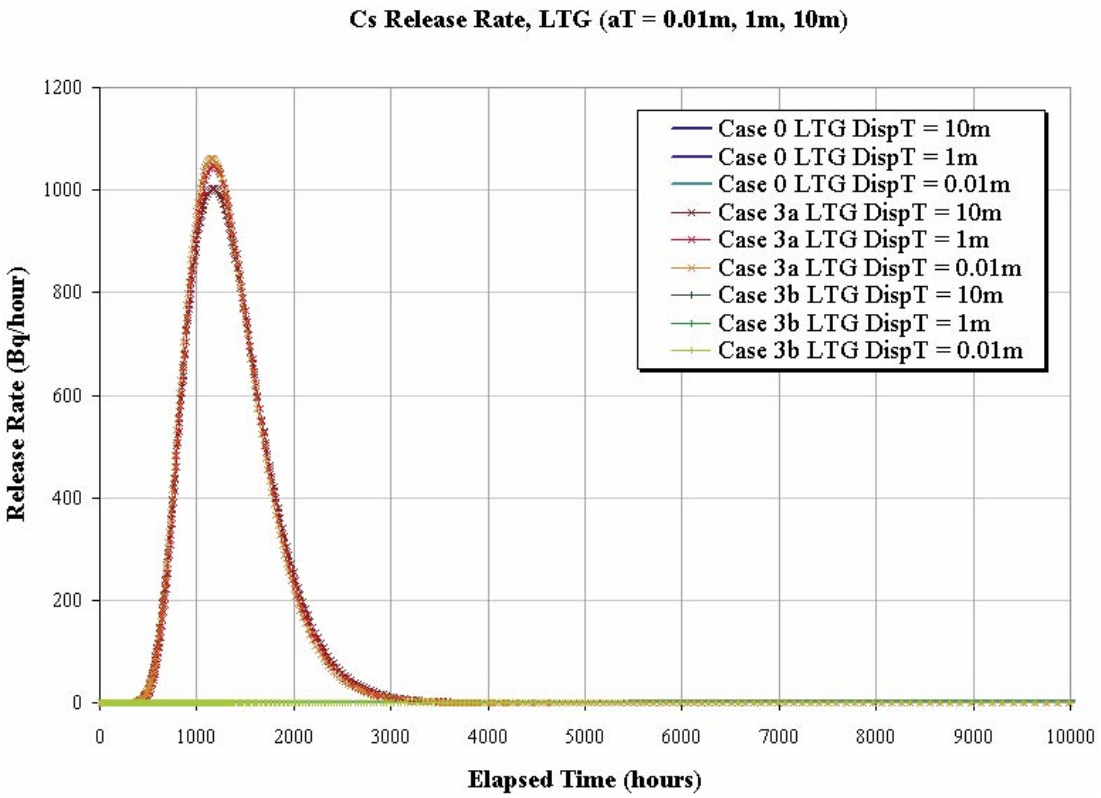

Figure 3-55. *Breakthrough curves for Cs for a single realization of the Base case, Case 3a, and 3b(α_T = 0.01, 1 and 10 m), LTG.*

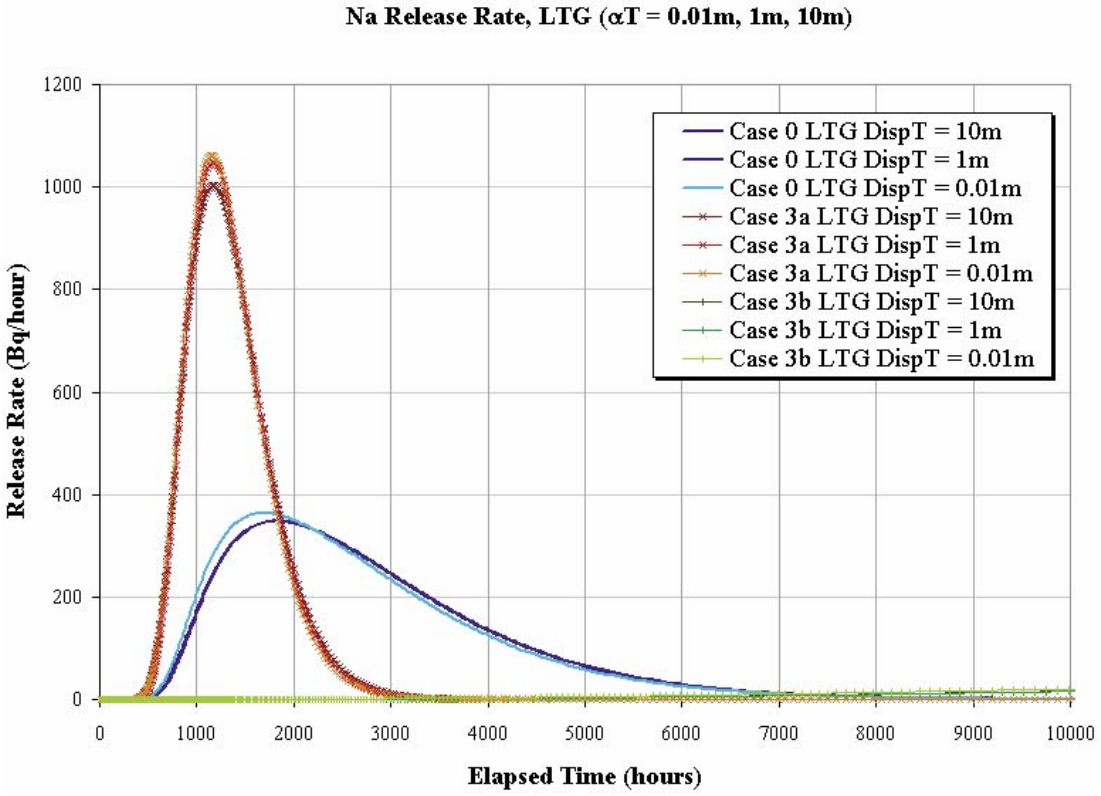

Figure 3-56. *Breakthrough curves for Na for a single realization of the Base case, Case 3a, and 3b(α_T = 0.01, 1 and 10 m), LTG.*

3.4 Case 2: source term size

The simulations reported in Sections 3.2.1 and 3.2.2 used a source term of 0.05 m length on the upgradient side of the fracture, with the sink defined over the entire 20 m length of the downgradient side of the fracture. To a certain extent, this is maximizing the possible effect of transverse dispersion, since diffusive processes are necessary to transform the transport pathways from 1D to 2D. At the same time, however, the effect of channelization might be larger with a source terms which introduces tracer into a larger portion of the fracture plane.

Cases 2a, 2b, and 2c study the effect of source terms sizes of 1, 5, and 10 m scale respectively. Figure 3-57 through Figure 3-65 present particle tracks for these simulations. The particle pathways are clearly influenced by the source term's size. However, the effect of transverse dispersions of 0.01, 1, and 10 m are fairly comparable between the different source term scales. For the 0.01 m transverse dispersion, pathways are clear and distinct for all the source sizes. For the 10 m transverse dispersion, the pathways merge into a single wide path. Results of these simulations are summarized in Table 3-7 and Table 3-8.

These simulations were carried out using the Base case stochastic field. The simulation results from LTG illustrating the effect of source term size are shown in Figure 3-66 through Figure 3-68. The mean and standard deviation for transport statistics for each of the cases are provided in Figure 3-69 through Figure 3-74.

Table 3-7. Statistical summary Case 2 source term, LTG simulations.

Case	Transverse dispersion	t_5 (μ,σ)	t_{50} (μ,σ)	t_{95} (μ,σ)
0–L	(A) 0.1 m	1,168.1, 79.3	2,369.4, 139.7	4,512.4, 219.5
	(B) 1 m	1,167.0, 45.7	2,383.5, 80.1	4,536.1, 112.8
	(C) 10 m	1,148.0, 23.3	2,377.0, 38.1	4,542.8, 58.4
2a–L	(A) 0.1 m	1,162.3, 73.8	2,365.6, 136.3	4,515.4, 224.7
	(B) 1 m	1,165.8, 46.4	2,381.9, 80.8	4,534.2, 113.6
	(C) 10 m	1,147.6, 23.4	2,376.4, 38.3	4,542.1, 58.7
2b–L	(A) 0.1 m	1,163.2, 70.8	2,382.4, 142.7	4,573.4, 264.9
	(B) 1 m	1,165.7, 46.4	2,382.9, 77.9	4,537.3, 105.8
	(C) 10 m	1,148.0, 22.5	2,377.0, 36.8	4,542.8, 56.7
2c–L	(A) 0.1 m	1,148.3, 56.9	2,372.1, 116.3	4,584.1, 221.0
	(B) 1 m	1,161.1, 37.5	2,379.3, 62.0	4,536.7, 82.6
	(C) 10 m	1,147.2, 20.9	2,376.5, 36.7	4,542.7, 59.0

Table 3-8. Statistical summary Case 2 source term, particle tracking simulations.

Case	Transverse Dispersion	Q (μ,σ)	1/v (μ,σ)	1/bv (μ,σ)	β (μ,σ)	τ (μ,σ)
0–P	(A) 0.1 m	1.5×10^{-8}, 8.3×10^{-6}	2.4×10^{5}, 3.3×10^{4}	2.4×10^{11}, 2.6×10^{13}	2.6×10^{9}, 5.5×10^{8}	5.2×10^{6}, 8.1×10^{5}
	(B) 1 m	1.8×10^{-8}, 1.5×10^{-5}	2.2×10^{5}, 4.4×10^{4}	5.8×10^{11}, 4.6×10^{13}	3.0×10^{9}, 7.3×10^{8}	5.9×10^{6}, 1.3×10^{5}
	(C) 10 m	2.2×10^{-8}, 1.8×10^{-5}	2.3×10^{5}, 5.7×10^{4}	3.9×10^{11}, 2.1×10^{13}	3.2×10^{9}, 9.2×10^{8}	6.4×10^{6}, 1.7×10^{5}

Case	Transverse Dispersion	Q (μ,σ)	1/v (μ,σ)	1/bv (μ,σ)	β (μ,σ)	τ (μ,σ)
2a–P	(A) 0.1 m	1.5×10^{-8}, 6.6×10^{-6}	2.4×10^{5}, 3.2×10^{4}	1.3×10^{11}, 1.2×10^{13}	2.5×10^{9}, 5.3×10^{8}	5.2×10^{6}, 7.9×10^{5}
	(B) 1 m	1.8×10^{-8}, 1.2×10^{-5}	2.2×10^{5}, 4.2×10^{4}	2.9×10^{11}, 3.3×10^{13}	2.9×10^{9}, 7.2×10^{8}	5.9×10^{6}, 1.3×10^{6}
	(C) 10 m	1.9×10^{-8}, 1.4×10^{-5}	2.3×10^{5}, 5.5×10^{4}	3.2×10^{11}, 3.0×10^{13}	3.2×10^{9}, 8.9×10^{8}	6.5×10^{6}, 1.7×10^{6}
2b–P	(A) 0.1 m	1.5×10^{-8}, 7.3×10^{-6}	2.4×10^{5}, 3.3×10^{4}	4.9×10^{10}, 5.7×10^{12}	2.5×10^{9}, 5.6×10^{8}	5.2×10^{6}, 8.0×10^{5}
	(B) 1 m	1.8×10^{-8}, 1.4×10^{-5}	2.2×10^{5}, 4.4×10^{4}	1.6×10^{11}, 2.3×10^{13}	2.9×10^{9}, 7.5×10^{8}	5.9×10^{6}, 1.3×10^{6}
	(C) 10 m	1.9×10^{-8}, 1.5×10^{-5}	2.3×10^{5}, 5.6×10^{4}	1.4×10^{11}, 1.6×10^{13}	3.2×10^{9}, 9.1×10^{8}	6.5×10^{6}, 1.7×10^{6}
2c–P	(A) 0.1 m	1.5×10^{-8}, 7.4×10^{-6}	2.4×10^{5}, 3.5×10^{4}	2.6×10^{10}, 3.7×10^{12}	2.5×10^{9}, 6.1×10^{8}	5.2×10^{6}, 8.4×10^{5}
	(B) 1 m	1.8×10^{-8}, 1.4×10^{-5}	2.2×10^{5}, 4.6×10^{4}	1.0×10^{11}, 1.5×10^{13}	2.9×10^{9}, 7.9×10^{8}	5.9×10^{6}, 1.3×10^{6}
	(C) 10 m	1.9×10^{-8}, 1.6×10^{-5}	2.3×10^{5}, 5.9×10^{4}	9.7×10^{10}, 1.3×10^{13}	3.2×10^{9}, 9.6×10^{8}	6.4×10^{6}, 1.7×10^{6}

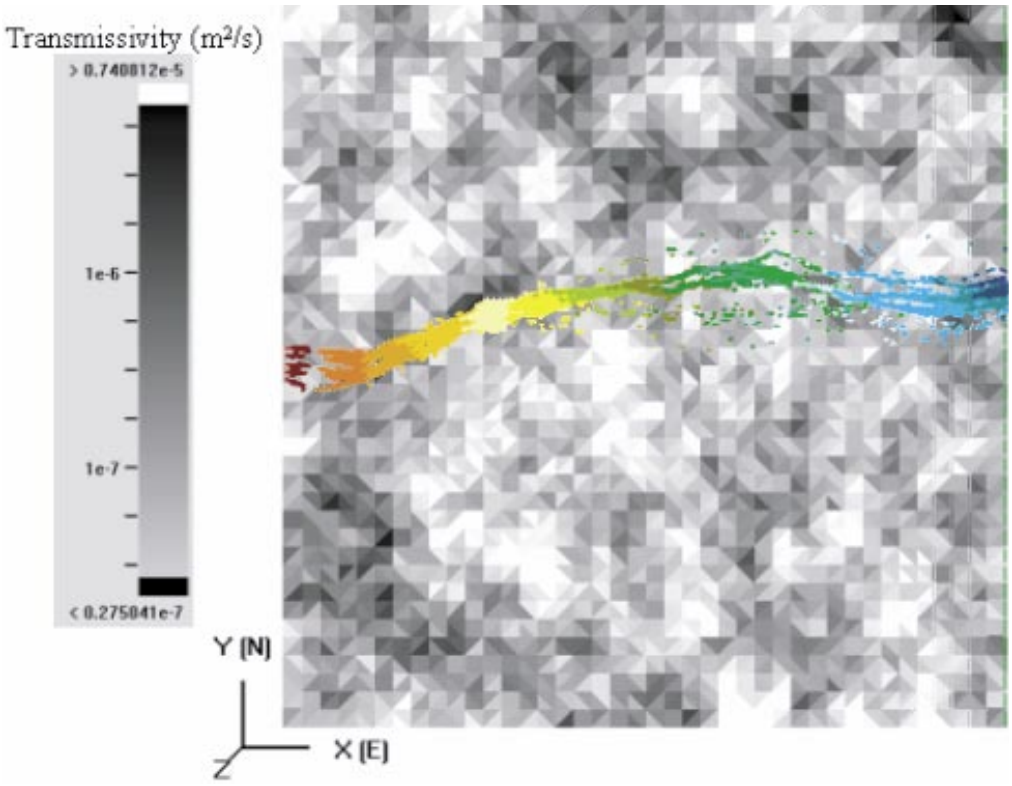

Figure 3-57. *Case 2a Source 1 m, α_T = 0.01 m, particle tracking.*

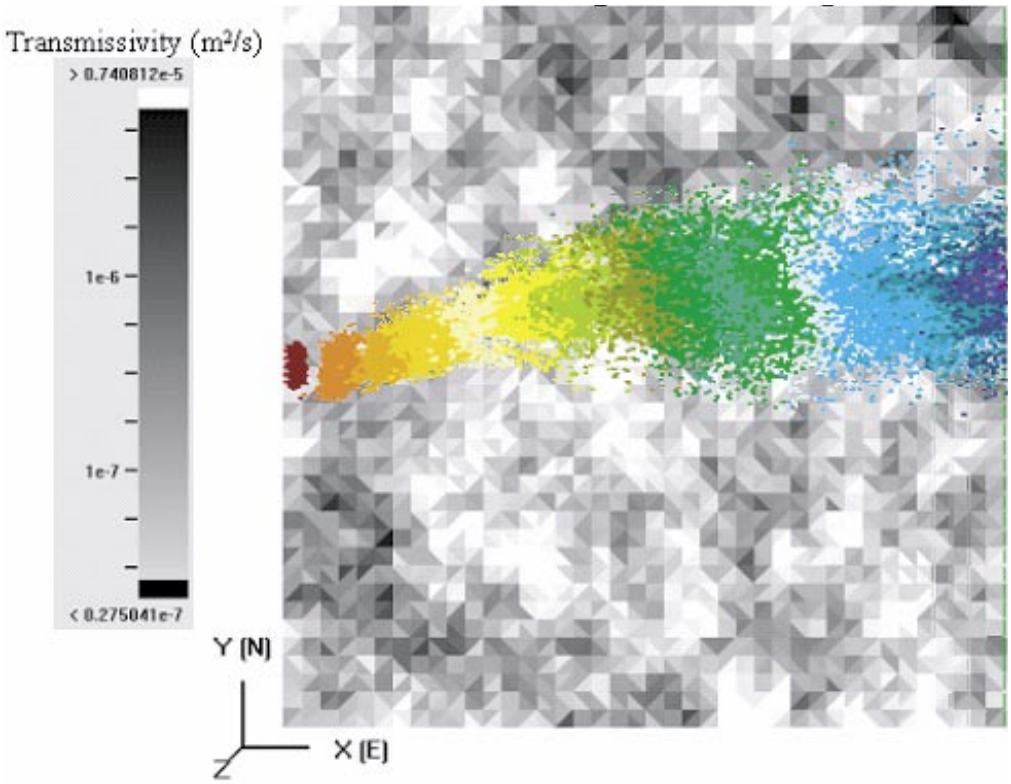

Figure 3-58. *Case 2a Source 1 m, α_T = 1.0 m, particle tracking.*

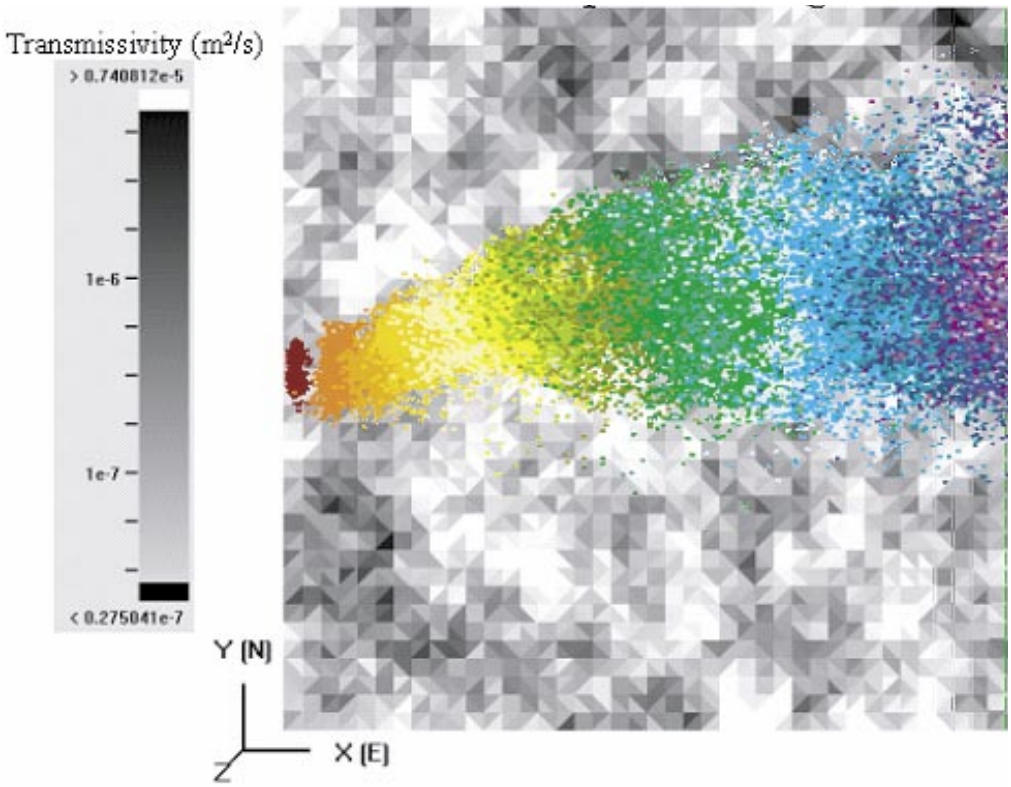

Figure 3-59. *Case 2a Source 1 m, α_T = 10.0 m, particle tracking.*

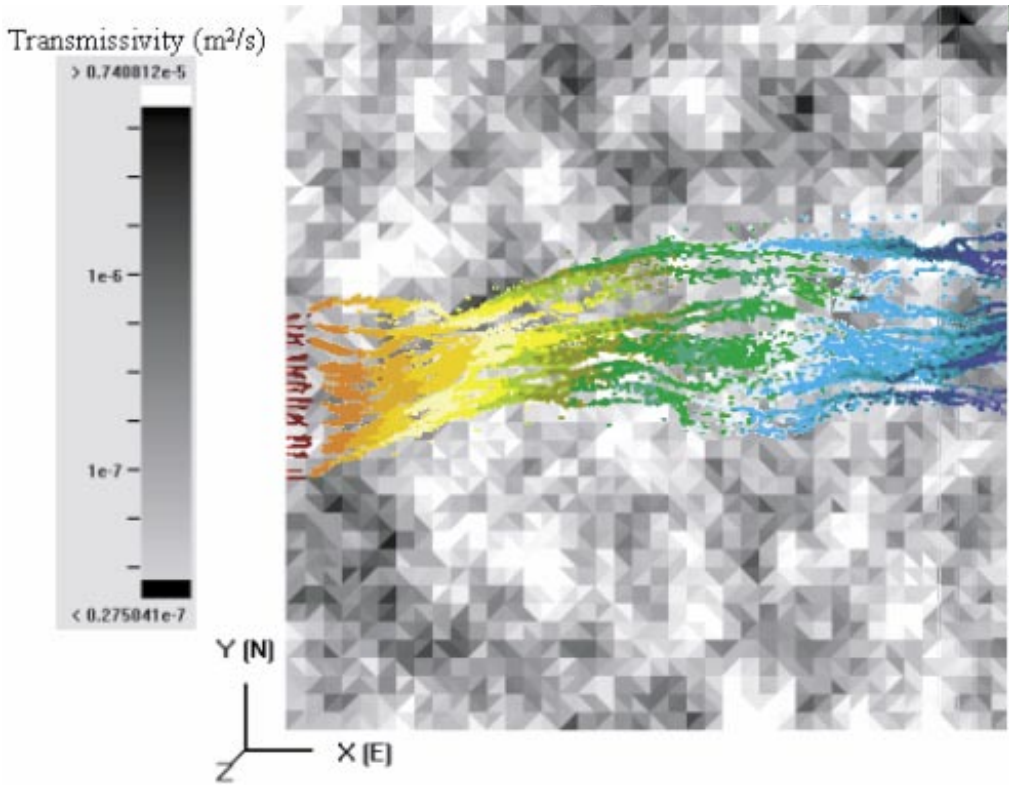

Figure 3-60. *Case 2b Source 5 m, α_T = 0.01 m, particle tracking.*

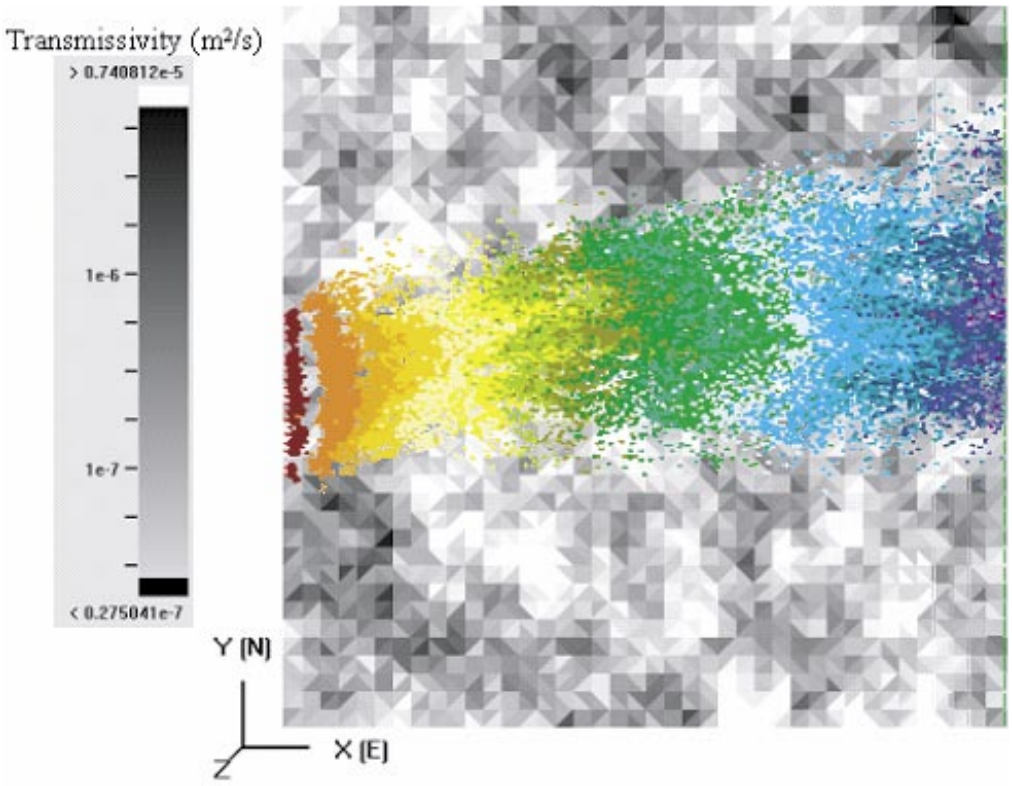

Figure 3-61. *Case 2b Source 5 m, α_T = 1.0 m, particle tracking.*

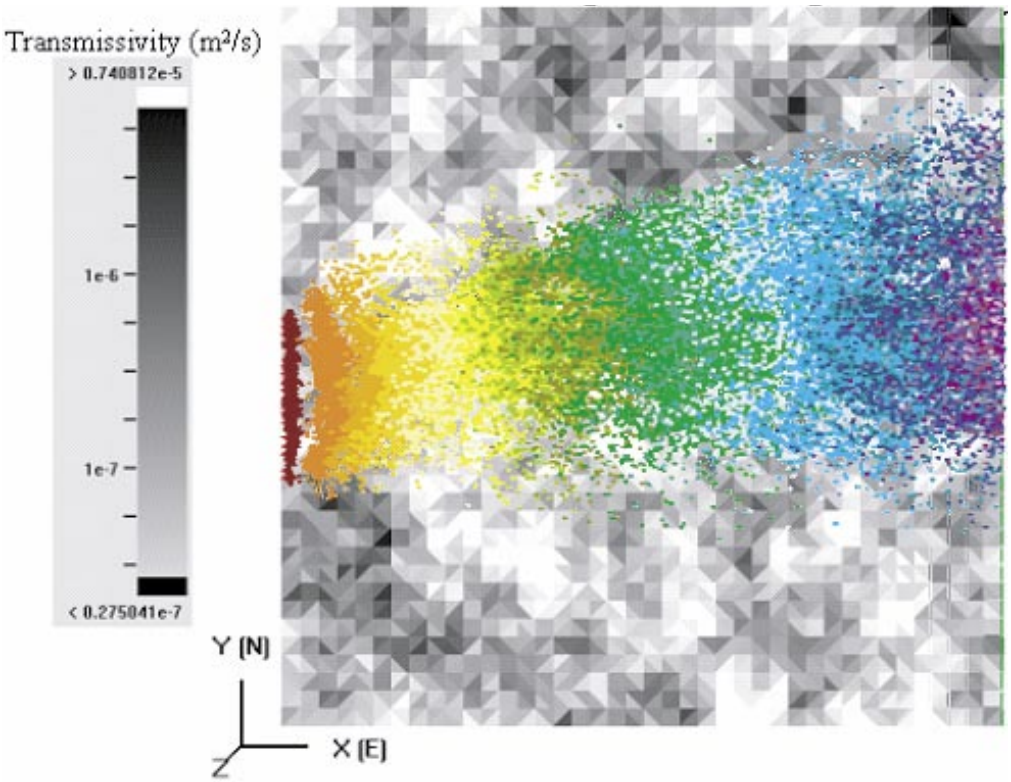

Figure 3-62. *Case 2b Source 5 m, α_T = 10.0 m, particle tracking.*

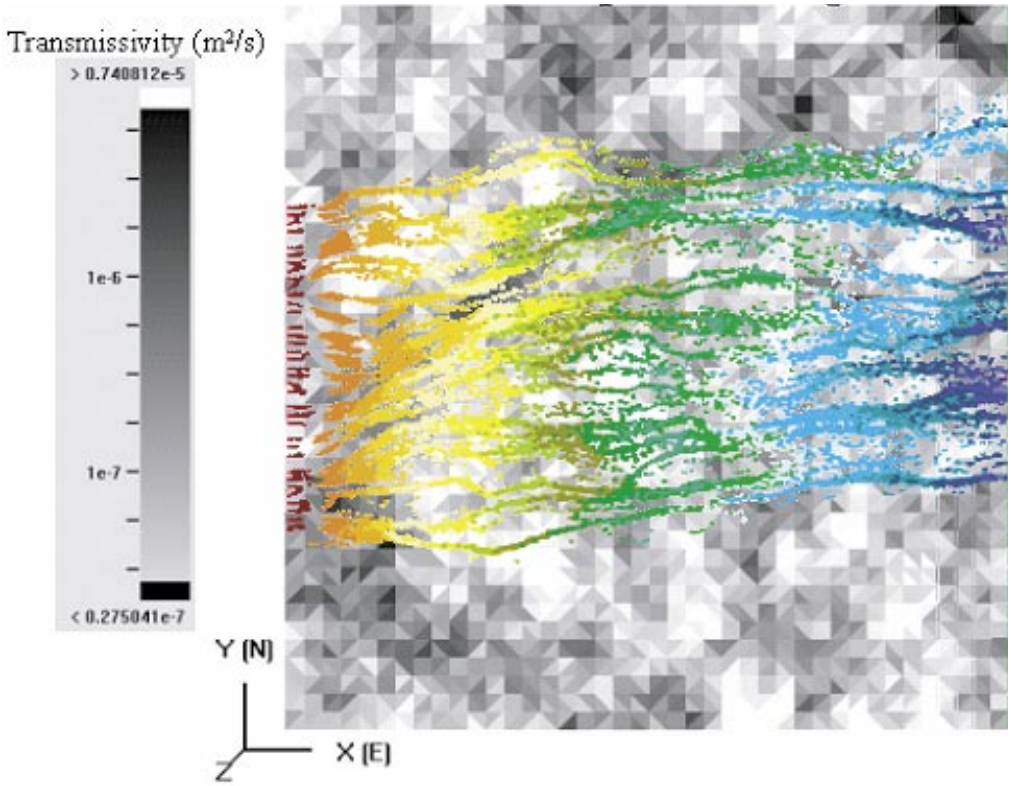

Figure 3-63. *Case 2c Source 10 m, α_T = 0.01 m, particle tracking.*

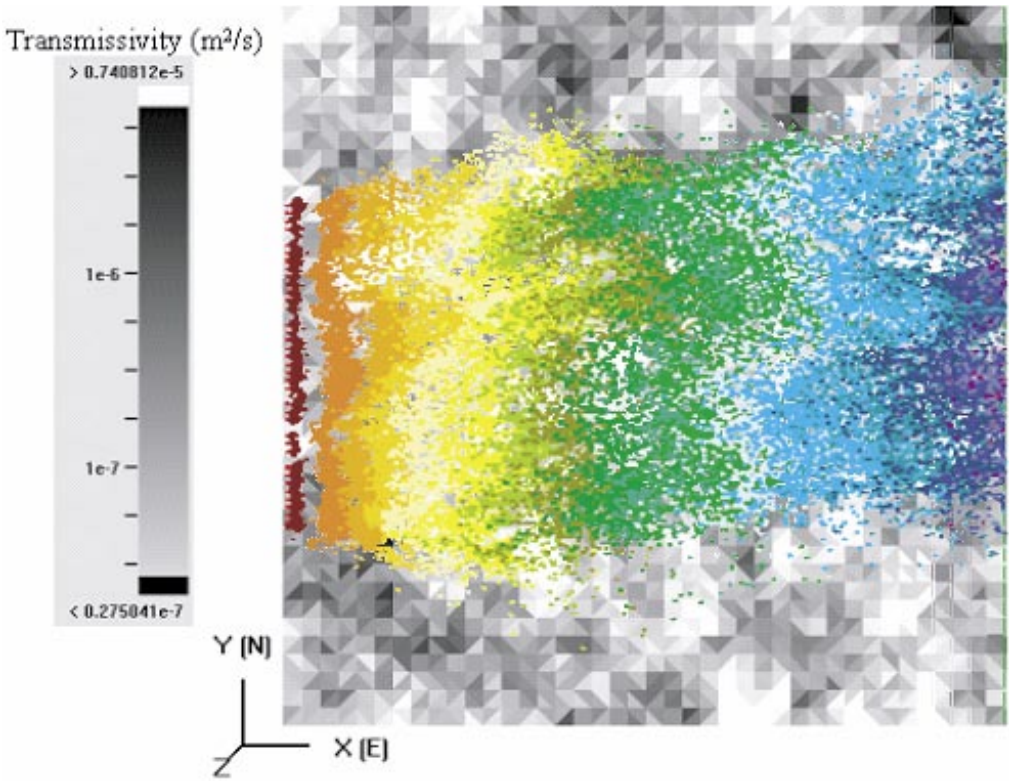

Figure 3-64. *Case 2c Source 10 m, α_T = 1.0 m, particle tracking.*

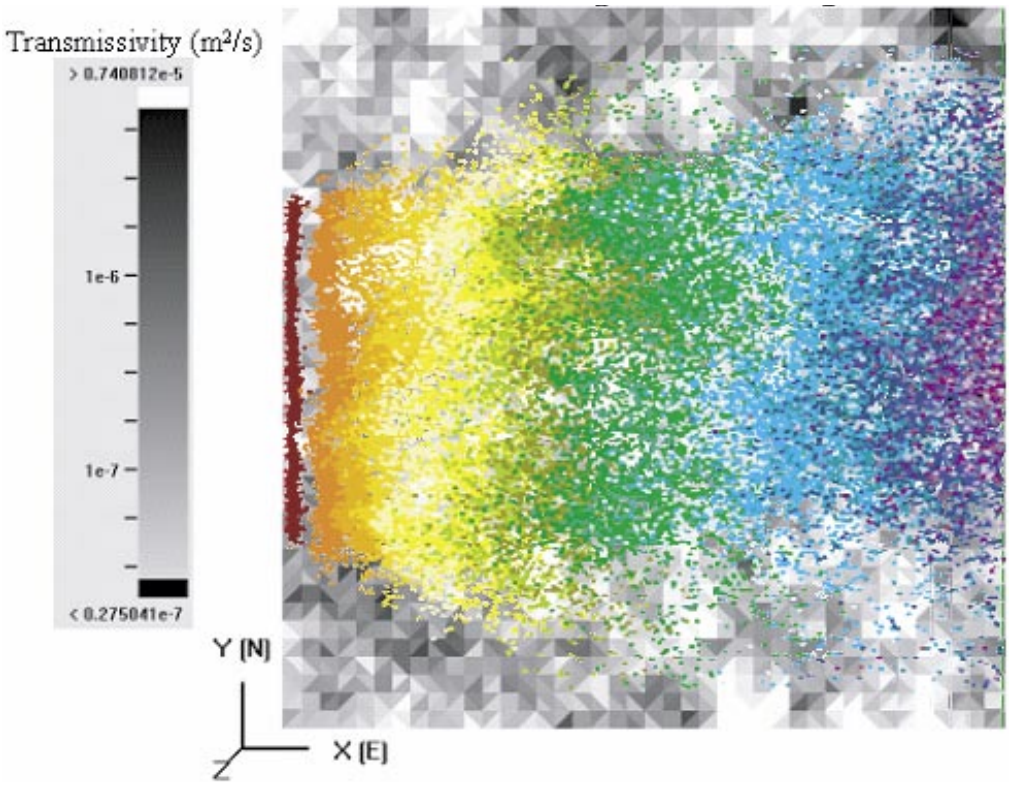

Figure 3-65. *Case 2c Source 1 m, α_T = 10.0 m, particle tracking.*

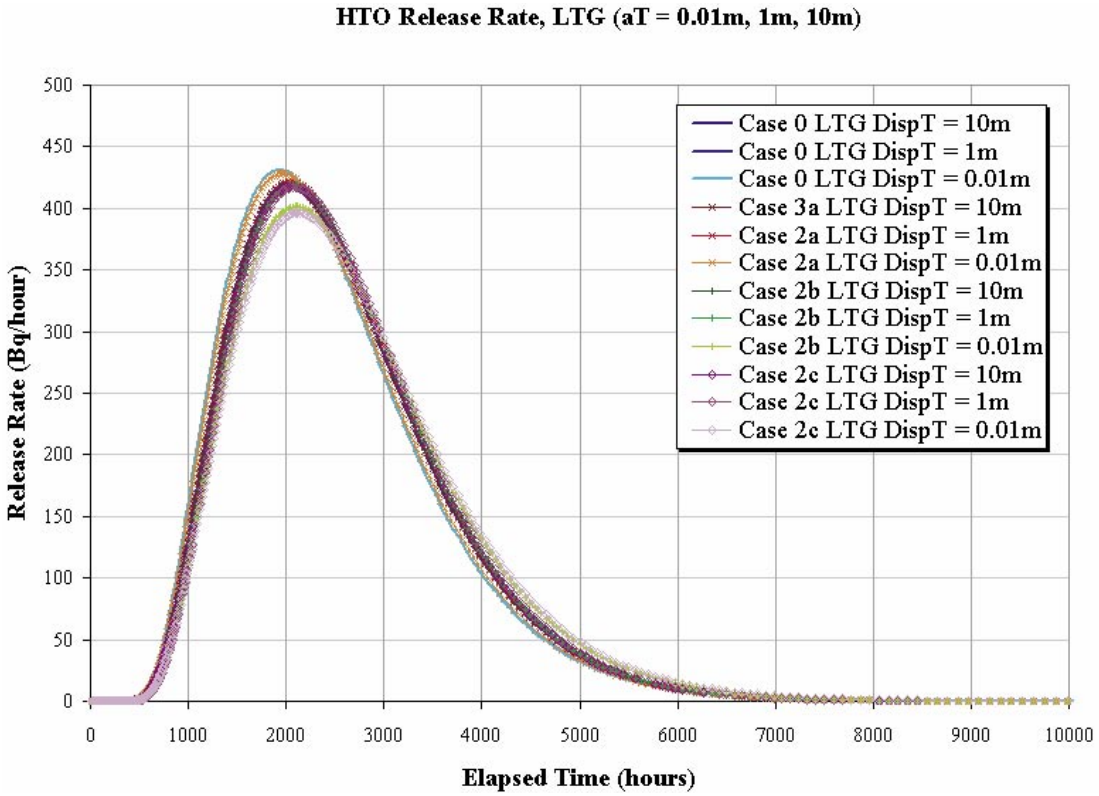

Figure 3-66. *Breakthrough curves for HTO for a single realization of the Base case, Case 2a, 2b, and 2c (α_T = 0.01, 1 and 10 m), LTG.*

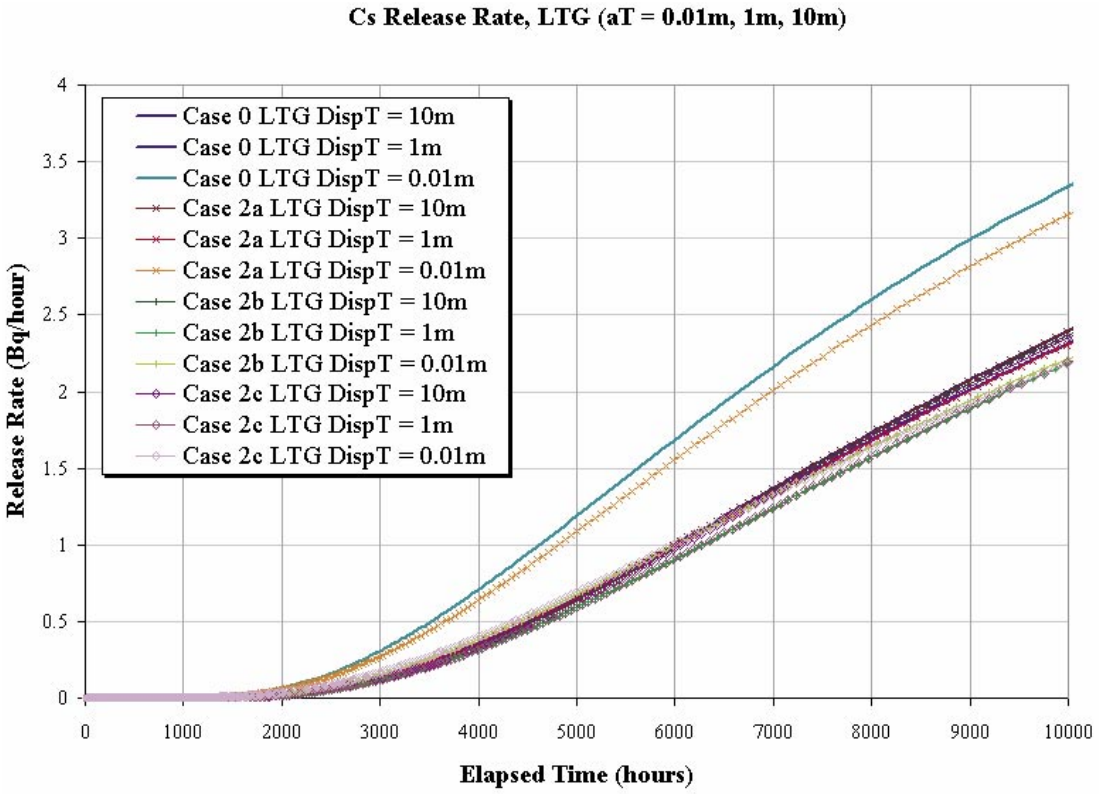

Figure 3-67. *Breakthrough curves for Cs for a single realization of the Base case, Case 2a, 2b, and 2c (α_T = 0.01, 1 and 10 m), LTG.*

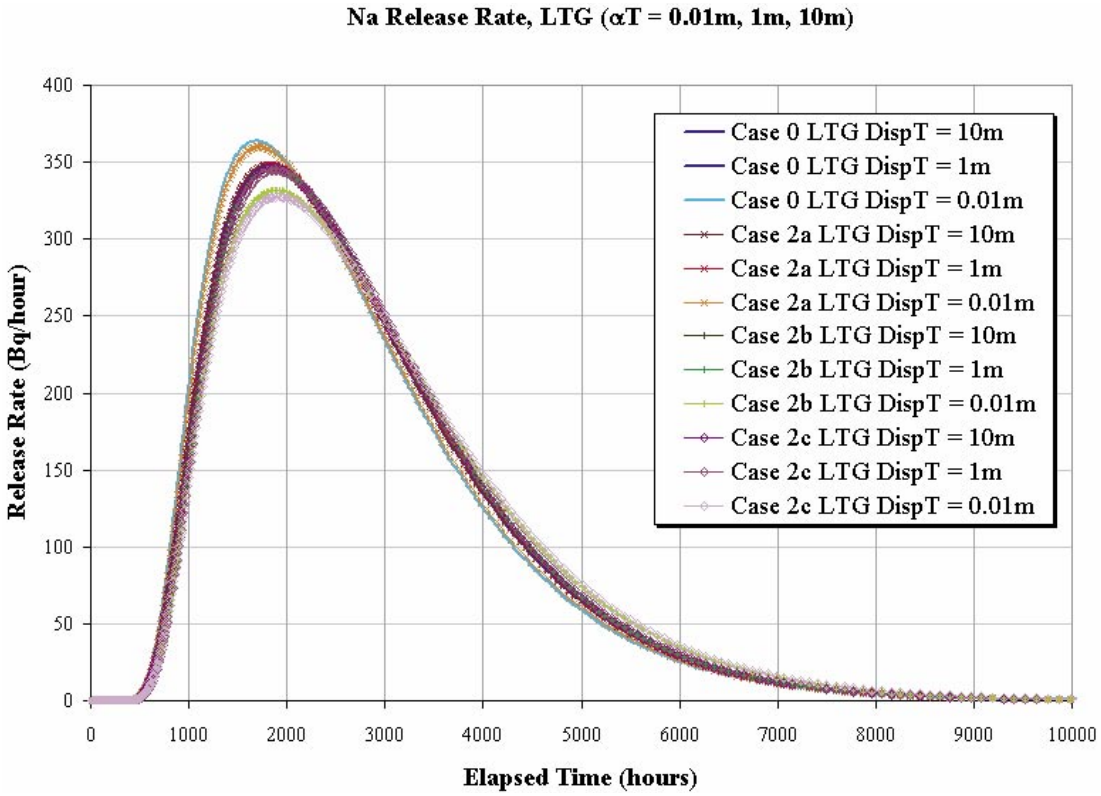

Figure 3-68. *Breakthrough curves for Na for a single realization of the Base case, Case 2a, 2b, and 2c (α_T = 0.01, 1 and 10 m), LTG.*

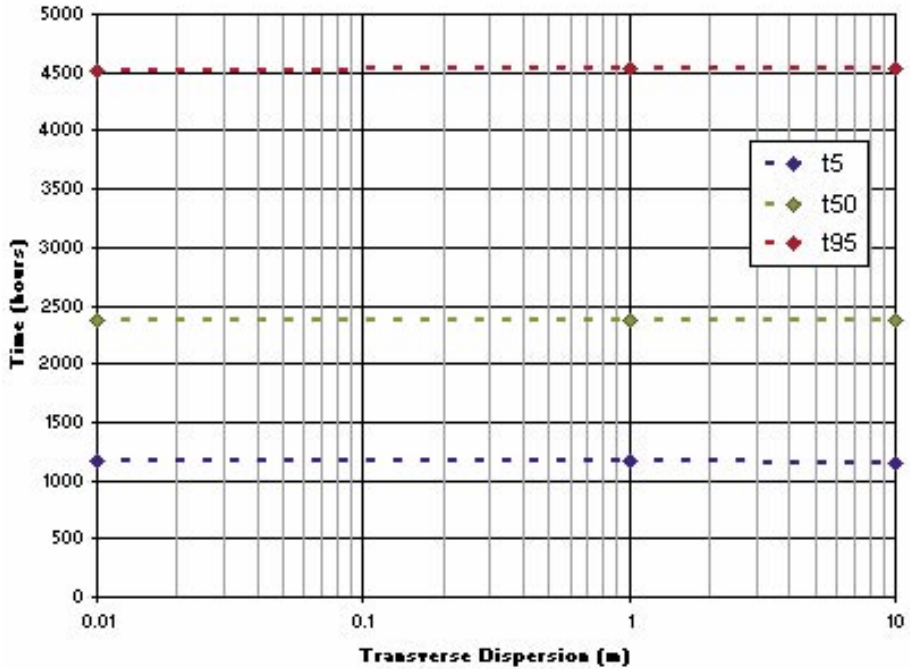

Figure 3-69. *Case 2a, HTO, distribution of mean t_5, t_{50}, t_{95}, LTG.*

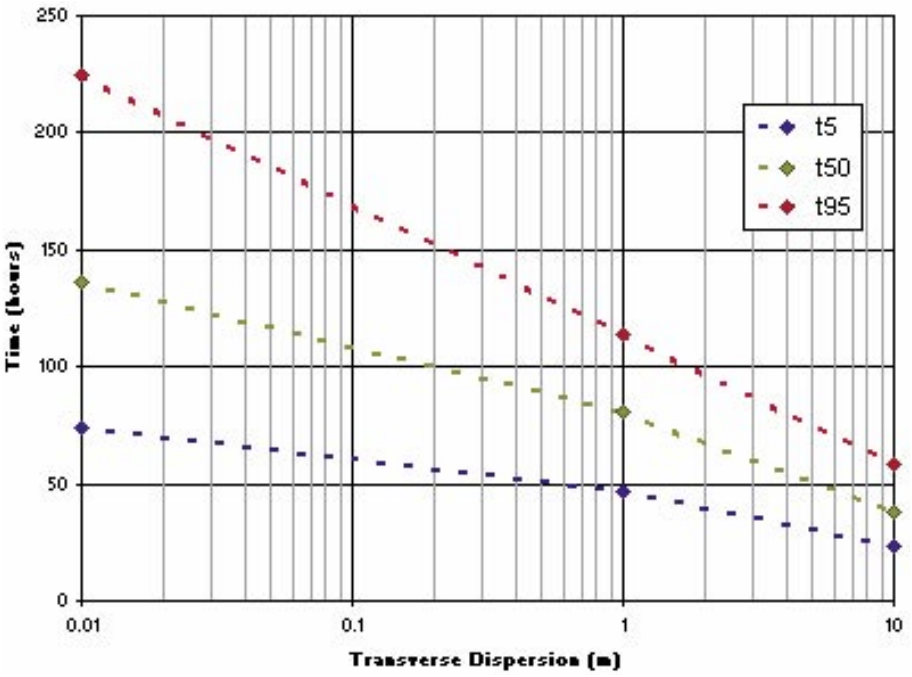

Figure 3-70. *Case 2a, HTO, distribution of st dev t_5, t_{50}, t_{95}, LTG.*

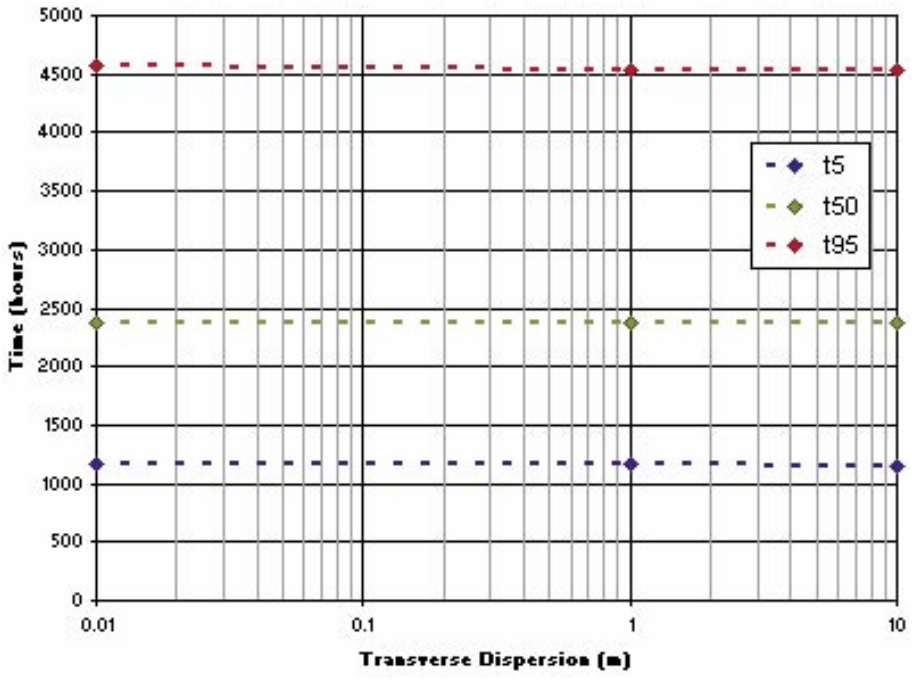

Figure 3-71. *Case 2b, HTO, distribution of mean t_5, t_{50}, t_{95}, LTG.*

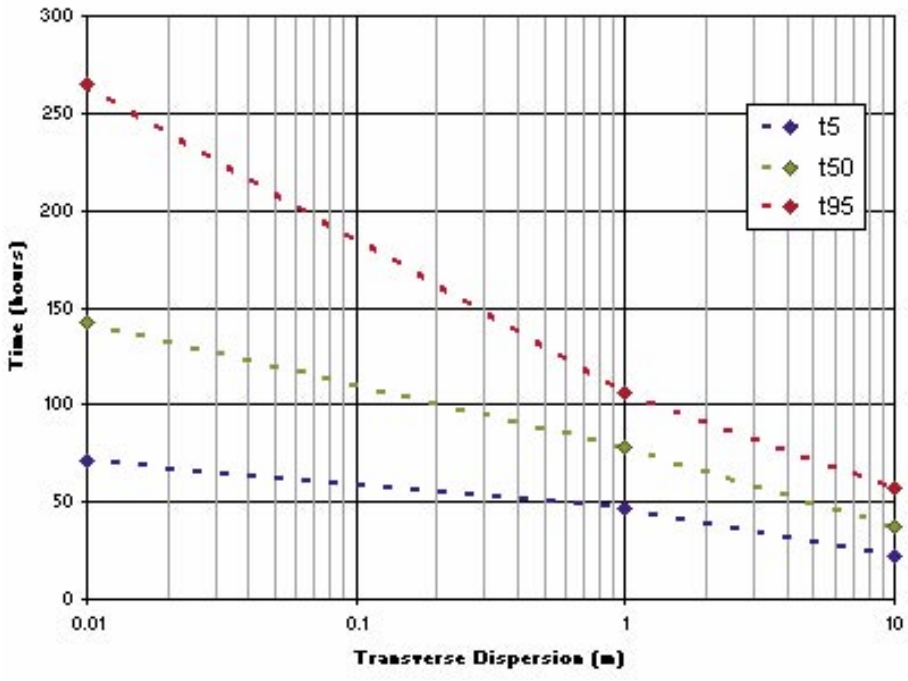

Figure 3-72. *Case 2b, HTO, distribution of st dev t_5, t_{50}, t_{95}, LTG.*

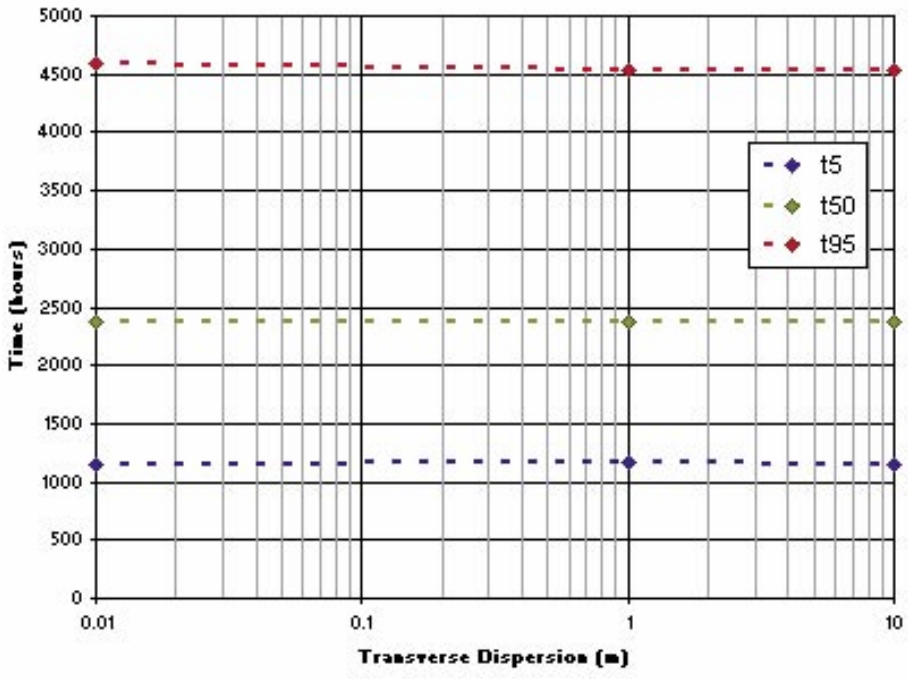

Figure 3-73. *Case 2c, HTO, distribution of mean t_5, t_{50}, t_{95}, LTG.*

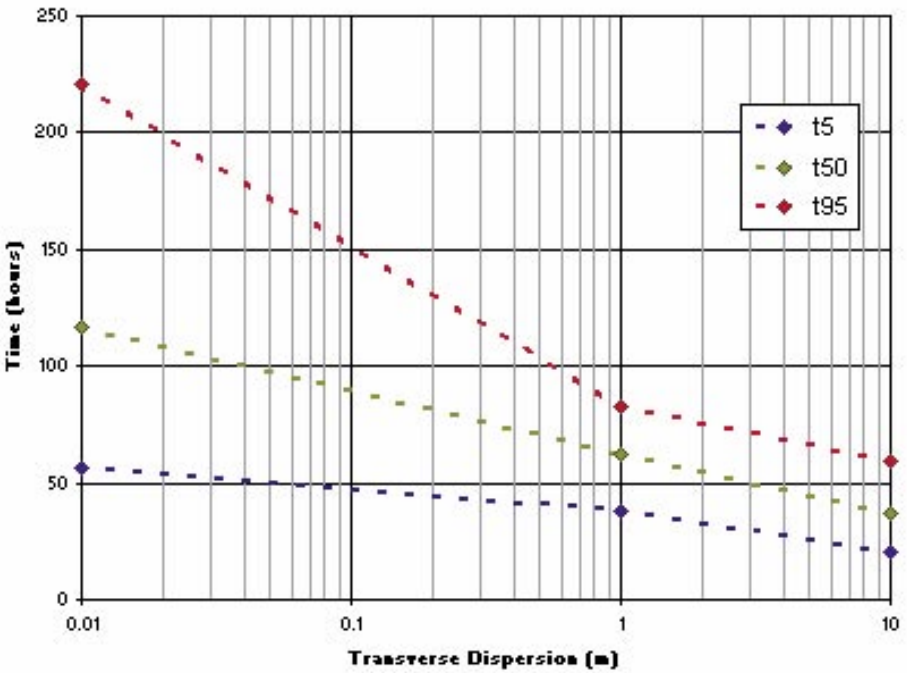

Figure 3-74. *Case 2c, HTO, distribution of st dev t_5, t_{50}, t_{95}, LTG.*

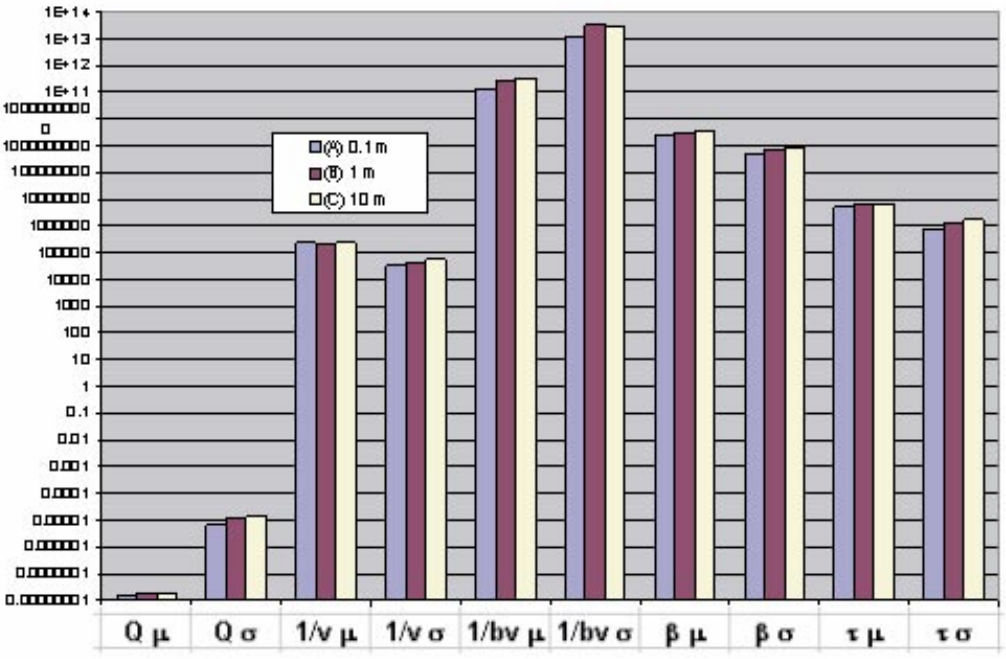

Figure 3-75. *Case 2a, 1 m Source summary statistics for all transport measures.*

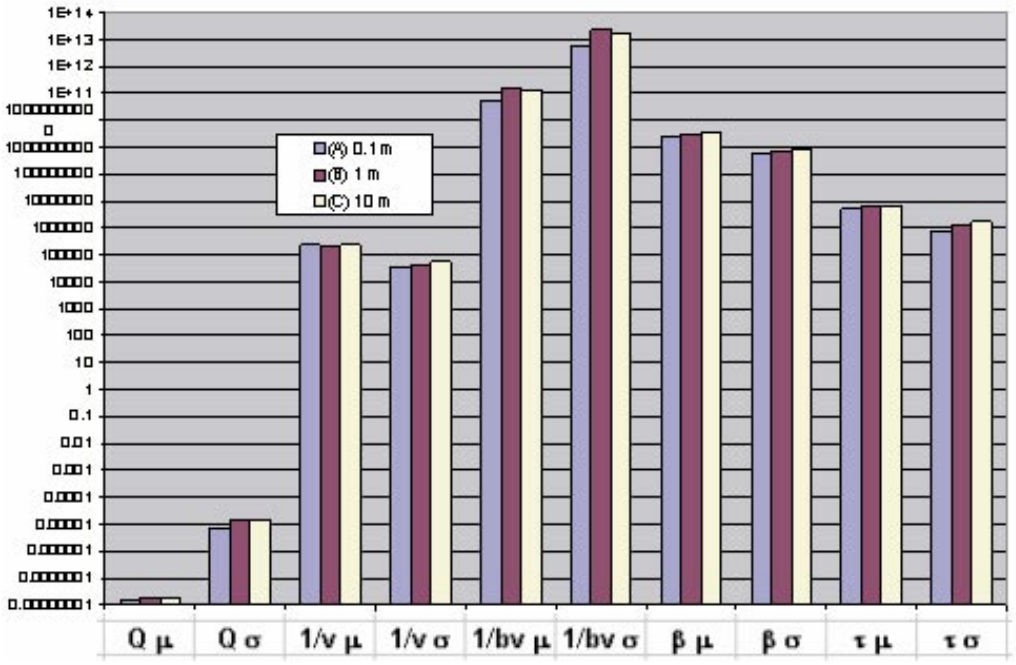

Figure 3-76. *Case 2b, 5 m source summary statistics for all transport measures.*

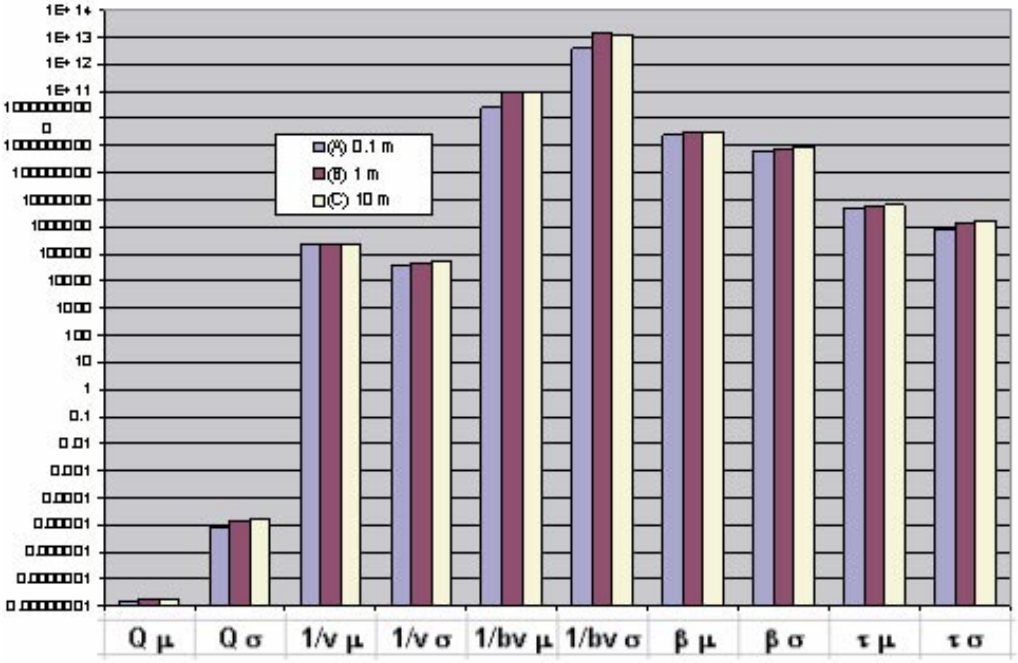

Figure 3-77. *Case 2c, 10 m source summary statistics for all transport measures.*

3.5 Case 4: million year sorbing tracer transport

While experimental measurements are general on the 0.1 to 2 year time scale, repository safety simulations are on the 10^5 to 10^7 year time scale. Case 4 was run for 10^8 years, by reducing the gradient to 0.00025%. Simulations were run using the Base case spatial fields, and immobile zone models. Simulations were carried out for the conservative tracer HTO, as well as sorbing tracers Cs and Na. Results are summarized in Table 3-9.

These simulations were carried out using the Base case stochastic field. The simulation results from LTG are illustrated in Figure 3-78 through Figure 3-80. The simulations to 10 million years show less variation between realizations and less variation as a result of transmissivity than any of the other cases studied. Particle tracks from these simulations are provided in Figure 3-81 through Figure 3-83. Figure 3-84 provides summary statistics for Case 4.

Table 3-9. Million year simulations, sorbing tracer results.

Case	Transverse dispersion	t_5 (μ,σ)	t_{50} (μ,σ)	t_{95} (μ,σ)
4a–L HTO	(A) 0.1 m	845.8, 16.0	2,402.4, 33.2	6,693.6, 105.1
	(B) 1 m	845.2, 15.2	2,401.8, 32.5	6,694.3, 105.5
	(C) 10 m	841.4, 12.6	2,398.3, 30.8	6,700.0, 107.8
4a–L Cs	(A) 0.1 m	4.6×10^4, 1.4×10^3	3.4×10^5, 3.4×10^5	3.4×10^5, 5.0×10^3
	(B) 1 m	4.6×10^4, 1.3×10^3	3.4×10^5, 3.4×10^5	3.4×10^5, 5.0×10^3
	(C) 10 m	4.6×10^4, 8.3×10^2	3.4×10^5, 3.4×10^5	3.4×10^5, 5.2×10^3
4a–L Na	(A) 0.1 m	1,133.7, 27.8	2,745.8, 47.1	6,639.3, 102.6
	(B) 1 m	1,132.6, 25.1	2,745.0, 43.4	6,639.5, 102.1
	(C) 10 m	1,126.2, 17.9	2,739.6, 36.5	6,644.4, 105.3
4a–F HTO		28,818.2	48,636.4	81,545.5
4a–F Cs		1,359,090.0	2,454,550.0	4,218,180.0
4a–F Na		30,818.2	52,818.2	89,090.9

Case	Transverse dispersion	Q (μ,σ)	1/v (μ,σ)	1/bv (μ,σ)	β (μ,σ)	τ (μ,σ)
4a–P	(A) 0.1 m	1.4×10^{-12}, 9.2×10^{-6}	2.6×10^9, 1.0×10^9	1.6×10^{15}, 1.3×10^{17}	2.7×10^{13}, 1.1×10^{13}	5.6×10^{10}, 2.3×10^{10}
	(B) 1 m	1.6×10^{-12}, 1.2×10^{-5}	2.4×10^9, 6.5×10^8	3.8×10^{15}, 3.9×10^{17}	2.9×10^{13}, 9.3×10^{12}	5.8×10^{10}, 1.7×10^{10}
	(C) 10 m	1.7×10^{-12}, 1.5×10^{-5}	2.3×10^9, 6.4×10^8	4.2×10^{15}, 2.7×10^{17}	3.0×10^{13}, 9.6×10^{12}	6.0×10^{10}, 1.8×10^{10}
4a–F		6.25×10^{-10}	1.99×10^5	1.6×10^8	3.2×10^9	3.98×10^6

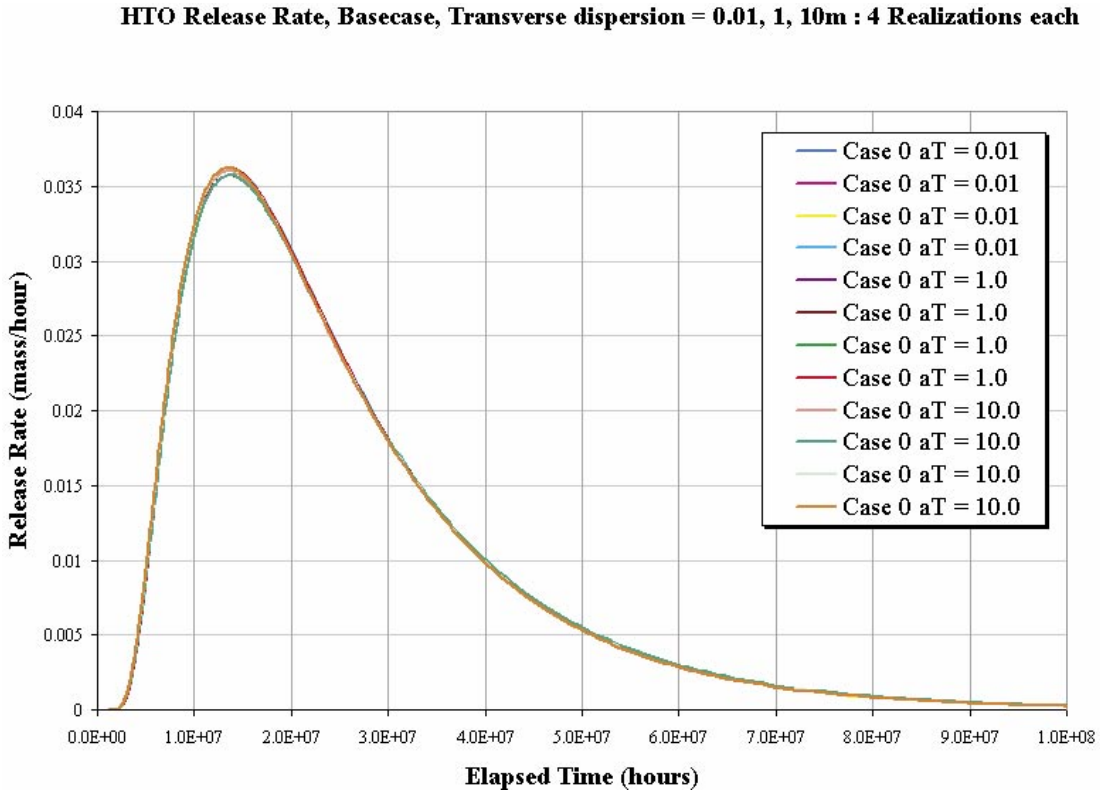

Figure 3-78. *Breakthrough curves for HTO for a 4 realizations of million year simulation (α_T = 0.01, 1 and 10 m), LTG.*

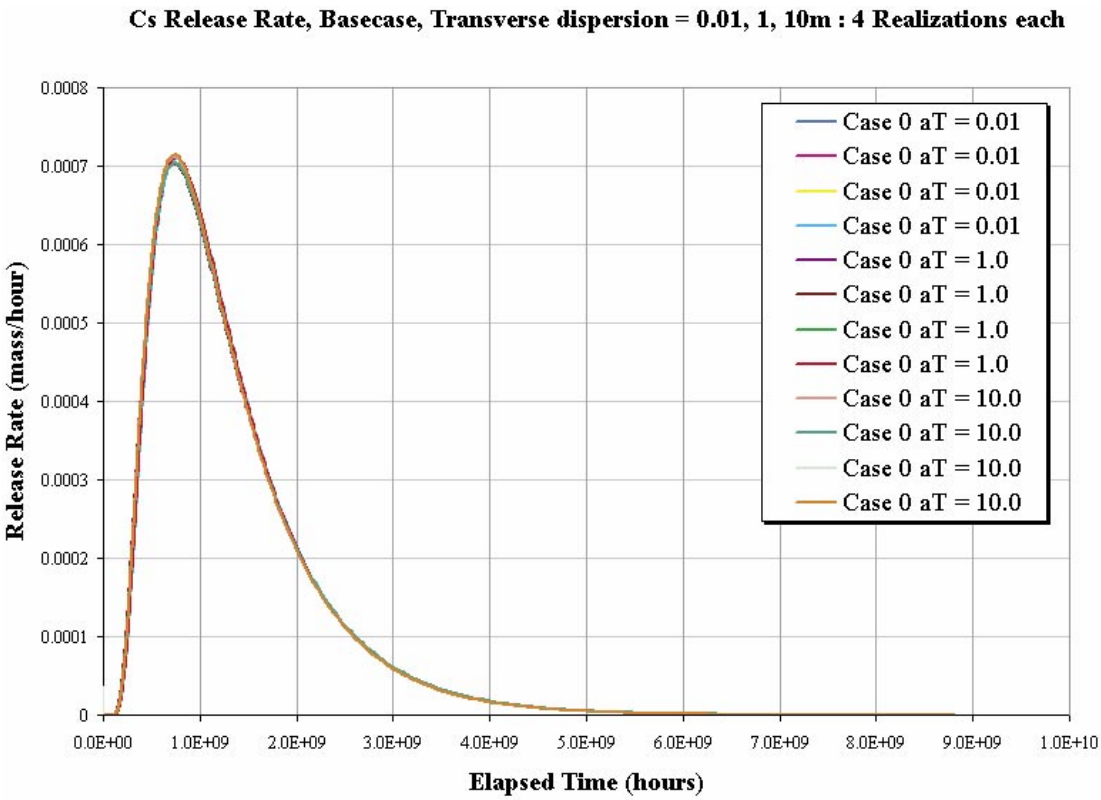

Figure 3-79. *Breakthrough curves for Cs for 4 realizations of million year simulation (α_T = 0.01, 1 and 10 m), LTG.*

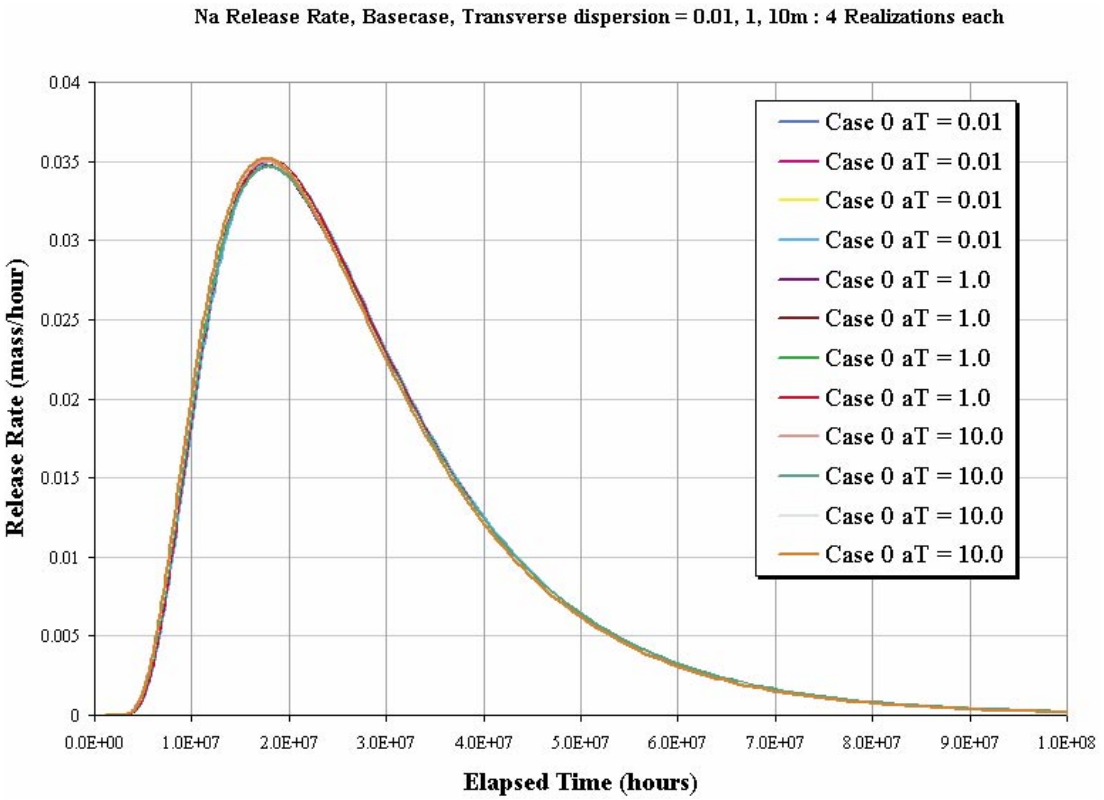

Figure 3-80. *Breakthrough curves for Na for 4 realizations of the million year simulation (α_T = 0.01, 1 and 10 m), LTG.*

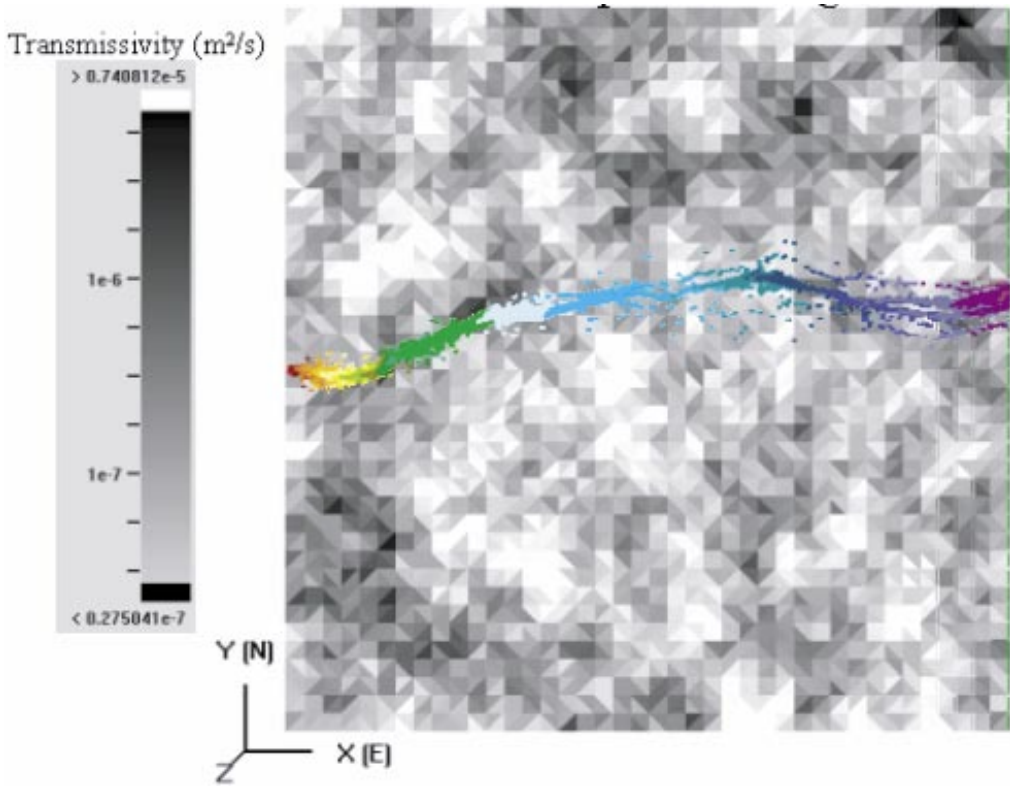

Figure 3-81. *Case 4, million year, α_T = 0.01 m, particle tracking.*

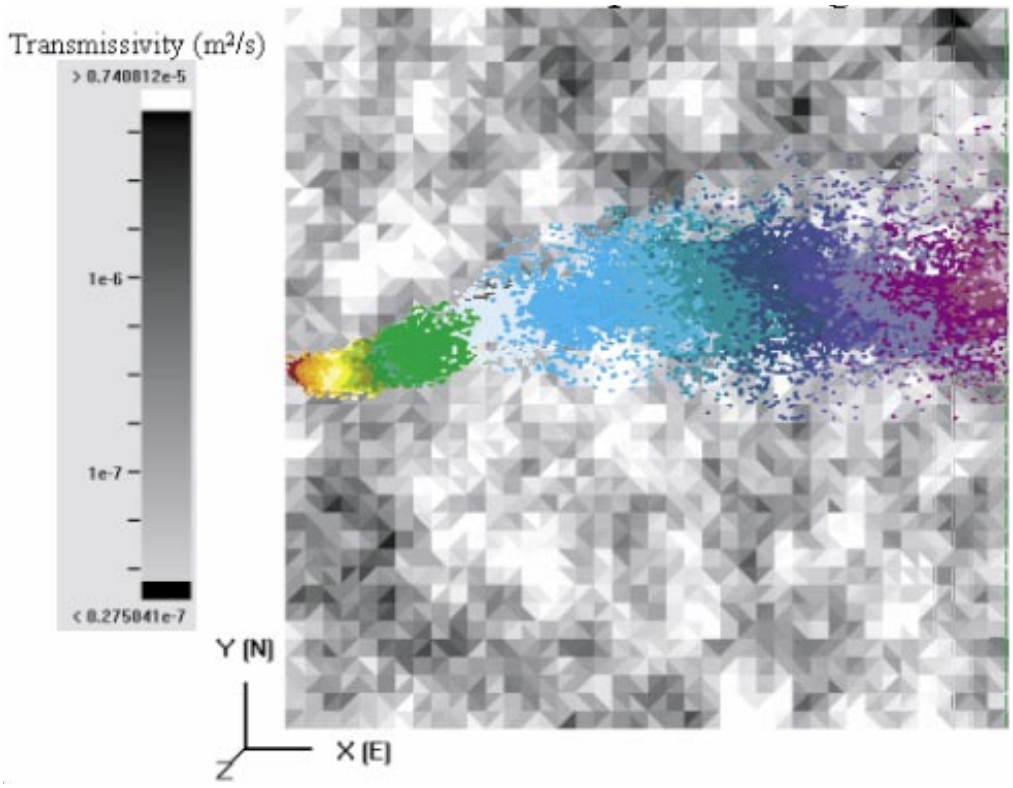

Figure 3-82. *Case 4, million year, α_T = 1.0 m, particle tracking.*

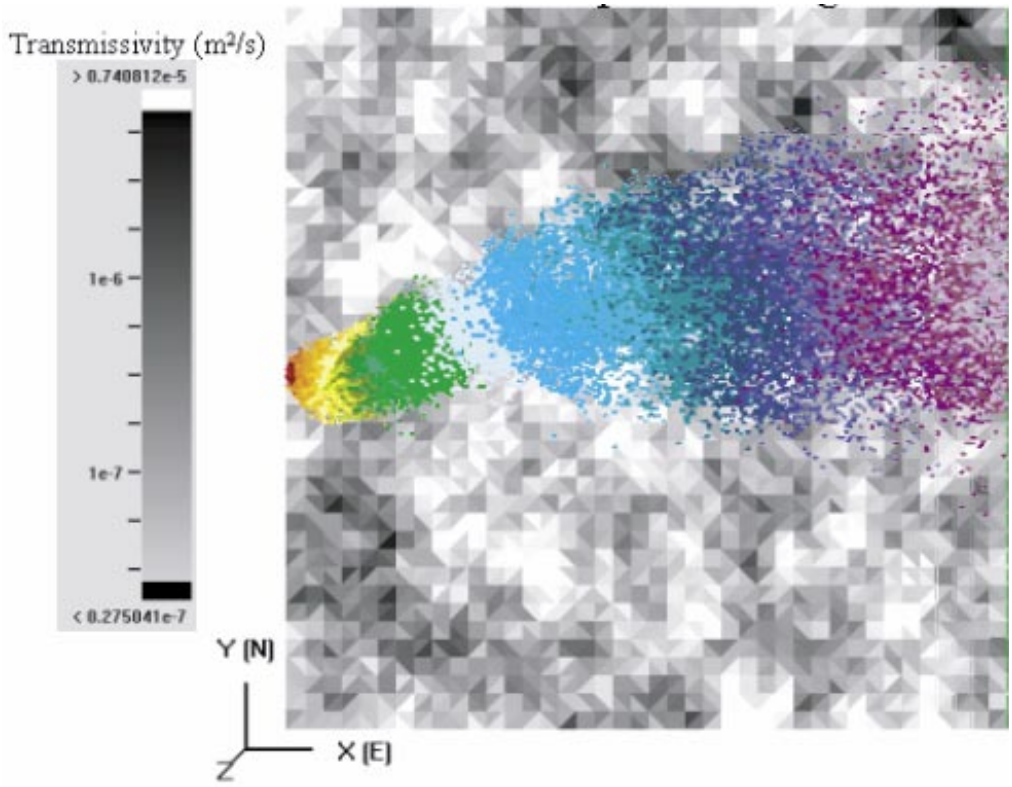

Figure 3-83. *Case 4, million year, α_T = 10.0 m, particle tracking.*

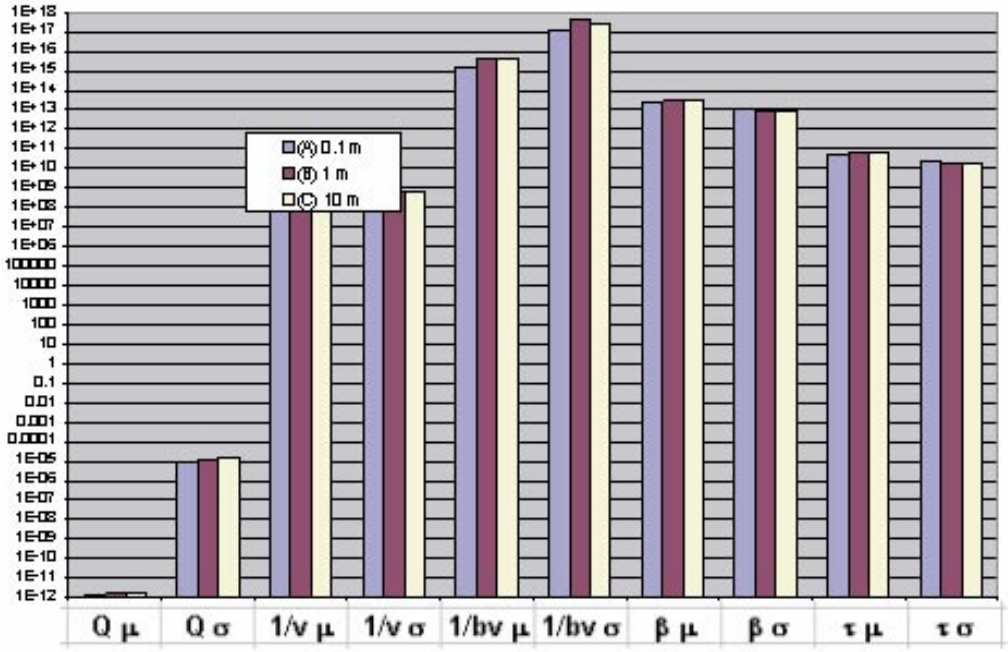

Figure 3-84. *Case 4, million year time scale, statistic for all transport measures.*

3.6 Case 5: simple channel model

The cases presented above show a smaller influence of transverse dispersion on solute transport than was initially anticipated. The purpose of Case 5 is to evaluate the role of the functional relationship between aperture and transmissivity in determining the sensitivity of solute transport to transverse dispersion and heterogeneity.

3.6.1 Case 5a simulations

Figure 2-5 shows the geometry defined for Case 5. This case has a constant transmissivity of 10^{-9} m^2/s, with a single channel, 1 m wide of T = 10^{-6} m^2/s in the middle. The head and tracer injection boundary condition is the same as was specified in the Base case, with a constant head of 0.5 m on the upgradient edge of the fracture and a constant head of 0 m on the downgradient edge of the fracture. With this boundary condition, the entire fracture is available for advection. However, the 10^{-9} m^2/s regions on either side are labeled as "stagnant zones" because the transmissivity is three orders of magnitude lower and there would presumably be much less flow there.

Case 5a is comparable to the Base case (Section 3.1), since it uses the empirical correlation between transmissivity T and aperture e (for units of seconds and meters),

$e = 15\ T^{0.6}$

Tracer breakthrough for this case is illustrated in Figure 3-85, for transverse dispersion values of α_T = 0.01 m and 1 m. Even though this is an extreme variation of transverse dispersivity, the breakthrough curves are similar. This is consistent with the small effect of transverse dispersion seen in Cases 1 through 4 and the Base case.

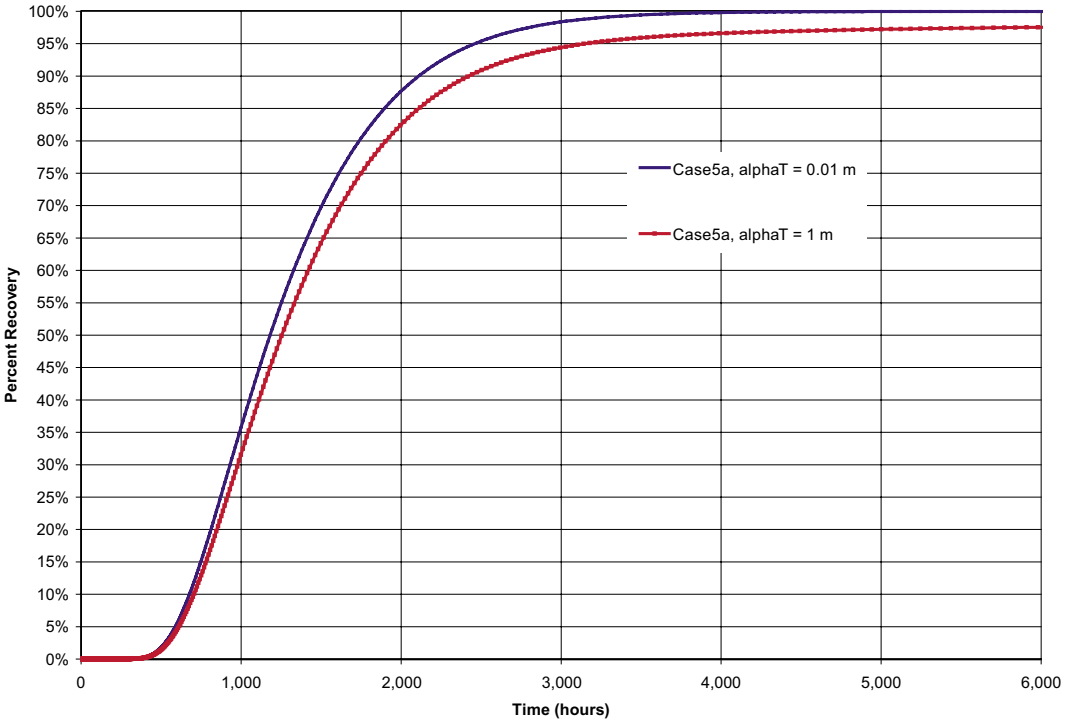

Figure 3-85. *Tracer breakthrough for Case 5a – transmissivity correlated to aperture, LTG.*

3.6.2 Case 5b simulations: constant aperture

Case 5a showed that the groundwater velocity in the "stagnant zones" at the sides of the "advective channel" actually have transport velocities comparable to those in the advective channel. Consequently, the mass transferred to the "stagnant zone" by transverse dispersion still breaks through to the down-gradient edge of the fracture with only a slight delay.

Case 5b applies a constant transport aperture e of 3.77 mm over the entire fracture surface. This transport aperture is the value applied just for the high transmissivity channel in Case 5a.

The increased aperture decreases the velocity for any solute mass dispersed to the "stagnant zone." Solute breakthrough for this simulation can be seen in Figure 3-86 for transverse dispersion values of α_T = 0.01 m and 1 m. In this case, increased transverse dispersion has a very significant effect on the breakthrough. For example, the increase in transverse dispersion from 0.01 to 1 m delays the t_{95} from 2,658 hours to 5,183 hours (95%). In contrast, in Case 5a, the t_{95} is only delayed from 2,457 hours to 3,141 hours (28%). This indicates that the form of correlation defined between transport aperture and transmissivity assumed in Case 5a (and in all previous cases) does significantly reduce the sensitivity of breakthrough to transverse dispersion.

The physical mechanism for this is as follows. Increased transverse dispersivity results in transfer of additional solute mass from the advective channel of the fracture ($T=10^{-6}$ m^2/s) to the "stagnant" portion of the fracture ($T=10^{-9}$ m^2/s). The total flow of water is much smaller in the "stagnant" region, due to the lower transmissivity. However, because the transport aperture in the "stagnant" portion of the fracture is so much smaller (0.06 mm vs. 3.77 mm), the transport velocity for the mass which is in the "stagnant" portion of the fracture is comparable to that in the advective zone of $T=10^{-6}$ m^2/s.

Results for Case 5a and 5b are summarized in Table 3-10.

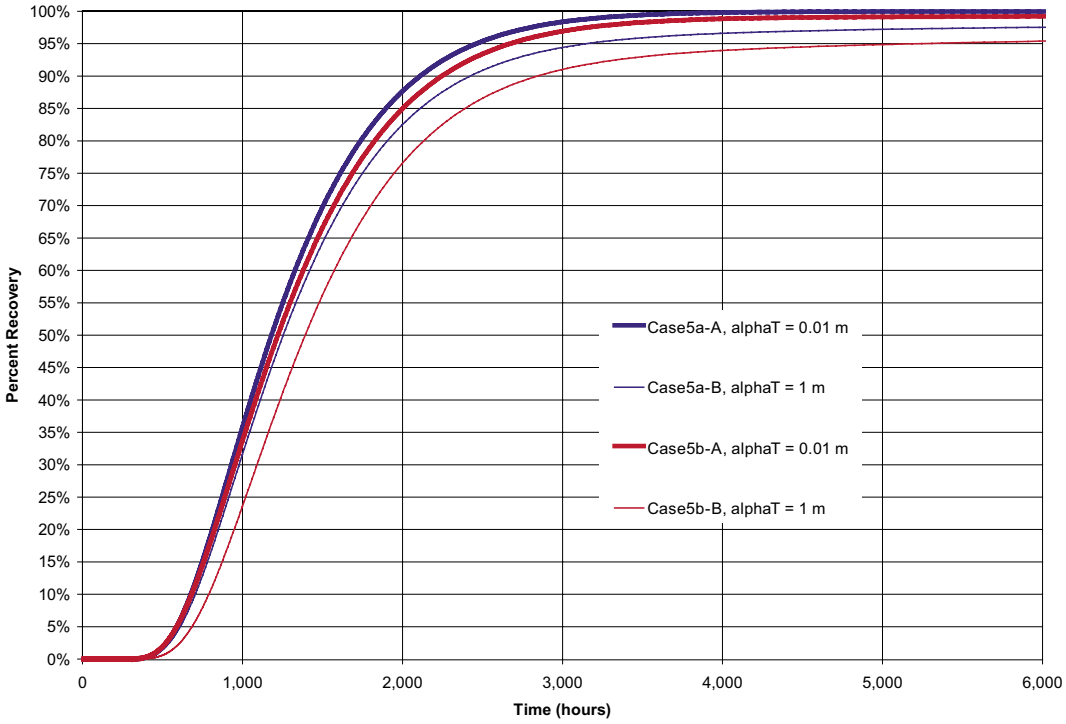

Figure 3-86. *Tracer breakthrough for Case 5b – constant aperture, LTG.*

Table 3-10. Statistical summary of Case 5 (breakthrough time, hours).

Stats	Case 5a			Case 5b		
	0.01 m	1 m	% delay	0.01 m	1 m	% delay
t_5 %	584.	605	3.6%	584	682	16.8%
t_{50} %	1,181	1,253	6.1%	1,209	1,379	14.0%
t_{95} %	2,457	3,141	28.5%	2,658	5,183	95.0%

3.6.2.1 Case 5c: alternative boundary conditions

Having established the importance of the aperture-transmissivity relationship, the next issue which can be addressed with the simplified channel model is the effect of boundary condition assumptions. The boundary condition used in the Base case and Cases 1 through 4 is a one-dimensional advective field throughout the fracture, with the same gradient across the entire fracture. In Cases 5a and 5b, once transverse dispersion moves tracer mass to the "stagnant" zone, the mass moves parallel to the flow field at the velocity determined by the gradient, transmissivity, and transport aperture.

To further clarify this mechanism, Case 5c changes this boundary condition. In Case 5c, the goal is that whenever solute mass moves to the "stagnant" zone by transverse dispersion, it must ultimately return to the advective channel to breakthrough to the down-gradient edge of the fracture. This was achieved by changing the down-gradient boundary from a constant head of 0 m, to no-flow, except at the outlet of the 1 m wide "advective" channel. The down-gradient constant head of 0 m is applied only at the 1 m wide downstream edge of the "advective channel". With this redefinition of the flow field, tracer mass must return to the 1 m wide channel to be released from the model.

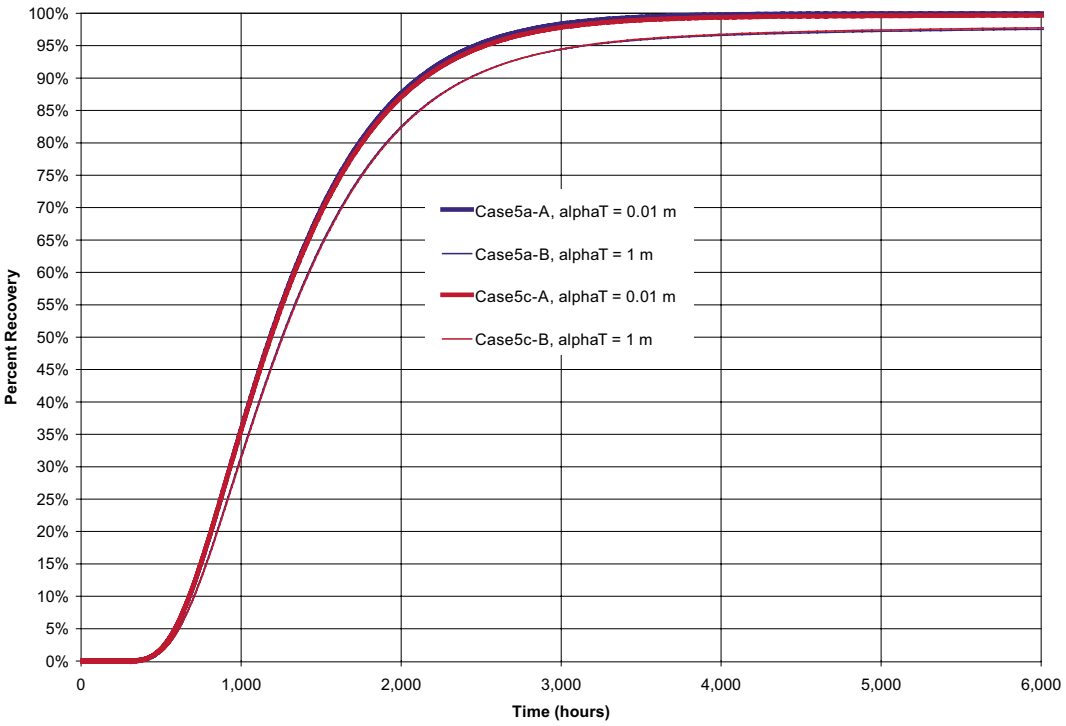

Figure 3-87. *Tracer breakthrough for Case 5c – channel with restricted outlet, LTG.*

Results from these simulations are illustrated in Figure 3-87, for the same aperture-transmissivity correlation used in Case 5a. Results are functionally identical, indicating that the advective transport back to the flow channel for mass transferred to the diffusive zone does not provide a significant delay in transport. For the low dispersion $\alpha T = 0.01$ m, the result for Case 5c is essentially the same as for Case 5a. For the high dispersion $\alpha T =$ 1 m, Case 5c shows some increased travel time compared to Case 5a, but significantly less than in Case 5b. This indicates that the assumed one-dimensional flow boundary condition is not critical to the simulation results.

3.6.2.2 Additional transmissivity correlations

Having established the aperture-transmissivity correlation as a key to understanding the effect of transverse dispersion, the scope of this effect was evaluated through a series of sensitivity studies. A total of four cases were defined, including the two correlations already defined as Case 5a and Case 5b. These relationships are listed in Table 3-11. All of these relationships are defined by empirical equations of the form

$$e_t = a\, T^b$$

where e_t is transport aperture in meters, a and b are coefficients, and T is transmissivity in m^2/s.

Table 3-11. Aperture-transmissivity correlation cases studied.

Case	Aperture-transmissivity correlation	Coefficient a	Coefficient b	Basis
5a	Base case	15	0.6	Calibration to STT1b (this report)
5b	Constant aperture	3.77 mm	0	Aperture from $T = 10^{-6}$ m^2/s (Base case)

Case	Aperture-transmissivity correlation	Coefficient a	Coefficient b	Basis
5d	Cubic law	0.011	0.3333	/Domenico and Schwartz, 1990, p 87/
5e	Breccia-filled fracture	1,000	1	T = e K Hydraulic conductivity K = 10^{-3} m/s

Because the average transport aperture is different between each of these cases, the breakthrough times are different. The results of these simulations are therefore presented as the percent delay in tracer breakthrough for a transverse dispersion of 1 m relative to that for a transverse dispersion of 0.01 m. These results are provided in Table 3-12.

Table 3-12. Delay in cumulative mass recovery of Case 5 for increase of transverse dispersion from 0.01 m to 1.0 m, channelized fracture.

Case	Percent delay t_5	Percent delay t_{50}	Percent delay t_{95}
Case 5a	3.6%	6.1%	28.5%
Case 5b	16.8%	14.0%	95.0%
Case 5d	21.0%	21.0%	46.5%
Case 5e	6.1%	12.7%	39.7%

3.6.2.3 Additional heterogeneous cases

Based on the results of Case 5 studies, it could be concluded that the correlation between transmissivity and aperture used in the Base case and Cases 1 through 4 minimized the effect of transverse dispersion on solute transport. In addition, however, Case 5 indicates that the effect of transverse dispersion is to delay solute breakthrough, with the most dramatic effect being an increase in the length of the tail of the breakthrough curve. For radioactive waste repositories, this would generally be considered a conservative result, since ignoring the effect of transverse dispersion causes simulated breakthrough to be earlier than it actually would be including the effect of transverse dispersion.

In order to address this effect, additional simulations were carried out for the Base case (Figure 2-1) spatial field for the transmissivity-aperture correlations of Table 3-11. Results of these simulations a summarized in Table 3-13.

Table 3-13. Delay in cumulative mass recovery of Case 5 for increase of transverse dispersion from 0.01 m to 1.0 m, base case spatial field.

Aperture-transmissivity correlation	Percent delay t_5	Percent delay t_{50}	Percent delay t_{95}
Base case	3.6%	3.6%	2.4%
Constant aperture	22.5%	25.4%	24.0%
Cubic law	43.0%	28.5%	19.6%
Breccia-filled fracture	18.2%	21.0%	16.8%

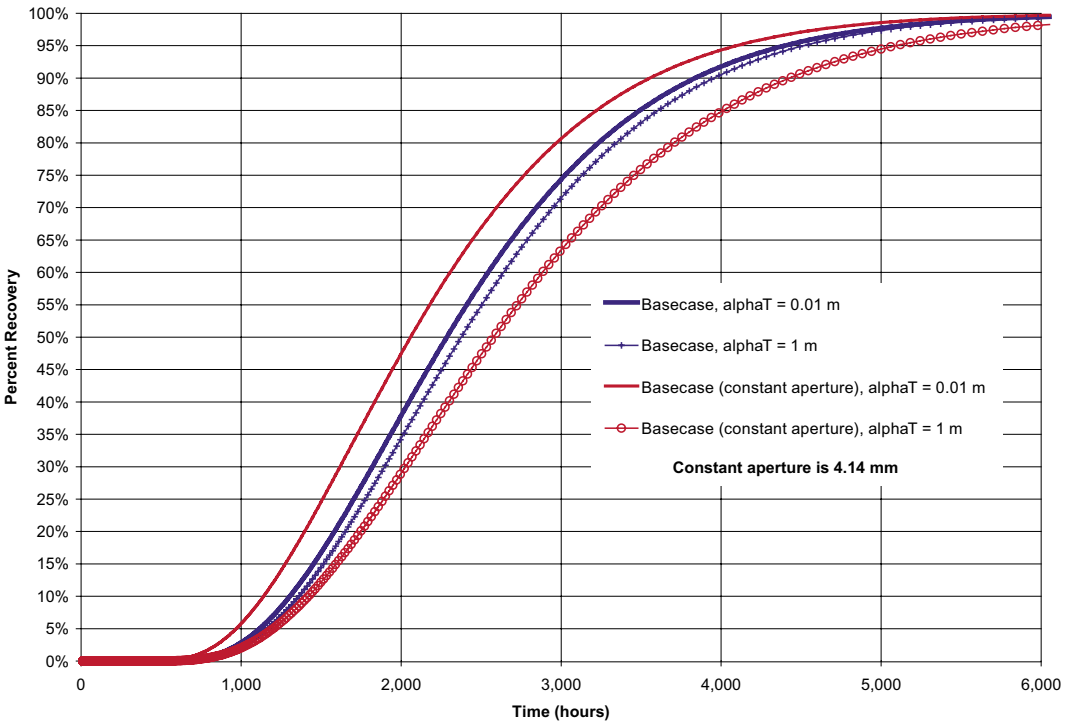

Figure 3-88. *Effect of constant aperture on heterogeneous fracture (Base case), LTG.*

Figure 3-88 presents a comparison of the Base case spatial field with the original transmissivity-aperture correlation, against the constant aperture assumption. For this figure, the aperture was modified slightly from those used for Table 3-13, to improve visibility. As noted in Section 3.2 above, for the Base case with the correlation between transmissivity and aperture, increased transverse dispersion delays breakthrough, but only within the statistical variability between realizations. For the case with constant aperture, the effect of increased transmissivity on the Base case is much more significant. At time t_{50}, the increased transverse dispersion for the Base case simulation is only 3.6%. For the case with a constant aperture the value of t_{50} is increased by 25.4%.

3.6.2.4 Summary of Case 5 simulations

Case 5 simulations were run with a range of different functional relationships between aperture and transmissivity. These cases demonstrate that increased transverse dispersion can have a significant influence on breakthrough, almost doubling the breakthrough time t_{95} as transverse dispersion is increased from 0.01 m to 1 m for the case of constant aperture. However, for the cubic and quadratic law relationships between aperture and transmissivity, the effect is significantly smaller. Increase in transverse dispersivity from 0.01 to 1 m generally results in a 5 to 20% delay in breakthrough times t_5, t_{50}, and t_{95}.

No cases were observed in which increase in transverse aperture resulted in a statistically significant decrease in travel times. Consequently, it can be concluded that for most realistic cases, the effect of ignoring transverse dispersion is conservative.

3.7 Comparison of 2D LTG transport against FARF31

The Base case addresses the issue of whether transverse dispersion is a significant process which can make 1D pipe approaches unrealistic. The studies presented above indicate that for the assumptions made in the present study, transverse dispersion is not in general a significant process for solute transport in a single fracture.

This section presents a direct comparison between the 2D LTG transport solution for a single fracture against a 1D-pipe transport solution. The 1D pipe transport solution was implemented using GoldSim /Miller and Kossik, 2002/, with settings to approximate FARF31 /Norman and Kjellbert, 1990/. These solutions are also compared against an analytical solution /Domenico and Schwartz, 1990, p 636/ 1-D advective dispersive transport with no matrix diffusion.

$C/Co = ½\ \mathrm{erfc}((x–v_t)/(2(a_L \times v_t)^{½}))$ where $C(0, t) = Co$ and $C(x, 0) = 0$

where erfc is the complementary error function. This solution is for a step injection starting at t = 0. For comparison against GoldSim/FARF31 and LTG, we have use superposition to apply this case for a 10 second long step pulse injection from t = 0 to 10 seconds. Note that both GoldSim/LTG and the analytical solution use simple pipe transport solutions which do not consider fracture geometric information.

The comparison between the analytical solution, 2D LTG solution, and GoldSim/FARF31 solution for a 10 second step pulse injection is shown in Figure 3-89. The match between the 2D LTG solution and the analytical solution is fairly good. The match to the GoldSim model is not as good. This is due to the fact that the GoldSim solution considers the effect of diffusive transport as well as advective transport within the pipe. This delays the break-through curve by approximately 10%.

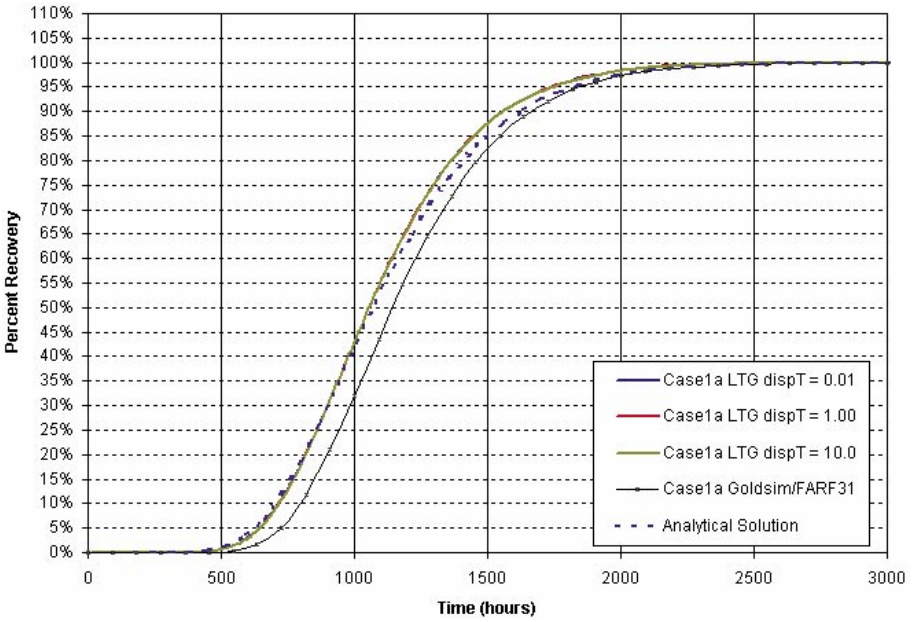

Figure 3-89. *Analytical, LTG/Plate and GoldSim/FARF31 solutions for homogeneous fracture (Case 1a).*

For a stochastic field, it is necessary to represent the stochastic field on the fracture plane using a stochastic distribution of properties on the pipes. The Base case has transmissivity mean and standard deviation of 5×10^{-7}. The GoldSim/FARF31 implementation of this therefore used transmissivity mean and standard deviation of 5×10^{-7}, among the six pipes connected in series which constitute the model. The effective dispersivity $\alpha_{'L}$ in each pipe can be approximated using the formula,

$$\alpha_{'L} = \alpha_L + (\sigma_{LN}(T))^2 \times \rho$$

where α_L is the specified dispersivity, $\sigma_{LN}(T)$ is the standard deviation of log transmissivity, and ρ is the correlation length (m)

Results for this GoldSim/FARF31 simulation of the Base case with HTO, Cs, and Na tracers are compared against the LTG solution in Figure 3-90 through Figure 3-92. Statistical results for these simulations are compared in Figure 3-93 through Figure 3-98. There are significant differences between the one and two-dimensional solutions, probably due to the differences in the treatment of heterogeneity, and the effect of greater available reactive area in the LTG models.

Clearly, the 1-D single pipe approach cannot address the 2D effects of in plane heterogeneity such as dilution and dispersion. However, it is possible that a 1-D approach can mimic the breakthrough curves that are obtained from 2D approaches, and by extension the results from full 3D DFN modeling. Comparison of the t_5, t_{50}, and t_{95} statistics from the 2-D and 1-D models demonstrates that there are significant differences between the tracer breakthrough for 1D and 2D models. Clearly, the additional information incorporated to the 2D models provides additional parameterization for the transport processes. However, where the 2D field is purely speculative, this advantage may be illusory.

Results for the Base case spatial field are summarized in Table 3-14.

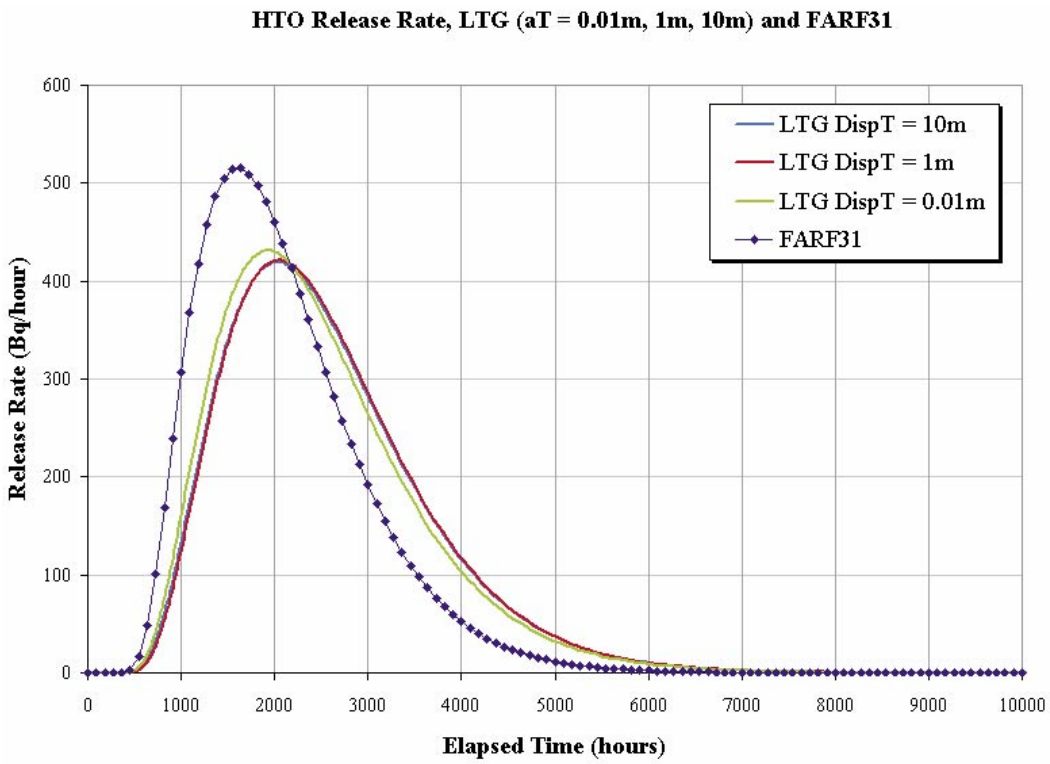

Figure 3-90. *Breakthrough curves for LTG (αT = 0.01, 1 and 10 m) and FARF31/GoldSim simulations of the Base case.*

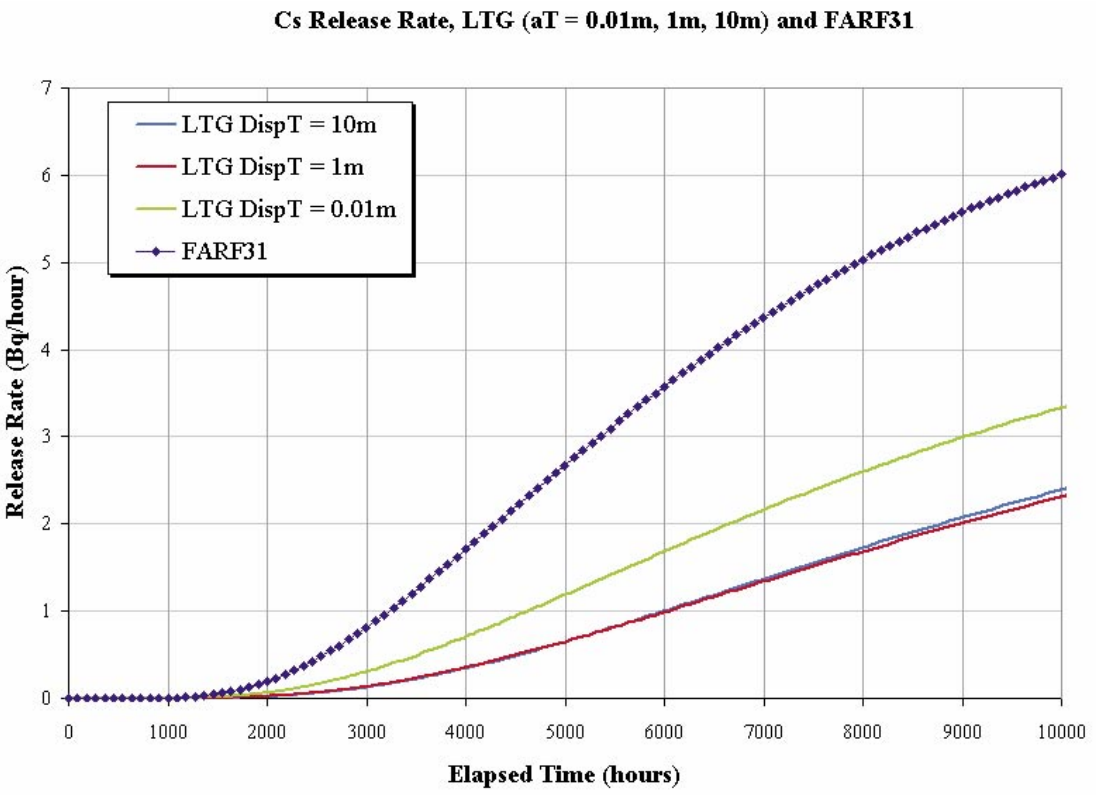

Figure 3-91. *Breakthrough curves for Cs, LTG (αT = 0.01, 1 and 10 m) and FARF31/GoldSim simulations of the Base case.*

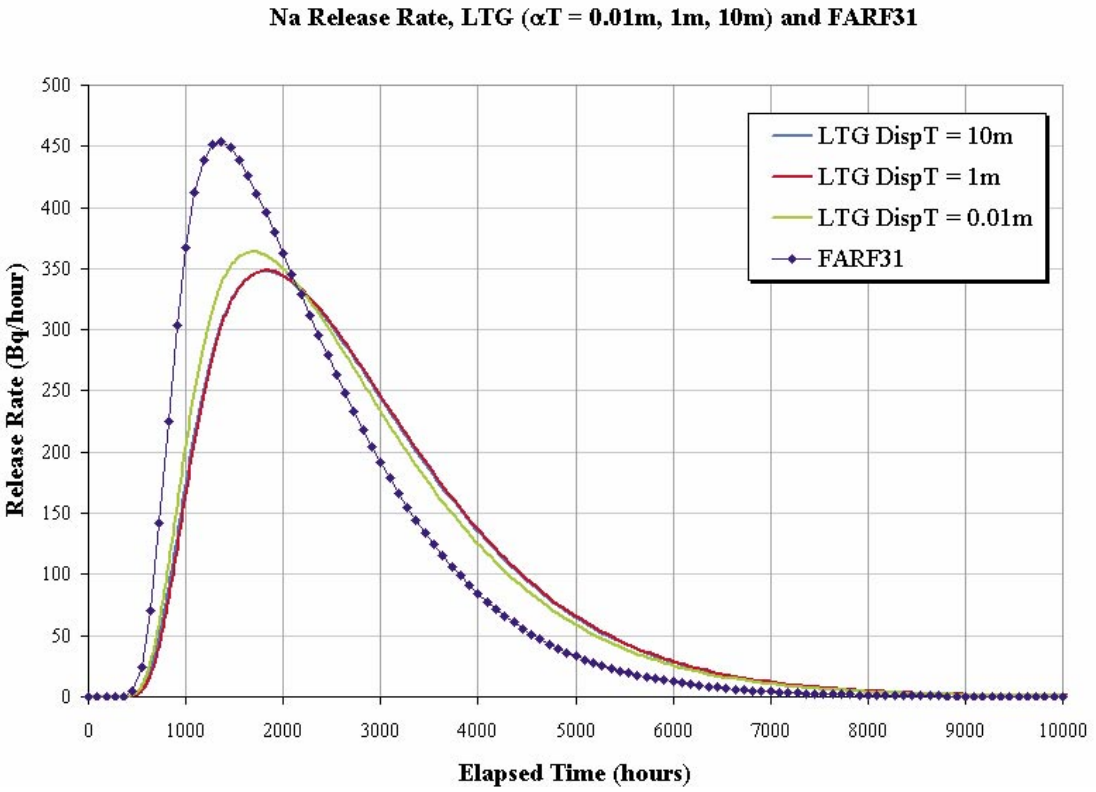

Figure 3-92. *Breakthrough curves for Na, LTG (αT = 0.01, 1 and 10 m) and FARF31/GoldSim simulations of the Base case.*

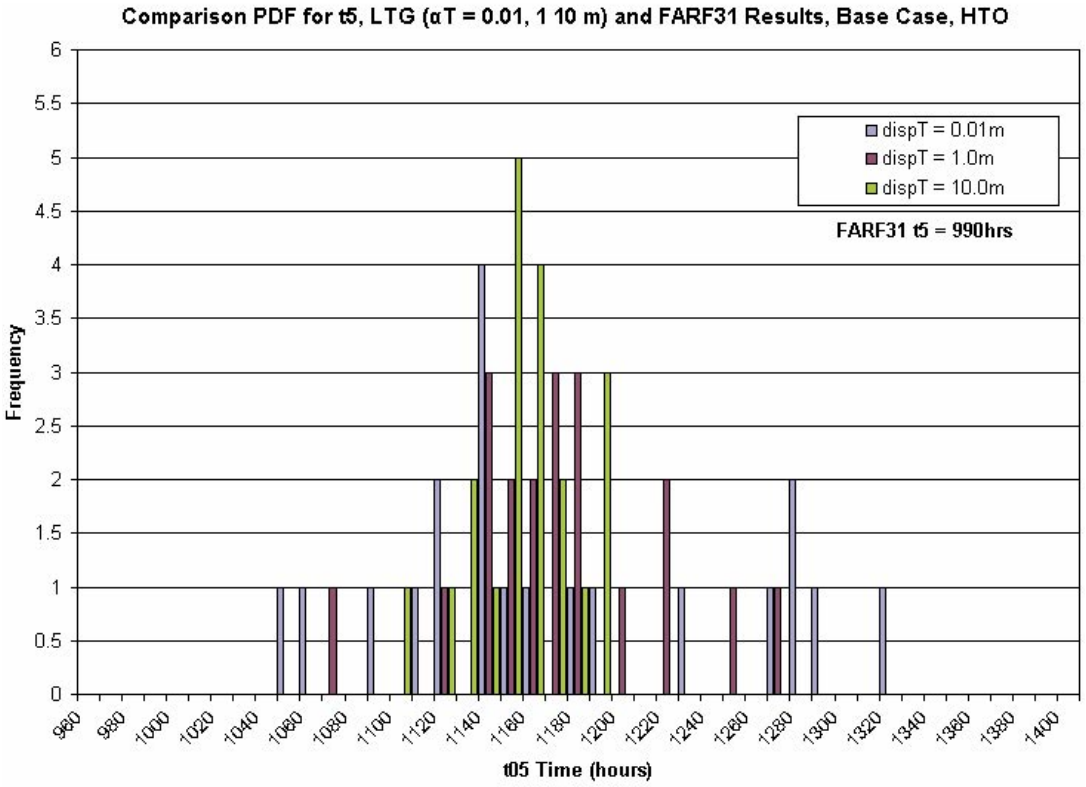

Figure 3-93. *Comparison PDF for t_5, LTG (αT = 0.1, 1 and 10 m) and FARF31 results, Base case, HTO.*

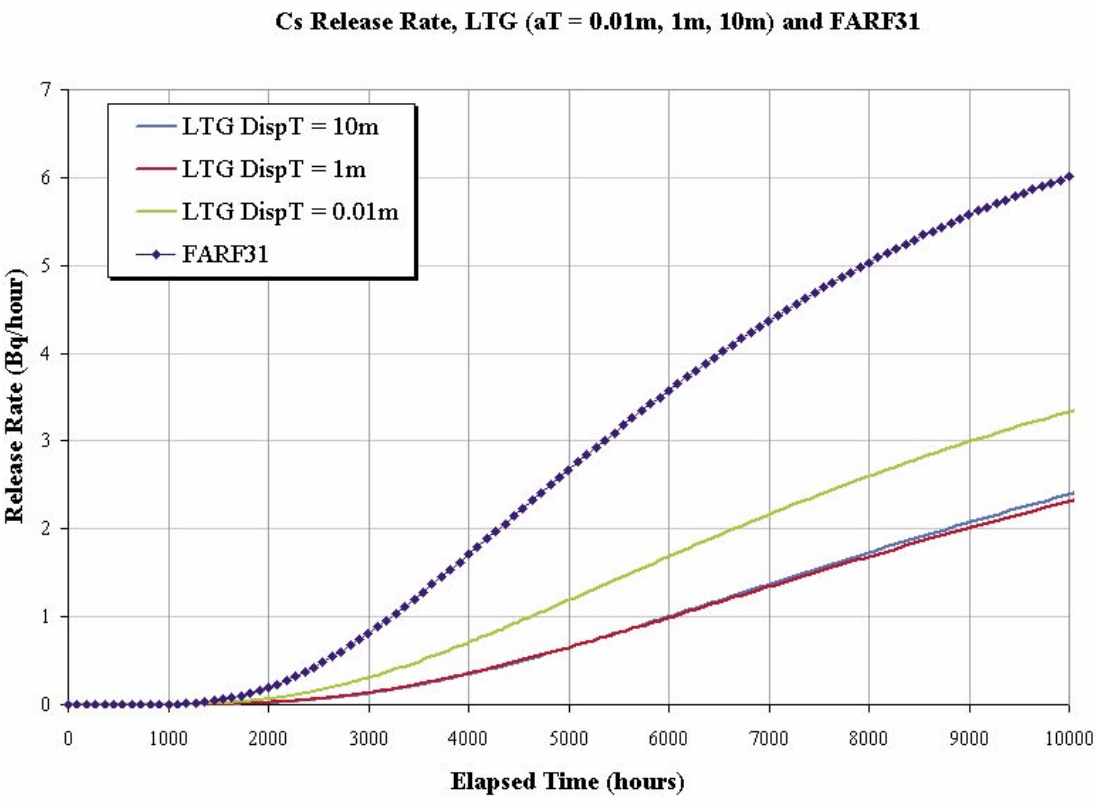

Figure 3-94. *Comparison PDF for t_{50}, LTG (αT = 0.01, 1 and 10 m) and FARF31 results, Base case, HTO.*

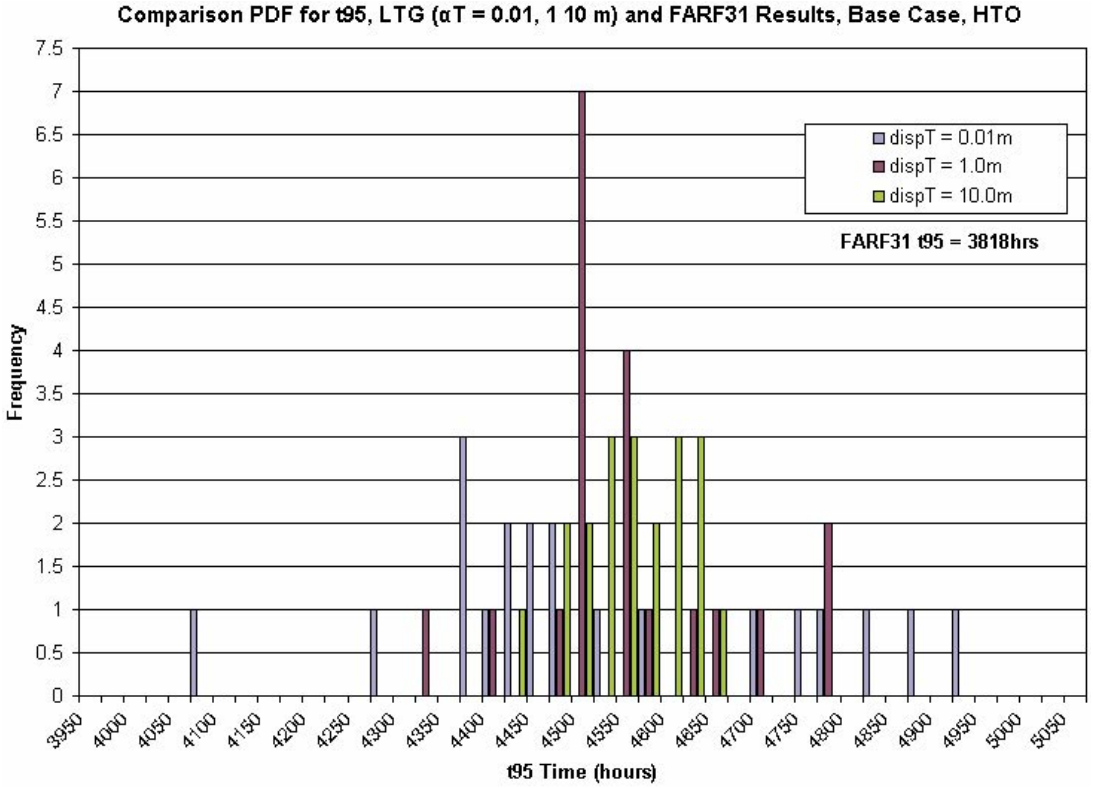

Figure 3-95. *Comparison PDF for t_{95}, LTG (αT = 0.01, 1 and 10 m) and FARF31 results, Base case, HTO.*

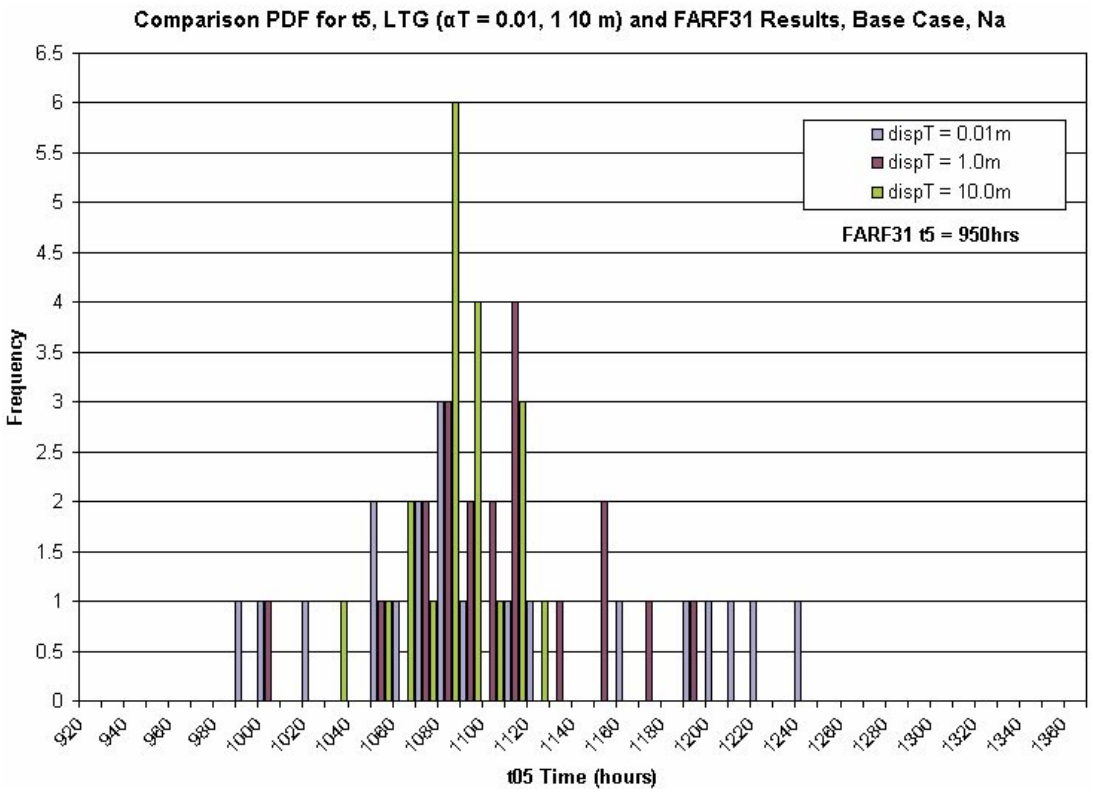

Figure 3-96. *Comparison PDF for t_{05}, LTG (αT = 0.1, 1 and 10 m) and FARF31 results, Base case, Na.*

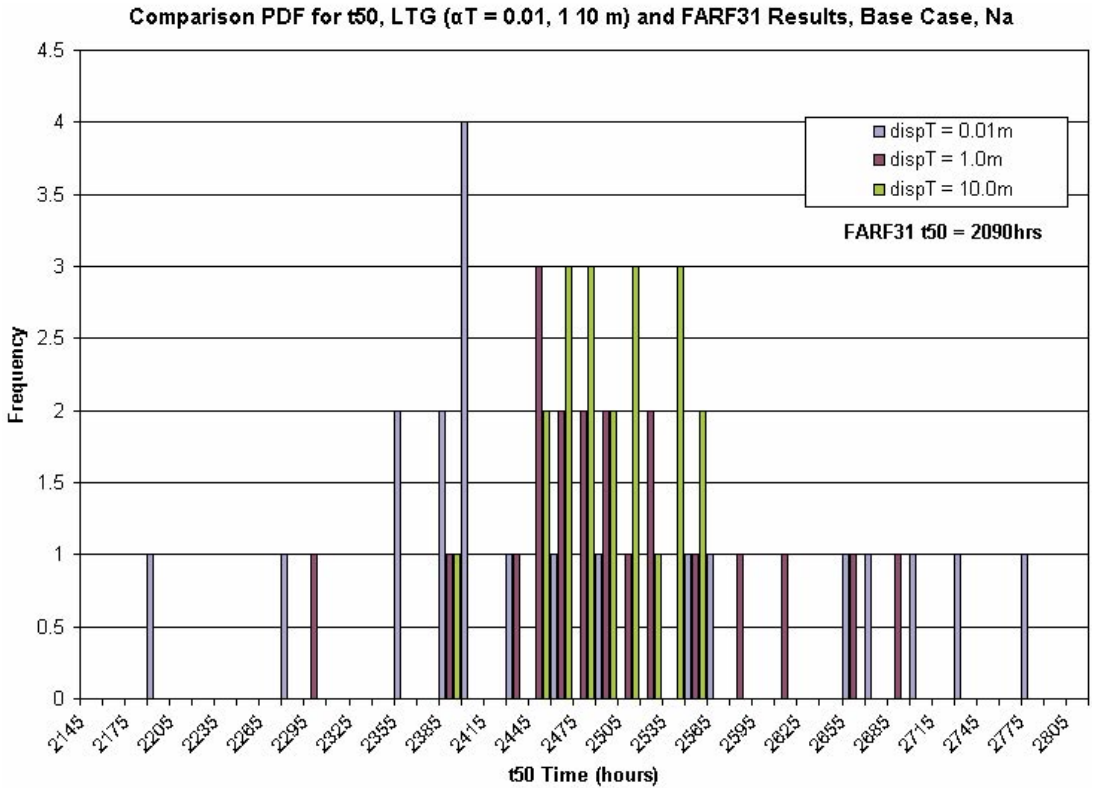

Figure 3-97. *Comparison PDF for t_{50}, LTG (αT = 0.01, 1 and 10 m) and FARF31 results, Base case, Na.*

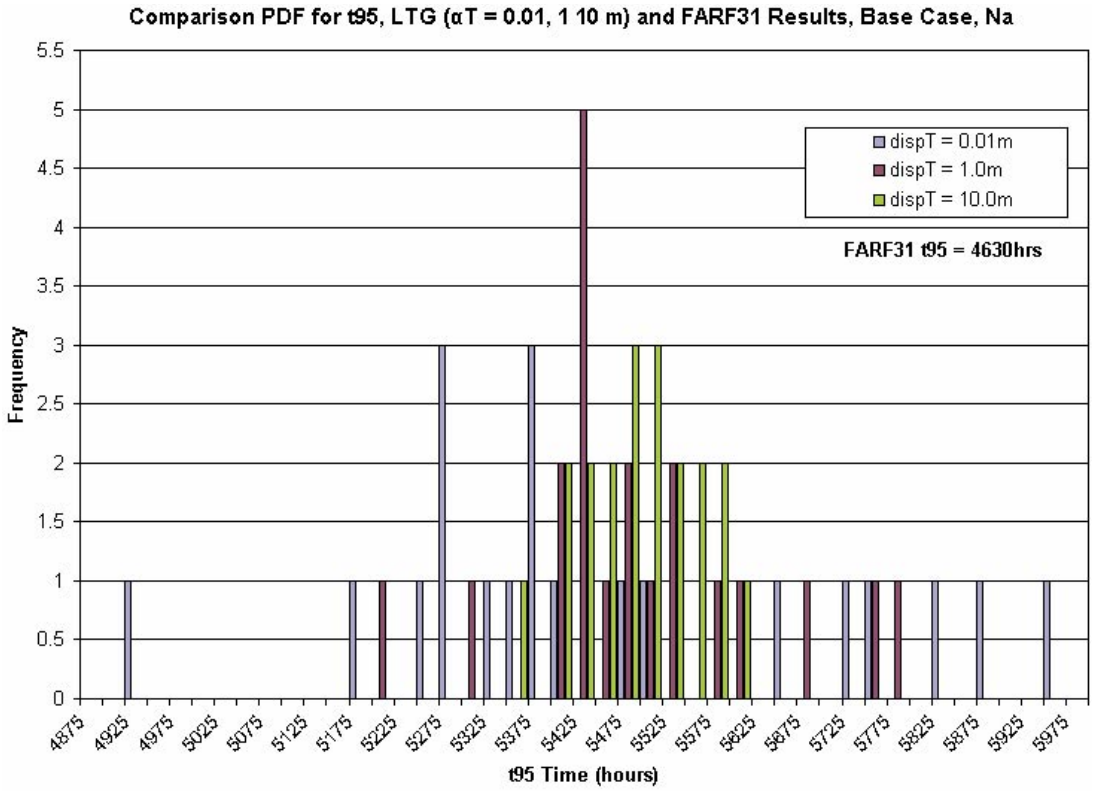

Figure 3-98. *Comparison PDF for t_{95}, LTG (αT = 0.01, 1 and 10 m) and FARF31 results, Base case, Na.*

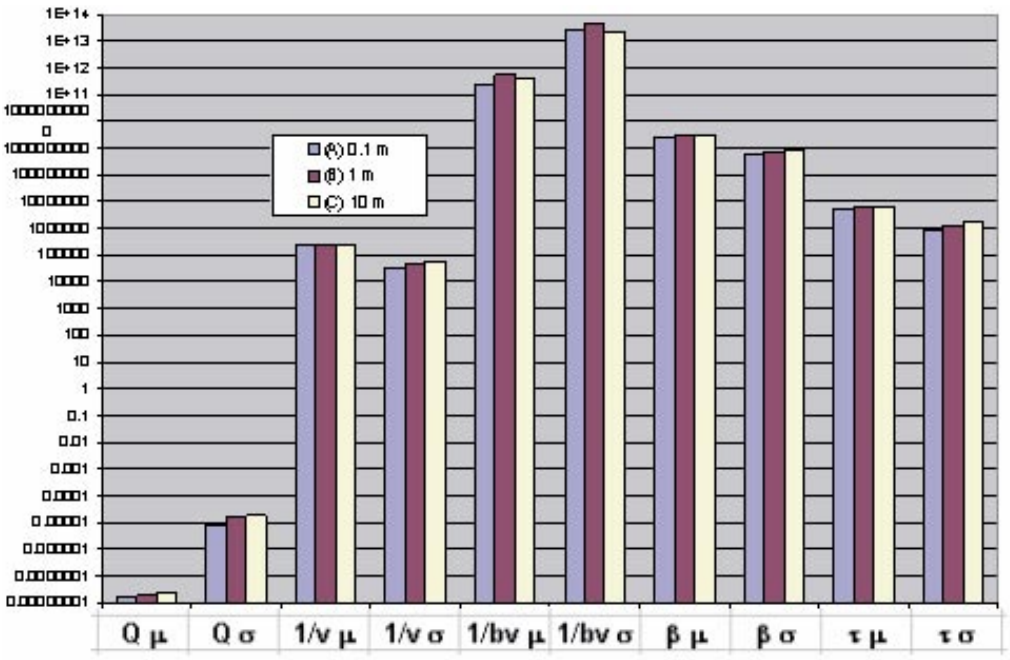

Figure 3-99. *Particle tracking results, Base case (αT = 0.01,1 and 10 m).*

Table 3-14. Comparison of 2D (LTG) and 1D (GoldSim /FARF31), Base case spatial field.

Case	Transverse dispersion	t_5 (hr) (μ,σ)	t_{50} (hr) (μ,σ)	t_{95} (hr) (μ,σ)
0–L HTO	(A) 0.1 m	1,168.1, 79.3	2,369.4, 139.7	4,512.4, 219.5
	(B) 1 m	1,167.0, 45.7	2,383.5, 80.1	4,536.1, 112.8
	(C) 10 m	1,148.0, 23.3	2,377.0, 38.1	4,542.8, 58.4
0–L Cs	(A) 0.1 m	Na	Na	Na
	(B) 1 m	Na	Na	Na
	(C) 10 m	Na	Na	Na
0–L Na	(A) 0.1 m	1,098.4, 72.8	2,471.6, 158.4	5,445.2, 262.6
	(B) 1 m	1,096.1, 42.0	2,488.8, 90.2	5,473.8, 137.8
	(C) 10 m	1,077.4, 22.0	2,482.8, 41.9	5,472.6, 65.3
0–F HTO	–	990	1,970	3,818
0–F Cs	–	Na	Na	Na
0–F Na	–	950	2,090	4,630

Case	Transverse dispersion	Q (m^3/s) (μ,σ)	1/v (s/m) (μ,σ)	1/bv (s/m^2) (μ,σ)	B (s/m) (μ,σ)	τ (s) (μ,σ)
0–P	(A) 0.1 m	1.53×10^{-8}, 8.27×10^{-6}	2.36×10^{5}, 3.26×10^{4}	2.40×10^{11}, 2.60×10^{13}	2.55×10^{9}, 5.48×10^{8}	5.24×10^{6}, 8.11×10^{5}
	(B) 1 m	1.76×10^{-8}, 1.50×10^{-5}	2.22×10^{5}, 4.38×10^{4}	5.78×10^{11}, 4.62×10^{13}	2.96×10^{9}, 7.34×10^{8}	5.91×10^{6}, 1.30×10^{5}
	(C) 10 m	2.15×10^{-8}, 1.77×10^{-5}	2.32×10^{5}, 5.74×10^{4}	3.89×10^{11}, 2.11×10^{13}	3.24×10^{9}, 9.15×10^{8}	6.42×10^{6}, 1.72×10^{5}
0–F	—	6.25×10^{-10}	1.99×10^{5}	1.6×10^{8}	3.2×10^{9}	3.98×10^{6}

4 Conclusions

Extensive single fracture simulations, under a wide variety of assumptions have demonstrated a distinctive difference in the pattern of solute transport with variations in the spatial heterogeneity on the fracture, and with different assumptions concerning transverse dispersion. These differences affect the spatial pattern of breakthrough and the spread of tracer across the fracture surface, with consequent effects on statistics such as the distributions of beta.

However, the influence of transverse dispersion on breakthrough and recovery times is much smaller than the variability of transmissivity would lead one to expect. This is due to the assumed power law relationships between transmissivity and aperture that lead to velocity fields which vary considerably less than transmissivity.

Transverse dispersion was shown to have a significant effect on solute transport for cases in which transmissivity and transport aperture are independent or only weakly correlated. This would seem unlikely for simple open fractures, but is possible for conducting features with complex internal structures.

5 References

Cvetkovic V, Cheng H, Selroos J O, 1999. Transport of Reactive Tracers in Rock Fractures. J. Fluid Mech., Vol 378, pp 335–356.

Dershowitz W, Cladouhos T, Uchida M, 2001. Tracer Tests with Sorbing Tracers. Task 4E-1:SST-1 Blind prediction. Task 4E-II: Analysis of STT-1 blind prediction. Task 4E-III: Predictions for STT1b. Task 4F: Prediction for STT-2. SKB ICR-01-02. Svensk Kärnbränslehantering AB.

Dershowitz W, Foxford T, Sudicky E, Shuttle D A, Eiben Th, Ahlstrom E, 2002. PAWorks: Pathways Analysis for Discrete Fracture Networks with LTG Solute Transport. User Documentation, Version 1.62. Golder Associates Inc., Seattle.

Dershowitz W, Lee G, Geier J, Foxford T, LaPointe P, Thomas A, 2003. FracMan: Interactive Discrete Feature Data Analysis, Geometric Modeling, and Exploration Simulation. User Documentation, Version 2.6. Golder Associates Inc, Seattle.

Domenico P, Schwartz F, 1990. Physical and Chemical Hydrogeology. J. Wiley and Sons, New York.

Marschall P, Elert M, 2003. Overall evaluation of the modeling of the TRUE-1 tracer tests - Task 4. The Äspö Task Force on Modelling of Groundwater Flow and Transport of Solutes. SKB TR-03-12. Svensk Kärnbränslehantering AB.

Miller I, Kossik R, 2002. GoldSim Pro, Version 7.51.1. User Documentation. Golder Associates Inc., Seattle.

Miller I, Lee G, Dershowitz W, 2002. MAFIC Matrix/Fracture Interaction Code with Heat and Solute Transport. User Documentation, Version 1.6. Golder Associates Inc., Redmond WA.

Norman S, Kjellbert N, 1990. FARF31 - A Far-field Radionuclide Migration Code for Use with PROPERT. SKB TR-90-01. Svensk Kärnbränslehantering AB.

Oda M, 1984. Permeability Tensor for Discontinuous Rock Masses. Geotechnique, Vol. 35, pp 483–495.

Outters N, Shuttle D, 2000. Sensitivity analysis of a discrete fracture network model for performance assessment of Aberg. SKB R-99-42. ISSN 1402-3091. Svensk Kärnbränslehantering AB.

Outters N, Follin S, Dershowitz W, 2003. Discrete Fracture Network Transport. Sensitivity Analysis of a Discrete Fracture Network, SKB R-03-13. Svensk Kärnbränslehantering AB.

Sudicky E A, McLaren R, 1992. The Laplace transform Galerkin technique for large-scale simulation of mass transport in discretely fractured porous formations, Water Resources Research, Vol. 28, No. 2, pp 499–514.